DIFLUOROMETHYLORNITHINE AND 5-AZACYTIDINE PROMOTE TUMOR ASSOCIATED MACROPHAGES TOWARD M1 POLARIZATION IN AN OVARIAN CANCER MOUSE MODEL

by

Meghan E. Travers

A dissertation submitted to Johns Hopkins University in conformity with the requirements for the degree of Doctor of Philosophy.

Baltimore, Maryland

June, 2019

Abstract

Although ovarian cancer has a low incidence rate, it remains the most deadly gynecologic malignancy. Research conducted in our laboratory has led to the development of a novel combination therapy which combines a DNA methyl transferase inhibitor (DNMTi) and an ornithine decarboxylase inhibitor that together, alter the tumor microenvironment to inhibit ovarian tumor growth. Previous work demonstrated that the DNMTi, 5-Azacytidine (AZA), activates type I interferon signaling to increase IFNγ+ T cells and NK cells and to reduce the percentage of macrophages in the tumor microenvironment. To improve the efficacy of epigenetic therapy, we hypothesized that the addition of α-difluoromethylornithine (DFMO), an ornithine decarboxylase inhibitor that reduces intracellular polyamines, may further decrease immunosuppressive cell populations. We tested this hypothesis in the VEGF-β-Defensin ID8 (VDID8) model, an immunocompetent and immunosuppressive mouse model for ovarian cancer, and found that *in vivo* AZA, DFMO, and AZA+DFMO significantly decreased tumor burden, and increased both survival and recruitment of activated (IFNγ+) CD4+ T cells, CD8+ T cells, and NK cells compared to vehicle. Combination therapy further led to a dramatic decrease in immunosuppressive cells such as M2 polarized macrophages and an increase in tumor-killing M1 macrophages. Using a CSF1R blocking antibody, we found that depleting macrophages in this model reduced the efficacy of AZA+DFMO treatment, and resulted in fewer M1 macrophages in the tumor microenvironment. We thus conclude that our novel combination therapy modifies macrophage polarization in the tumor microenvironment, recruiting M1 macrophages and prolonging survival.

After establishing an important role for macrophages in the AZA+DFMO response, we next tested the drug combination in additional solid tumor models, including the p53-/- ID8 ovarian cancer model and the 2208L breast cancer model. In both tumor models, combination AZA+DFMO had the greatest survival benefit as observed in the VDID8 model; however, single agent DFMO had a pronounced benefit in survival compared to single agent AZA. Subsequent experiments in the VDID8 model analyzed macrophage subpopulations at a greater depth, assessing whether AZA and DFMO affected tissue resident peritoneal macrophages or led to recruitment of M1 macrophages from secondary lymphoid tissue. DFMO alone was found to impact these tissue resident macrophages, polarizing them to an M1 phenotype, while AZA treatment had no impact on tissue resident macrophages.

We therefore hypothesize that DFMO treatment promotes M1 macrophage polarization at the tissue level, while AZA treatment promotes M1 macrophages through a system wide interferon and anti-viral immune response. Combined AZA and DFMO work synergistically in the VDID8 ovarian model possibly due to the high vascularization, while solid tumors such as the p53-/- ID8 model and 2208L breast model, the benefit to combination therapy is less pronounced. In these solid tumors, decreased vascularization could diminish the ability of recruited immune cells to penetrate the tumor; however DFMO is able to impact the macrophages that are already present at the tissue site.

Thesis Advisor: Dr. Cynthia A. Zahnow

Thesis Reader: Dr. Robert A. Casero

Acknowledgements

I am so thankful for all of my mentors here at Hopkins, every member of my thesis committee, and the Cellular and Molecular Medicine (CMM) program that has felt more like a family than a program during my tenure here. First and foremost I have to thank my mentor Dr. Cynthia Zahnow and my informal co-mentor Dr. Robert Casero for providing me with every opportunity to succeed. Cindy and Bob together have helped mold me into the scientist I am today and I know that I can turn to them for advice even now, as I continue to the next stage of my career. I'm lucky to have had two outstanding mentors who encouraged me to follow my scientific instincts and interests, while also teaching me their lessons learned from years of experience. Without them, I would not be where I am today. I must also thank every member of my Thesis Committee: Dr. Fred Bunz, Dr. Zaver Bhujwalla, and Dr. Deborah Armstrong for all of their guidance and insight throughout my graduate career.

I am incredibly grateful for my informal, immunology and teaching mentor Dr. Alan Scott for providing me with wonderful teaching opportunities that made me even more excited about immunology research. I was very lucky to have Alan to turn to when I got a piece of data I wanted to discuss or an experiment I thought might be a good idea. His career advice has led me to an incredible postdoc opportunity at Harvard Medical School and I truly could not be more thankful for his mentorship and guidance.

All members of our bigger cancer epigenetics lab group at Hopkins—the Baylin lab and Casero lab—every person has been helpful, collaborative, and generous with both reagents and their own personal knowledge. It has been a wonderful work environment and has fostered some of the best science in the field. I have to single out our research technician in the Zahnow lab, Stephen Brown for all of his support. Twelve hour days in lab, countless hours of mouse work… nearly every single data point I collected was with Stephen's help and I cannot express how grateful I am for him.

The CMM program at Hopkins is truly very special. Our program director Dr. Rajini Rao, manager Colleen Graham, and administrator Leslie Lichter-Mason fostered an encouraging environment that is absolutely essential to success as a PhD student. These lovely women set the tone for our program as a whole, which was extremely supportive and collaborative. Me and my fellow 2015 classmates studied together, worked on homework sets together, and prepared for our qualifying exams together. Everyone in CMM is incredibly talented and I cannot wait to follow their careers and see where we all end up.

Finally, and most importantly, I want to thank my family: my mom, dad, grandparents, brother, sister, nieces, and nephew. I've missed you all so much since moving to Baltimore. I know it was not something that anyone wanted me to do, but you were supportive of my decision regardless and I'm so thankful for that. I'm lucky to have such a wonderful family, and can't wait to be back in Boston!

Table of Contents

List of Figures

List of Abbreviations

7AAD: 7-Aminoactinomycin D

ACK: Ammonium chloride potassium

ANOVA: Analysis of variance

ARG1: Arginase 1

AZA: 5-Azacytidine

BrdU: Bromodeoxyuridine

CCR: Chemokine receptor type 2

CD: Cluster of differentiation

CRISPR: Clustered regularly interspaced short palindromic repeats

CSF: Colony-stimulating factor

CSF1R: Colony-stimulating factor receptor

dcAdoMet: Decarboxylated S-adenosylmethionine

DFMO: Difluoromethylornithine

DNA: Deoxyribonucleic acid

DNMT: DNA methyl transferase

DNMTi: DNA methyl transferase inhibitor

ELISA: Enzyme-linked immunosorbent assay

ERV: Endogenous retrovirus

FBS: Fetal bovine serum

FcR: Fc receptor

FTE: Fallopian tube epithelium

GFP: Green fluorescent protein

GrB: Granzyme B

HDACi: Histone deacetylase inhibitor

HGSOC: High-grade serous ovarian carcinoma

HPLC: High-performance liquid chromatography

IFN: Interferon

IFNGR: Interferon γ receptor

Ig: Immunoglobulin

IL: Interleukin

iNOS2: Nitric oxide synthase

IP: Intraperitoneal

LPS: Lipopolysaccharide

M-CSF: Macrophage colony-stimulating factor

MDS: Myelodysplastic syndrome

MDSC: Myeloid-derived suppressor cell

MHC: Major histocompatibility complex

MOSE: Mouse ovarian surface epithelium

NK: Natural killer

ODC: Ornithine decarboxylase

OSE: Ovarian surface epithelium

PAOX: Peroxisomal N(1)-acetyl-spermine/spermidine oxidase

PBT: Polyamine blocking therapy

PD: Programmed death

PD-L1: Programmed death ligand

PMA: Phorbol 12-myristate 13-acetate

qRT-PCR: Real-time polymerase chain reaction

RAG: Recombination activating gene

RNA: Ribonucleic acid

RPMI: Roswell Park Memorial Institute

SEM: Standard error of the mean

SMOX: Spermine oxidase

SPDSY: Spermidine synthase

SPMSY: Spermine synthase

SSAT: Spermidine/spermine N(1)-acetyltransferase

TAM: Tumor associated macrophage

TGFβ: Transforming growth factor β

TNF-α: Tumor necrosis factor

VDID8: VEGF-β-Defensin ID8

VEGF: Vascular endothelial growth factor

WT: Wildtype

Background and Significance

1.1 Ovarian cancer and its tumor microenvironment

A patient diagnosed with ovarian high-grade serous ovarian carcinoma (HGSOC) today has only a slightly increased survival compared with the same patient diagnosed 30 years ago (1). This fact is disturbing given the amount of research that has been conducted in the cancer field. It remains the most deadly gynecological malignancy with a high recurrence of 60% (1,2). Nearly 60 new cancer drugs received FDA approval in the past 5 years (2012-2017); however only one of those drugs was approved to treat ovarian cancer (3). Although ovarian cancer is not the most prevalent malignancy, it remains the 5th leading cause of death for women, and therefore the need for novel therapeutics is high (1,2).

One of the biggest challenges related to ovarian HGSOC is its immunosuppressive tumor microenvironment, helping the tumor escape immune surveillance. Cancer immunotherapy treatment options have grown rapidly in the last decade and have demonstrated considerable promise in multiple disease types; however, ovarian tumors have thus far not responded well to current treatment options such as immune checkpoint blockade therapies using α-PD-1 and α-PD-L1 (4-7). Low intra-tumoral CD8+ T cells and high immunosuppressive cell populations such as myeloid derived suppressor cells (MDSCs) and macrophages are associated with poor prognosis in ovarian cancer and could impact the efficacy of these immune therapies (8-11). Drug treatment strategies

that alter the tumor and immune cell microenvironment could prolong survival for ovarian patients.

1.2 DNMTis and the antiviral immune response

One treatment strategy that impacts immune cell populations in the tumor microenvironment is epigenetic therapy such as DNA methyl transferase inhibitors (DNMTIs) and histone deacetylase inhibitors (HDACIs) (12-18). 5-azacytidine (AZA) is a demethylating agent that incorporates into nucleic acids as a cytidine analog, which cannot be methylated by DNA methyl transferases (DNMTs). AZA is FDA approved for myelodysplastic syndrome (MDS), and low nanomolar doses lead to decreased DNA promoter methylation and restored expression of hypermethylated genes in cancer (19). Additionally, AZA treatment induces the re-expression of hypermethylated, silenced endogenous retroviruses (ERVs) *in vitro*, which can elicit an anti-viral, interferon immune response that leads to T cell activation *in vivo* (14,17). Furthermore, AZA treatment of an ovarian cancer mouse model leads to increased immune cells in the tumor microenvironment, and combination AZA and HDACi sensitized tumors to α-PD-1 therapy (17). While first generation HDACIs combined with DNMTIs have demonstrated some promise in clinical trials for non-small cell lung cancer (20), there remains a need to discover novel treatment strategies that activate the immune system and provide long term remission for other solid tumors.

1.3 Polyamines as anti-inflammatory agents

While the impact of epigenetic therapy on the immune system has been well established, emerging literature has shown that additional drug therapies can also regulate the immune system. The second drug we chose to test in a novel combination with 5-azacytidine is α-difluoromethylornithine (DFMO), an inhibitor of ornithine decarboxylase (ODC). ODC, a transcriptional target of the oncogene MYC, catalyzes a rate limiting step of polyamine synthesis forming putrescine from the precursor ornithine (Fig 1.1) (21,22).

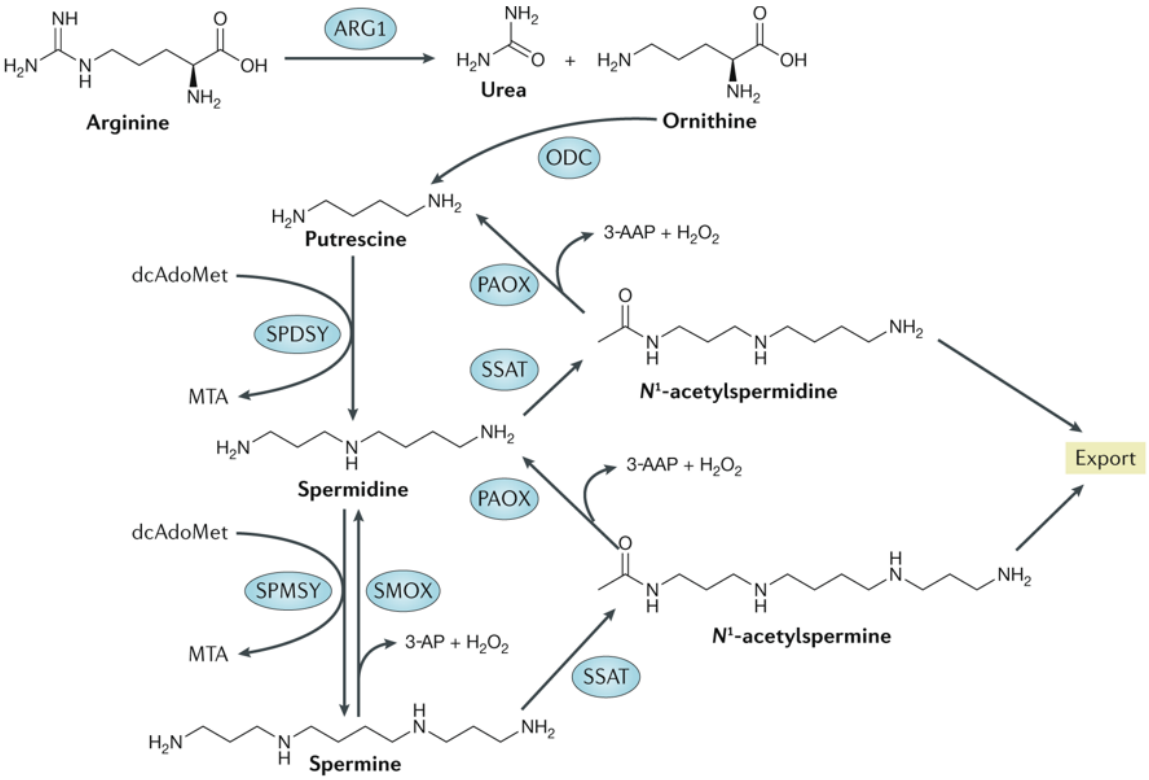

Figure 1.1: The enzyme arginase (ARG1) first catalyzes the conversion of arginine to ornithine, creating the substrate for ornithine decarboxylase (ODC). ODC then catalyzes the production of putrescine from ornithine, forming the first polyamine in the polyamine pathway. Subsequent polyamines spermidine and spermine are formed by the enzymes spermidine synthase (SPDSY) and spermine synthase (SPMSY) respectively using the aminopropyl group from decarboxylated S-adenosylmethionine (dcAdoMet). Once decarboxylated, S-adenosylmethionine can no longer be used as a methyl donor in methyltransferase reactions. Figure reproduced with permission from

Casero, et al. *Nature Reviews Cancer*. (22). SMOX = spermine oxidase; SSAT = spermidine/spermine N(1)-acetyltransferase; PAOX = Peroxisomal N(1)-acetyl-spermine/spermidine oxidase

Polyamines are polycationic alkylamines and in mammalian cells consist of spermidine, spermine and their diamine precursor, putrescine. Polyamines are essential for several biological processes including chromatin stability, regulation of gene expression at the transcriptional, translational, and posttranslational levels, play important roles in ion channel gating, membrane stability and act as free radical scavengers (22). Importantly, the metabolism of and requirements for polyamines are frequently dysregulated in cancer (22). This dysregulation, often leading to increased tumor polyamine levels is considered a prerequisite for the hyperproliferative nature of the cancer cells. Additionally, the increased polyamines may also contribute to an immunosuppressive tumor microenvironment. Spermidine regulates pro-inflammatory cytokines and has been shown to have anti-inflammatory effects (23). Microglial cells treated with spermidine prior to stimulation with lipopolysaccharide (LPS) demonstrated a decrease in inflammatory cytokines such as IL-6 and TNF-α (23). Polyamines may therefore promote immunosuppression via these anti-inflammatory mechanisms.

Polyamine blocking therapy (PBT) is a therapeutic strategy that uses an inhibitor of ODC, 2-difluoromethylornithine (DFMO) in combination with a polyamine transport inhibitor and results in greater polyamine depletion in cells and animals as compared to the use of DFMO alone (REF). This strategy has the potential to be used as both an anti-proliferative and pro-inflammatory strategy. Researchers found that use of PBT hindered tumor growth in immunocompetent

mice but not in athymic mice (24). It would seem that an essential action of the PBT was to activate the immune response and prevent tumor escape. If PBT was purely anti-proliferative, the athymic mice should have responded to treatment as well (24). It was further found that PBT led to decreased levels of myeloid suppressor cells and increased levels of CD3 positive T cells (24). Polyamine deprivation and PBT was also found to reverse immune abnormalities in the spleens of mice (25). Decreased IL-2 production in mice grafted with Lewis lung carcinoma recovered after PBT treatment, and an increase in natural killer (NK) cells was seen (25).

DFMO has traditionally been used for its anti-proliferative effects; however, these recent findings suggest it may play an important role in activating the antitumor immune response (26). Investigators demonstrated that treatment of immunocompetent mice with DFMO inhibited tumor growth, and this effect was eliminated when RAG1 knockout mice which have no functional T cell immunity were given the same treatment (26). DFMO treatment in immunocompetent mice was also shown to decrease myeloid-derived suppressor cells (MDSCs) activity and increase infiltration of CD8 positive T cells (26). Cancers with high infiltration of MDSCs are associated with a poorer prognosis, therefore decreasing the activity of these cells could be an effective way to relieve the immunosuppression and activate the immune response against the tumor (27).

Additional evidence in the literature supports the role of polyamines as anti-inflammatory agents. Pathogens such as the fungi *Batrachochytrium dendrobatidis* use polyamines to diminish immune responses in their prospective hosts (28). High

spermidine concentrations have been shown to inhibit lymphocyte proliferation (28). Ridding the body of infection from the bacterium *Helicobacter pylori*, which has been shown to increase risk of gastric cancer, is also impacted by polyamines (29). One mechanism for controlling *H. pylori* infection is through production of nitric oxide which can kill the bacterium (29). Production of nitric oxide is achieved primarily via gastric macrophages which upregulate expression of the enzyme iNOS2 that metabolizes arginine to nitric oxide (29,30). The polyamine spermine was shown to inhibit translation of inducible iNOS2, and ODC was found to be upregulated in macrophages of mice and human gastritis tissue—a condition known to be caused by chronic *H. pylori* infection (29,31). Treatment with DFMO was found to restore iNOS2 expression and consequently lower *H. pylori* colonization levels in mice infected with the bacterium (29).

Also in the case of *H. pylori* infection, others have found that myeloid-specific deletion of ODC increases inflammation and promotes gastric macrophages toward an M1 polarization (32). Importantly, an add-back experiment which introduced extraneous putrescine rescued the increased inflammation, and caused macrophages to reverse their phenotype (32). Taken together, polyamine metabolism has critical impacts on myeloid populations through metabolism of arginine, making them an attractive target for tumors rich in myeloid populations.

1.4 TAMs as both pro- and anti-tumorigenic

Macrophages demonstrate considerable plasticity in their development, responding to environmental signals such as cytokines and growth factors that

dictate their phenotype (33). Classically polarized or M1 type macrophages are considered to be anti-tumorigenic, producing pro-inflammatory cytokines and promoting T cell immunity (33-35). These M1 polarized macrophages can also have direct cytotoxic effects on tumor cells, killing them via extracellular mechanisms (36).

In contrast, alternatively polarized or M2 type macrophages, normally involved in wound repair, are anti-inflammatory and can promote tumorigenesis (33-35). Tumors and surrounding stromal cells can produce chemokines, cytokines, and growth factors that promote macrophages toward this M2 or pro-tumorigenic polarization (36,37). These M2 macrophages not only dampen the anti-tumor immune response by producing regulatory cytokines such as IL-10 and TGFβ, they can further directly assist tumors in processes essential for their survival such as angiogenesis and metastasis (36).

At the core of this polarization decision of a developing myeloid cell is how to use the metabolite arginine (Fig. 1.2) (30). M1 macrophages, whose differentiation is promoted by downstream signaling from IFNγ, upregulate the enzyme iNOS which metabolizes arginine to nitric oxide and L-citrulline (30). Via a nitric oxide dependent mechanism, these M1 macrophages are capable of promoting tumor rejection via T cell recruitment and promotion of T cell immunity (38). Conversely, M2 macrophages upregulate expression of the enzyme arginase (ARG1) via signaling downstream from cytokines such as IL-4, IL-10, and IL-13 (30,36). Arginase metabolizes L-arginine to L-ornithine and urea, and subsequently L-ornithine can be further metabolized to produce polyamines such as putrescine,

spermidine, and spermine. As indicated above, polyamines have been shown to have an anti-inflammatory role in the cell, and in fact spermine was shown to inhibit synthesis of inflammatory cytokines such as TNFα and IL-1 (39). DFMO, as an inhibitor of ODC, has potential to inhibit ARG1 via increased amounts of L-ornithine and product inhibition. DFMO treatment of melanoma cell lines was shown to decrease arginase enzyme activity (26), and DFMO treatment potentiates nitric oxide production in LPS stimulated macrophages (40). Therefore, one critical mechanism of action of DFMO is its function at the center of this macrophage polarization decision, and thus has great potential to stimulate myeloid cells toward an M1, anti-tumorigenic phenotype.

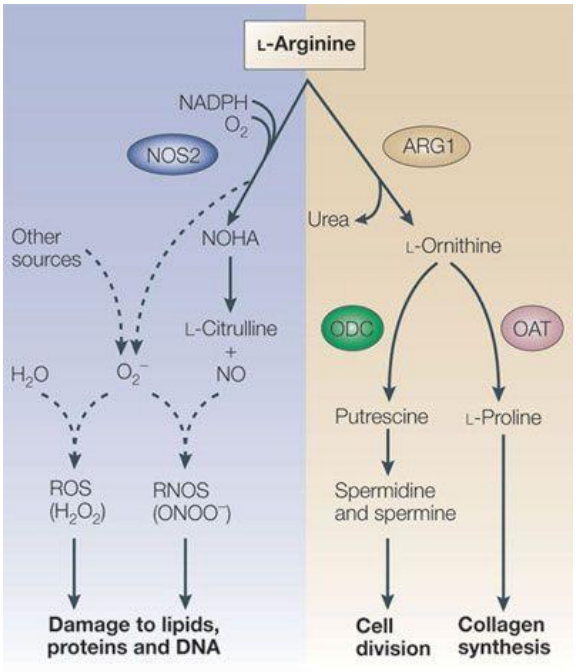

Figure 1.2: L-arginine metabolism pathways. M1 macrophages upregulate the enzyme iNOS2 (left) to mediate T cell recruitment to the tumor, while M2 macrophages upregulate ARG1 which favors production of polyamines and a pro-tumor microenvironment (17).

Lastly it should be noted that the oncogene MYC comprises approximately 40 percent of the transcriptional fingerprint of alternatively polarized M2 macrophages and is overexpressed in TAMs (36). The enzyme ODC is a transcriptional target of MYC, therefore TAMs which overexpress MYC are likely to upregulate ODC expression as well, enabling them to metabolize arginine down the polyamine pathway (21,22). AZA treatment has been shown to downregulate MYC, therefore the addition of AZA to DFMO treatment could further impact macrophage polarization (18). DFMO will inhibit the enzyme ODC directly, while AZA can attenuate expression of ODC via downregulation of its transcription factor MYC (18,21).

Experimental protocol

2.1 Animal Models

Female C57BL/6NHsd wild-type (WT) mice (7-8 wk old) were purchased from Envigo International Holdings, Inc. (Indianapolis, IN). Mice were housed at the Johns Hopkins Kimmel Cancer Center Animal Resources Core and cared for in accordance with the policies of The Johns Hopkins University Animal Care and Use Committee and our approved animal protocol.

2.1.1 VEGF-β-Defensin ID8 Ovarian Cancer Model

Dr. Katherine Roby developed the ID8 model via mild trypsinization of the ovarian surface epithelium, followed by long-term passage in vitro until the cells spontaneously immortalized (41). The parental ID8 clone has been further modified to enhance its usefulness as a tool by overexpressing VEGF and β-defensin, making the tumor more aggressive and immunosuppressive (42,43). The VEGF-β-Defensin ID8 (VDID8) cells are also positive for Luciferase and green fluorescent protein (GFP). While this model has proven to be an excellent research tool, it has limitations in representing high-grade serous ovarian cancer in humans because it is derived from mouse ovarian surface epithelium, not the fallopian tube, and is Trp53 wildtype (44). In mice however, ovarian cancer can arise from either fallopian tube epithelium (FTE) or ovarian surface epithelium (OSE) and ID8 is the most widely used MOSE model for immunotherapy studies in ovarian cancer.

2.1.2 p53-/- ID8 Ovarian Cancer Model

Mutations in the tumor suppressor TP53 are among the most common mutations seen in human ovarian cancers (44). To better study this mutation in animal models, Dr. Iain McNeish developed an ID8 tumor cell line null for p53 using CRISPR-Cas9 (44). This single mutation accelerated the rate of tumor growth such that median survival reduced from approximately 90 days to 60 days.

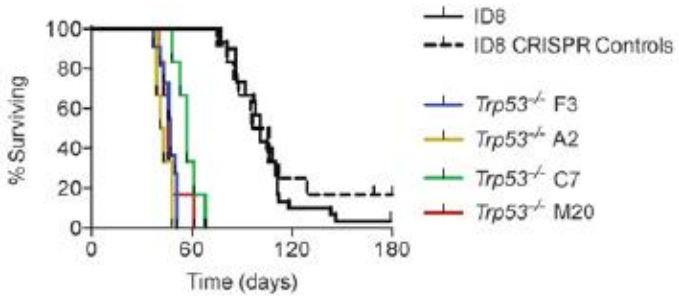

Figure 2.1: Percent survival of p53-/- ID8 tumor in WT C57BL/6NHsd mice (44).

2.1.3 2208L Breast Cancer Model

The 2208L model developed by the Medina and Rosen labs at Baylor college of Medicine is also a p53-/- tumor model (45). The model was adapted from whole p53 null mice that succumbed to tumors elsewhere in the body prior to developing mammary tumors (45). Thus in order to study only breast tumors, mammary glands were isolated from 6 week old p53-/- germline BALB/c mice, and transplanted into 3 week old wildtype BALB/c mice (45). Numerous mammary tumors developed and were characterized according to tumor type. The 2208L is an aggressive, infiltrating ductal carcinoma-like mouse tumor that is rich in MDSCs (45). Also

unique to this model is that the breast cancer cells have not been cultured on plastic and have only been passaged in mice, making them a better, less altered, model for *in vivo* tumor conditions (45).

2.2 Flow Cytometry

Cells were washed and blocked with FcR Blocking Reagent (Miltenyi Biotec 130-092-575) and stained for cell-surface markers including Live/Dead (eBioscience 65-0865-14), CD45 (BD Biosciences 563891), CD3 (BD Biosciences 560527), CD4 (BD Biosciences 563331), CD8 (BD Biosciences 563152), NK1.1 (BD Biosciences 562921), F4/80 (BioLegend 123113), CD11b (BioLegend 101222), MHC II (isotype control 400627; BioLegend 107619), CD206 (BioLegend 141708), CD11c (BD Biosciences 564079), Ly6C (BD Biosciences 562728), Ly6G (BD Biosciences 563005), CD80 (BD Biosciences 553769), and CD86 (BD Biosciences 558703). Cells were permeabilized and stained for intracellular IFNγ (isotype control 554686; BD Biosciences 554413). Flow cytometry acquisition was performed on an LSR II cytometer (BD Biosciences), and data were analyzed using FlowJo software version 10.2.

2.3 Statistical Analysis

Data were graphed in GraphPad Prism 7.0 and tested for a Gaussian distribution using the Shapiro-Wilk test. Significance was determined for sets of data with more than two groups using the one-way ANOVA or Kruskal Wallis test

dependent upon normality results from the Shapiro-Wilk test. If only two sets of data were compared, either the Mann-Whitney (non-parametric) or student's t test (parametric) were used dependent on normality results. Significances in survival data were determined by Mantel–Cox (log-rank) test. P values less than 0.05 were deemed significant. Outliers were removed from ascites volume datasets and ascites immune cell datasets using Peirce's criterion (46). Significances are shown as *P < 0.05, **P < 0.01, and ***P < 0.001 ****P < 0.0001.

Chapter 1: AZA and DFMO activate the immune system

3.1 Introduction

AZA treatment induces the re-expression of hypermethylated, silenced endogenous retroviruses (ERVs) *in vitro*, which can elicit an anti-viral, interferon immune response that leads to T cell activation *in vivo* (14,17). Furthermore, AZA treatment of an ovarian cancer mouse model leads to increased immune cells in the tumor microenvironment, and combination AZA and HDACi sensitized tumors to α-PD-1 therapy (17). DFMO treatment also alters immune cell populations in the tumor microenvironment (26). Investigators demonstrated that treatment of immunocompetent mice, but not RAG1 knockout mice, inhibited tumor growth, decreased MDSC activity and increased infiltration of CD8+ T cells (26). Since both single agents have demonstrated impacts on the immune system, we tested whether the two combined agents would have a synergistic effect in the VDID8 ovarian cancer mouse model.

3.2 Methods

To test the hypothesis that addition of DFMO to therapy using the DNMTi AZA would reduce tumor burden and improve overall survival in a mouse model of ovarian cancer, immunocompetent C57BL/6 mice were injected intraperitoneally (IP) with 250,000 VDID8 syngeneic MOSE cells. Mice were treated IP with AZA (0.5 mg/kg) or saline vehicle, DFMO (2% in water), or combination AZA and DFMO beginning three days post tumor injection (Fig 3.1). Hemorrhagic ascites fluid

consistently develops at approximately 4-5 weeks post VDID8 injection and is an accurate measurement of tumor burden in mice, allowing observation of tumor growth in real time (42,43).

When ascites fluid is collected from the mice, the cells obtained represent the tumor microenvironment and can be further analyzed to help illustrate the mixed population of cells surrounding the tumor. Ascites was collected, filtered, incubated in ACK buffer (Quality Biological) to lyse red blood cells, and washed. The mononuclear cells collected were then cultured for four hours in RPMI (Corning) with 10% FBS in the presence of phorbol 12-myristate 13-acetate (PMA) and ionomycin to stimulate cells, and brefeldin A and monensin (Invitrogen 00-4975-93) to cause aggregation of secreted proteins inside the cell. Cells were subsequently washed and stained with a panel of antibodies (one million cells per mouse) in accordance with experimental protocol 2.2 Flow Cytometry. Remaining cells from each treatment arm were pooled, washed, and pellets were frozen at -80C for later polyamine analysis. Polyamines were analyzed via high-performance liquid chromatography (HPLC) as previously described (47). *In vitro* polyamines were assessed by culturing VDID8 cells in 10% FBS RPMI + gentamicin for one week prior to beginning 10 day treatment. Cells were treated with 500nM AZA/saline for 10 days and 5mM DFMO/water for 3 days. AZA+DFMO cells were treated with 500nM AZA for the first 7 days, and 500nM AZA + 5mM DFMO for the final 3 days of treatment. Polyamines were then analyzed via HPLC as previously described (47).

3.3 Results

3.3.1 Combination treatment reduces tumor burden and increases survival

To confirm that DFMO inhibits ODC in the model systems used, VDID8 cells were treated in vitro and in vivo and polyamine levels were determined (Fig 3.2. 3.3). *In vitro* treatment of VDID8 tumor cells led to a significant decrease in putrescine and spermidine with DFMO alone and when combined with AZA. However, AZA alone appeared to have a stimulatory effect on putrescine and spermidine synthesis (Fig 3.2). In bulk ascites cells from treated animals, combination treatment led to a decrease in all three polyamines, including spermine (Fig 3.3). No significant changes to the polyamine pools were observed with AZA treatment alone, but putrescine and spermidine were decreased (although not significantly) by DFMO treatment (Fig 3.3).

Volumetric measurements of hemorrhagic ascites fluid are directly correlated to tumor burden in the VDID8 model of ovarian cancer (42,43). Mice treated with single agent AZA or DFMO have reduced tumor burden initially after the first ascites drain (week 4), but subsequently present with higher tumor burden at week 5 compared to mice treated with combination therapy (Fig. 3.4 and 3.5). Mice treated with combination therapy also exhibited the largest increase in overall survival with a median survival of 59 days compared to that of single agent AZA or DFMO of approximately 44 days (Fig. 3.6). Although single agent treatment with AZA or DFMO compared to vehicle treatment significantly increases total numbers

of lymphocytes, these numbers are not further enhanced with combination AZA+DFMO treatment (Fig. 3.7 and 3.8).

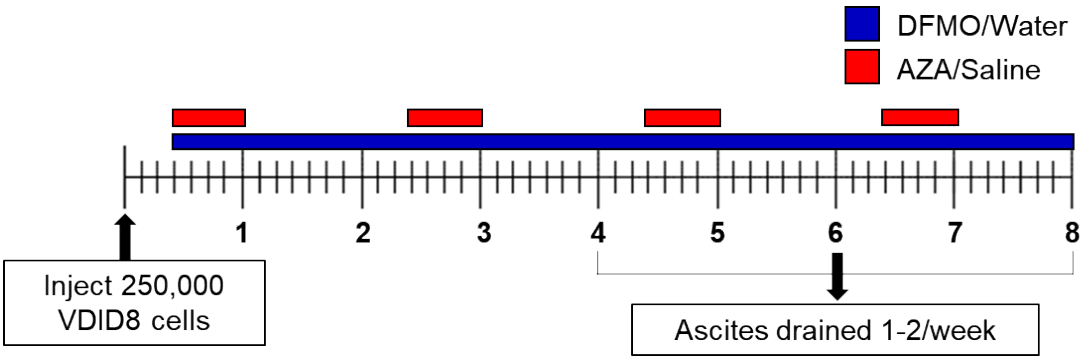

Figure 3.1: Tumor cell injection and treatment schematic. Mice were injected IP with 250,000 VDID8 cells and treated with 0.5 mg/kg of AZA/saline IP 5 days a week, every other week. 2% DFMO was provided in water bottles. Mice were treated throughout the duration of the experiment. Upon 25-30% weight gain, ascites fluid was drained from mice and processed for analysis of the tumor microenvironment.

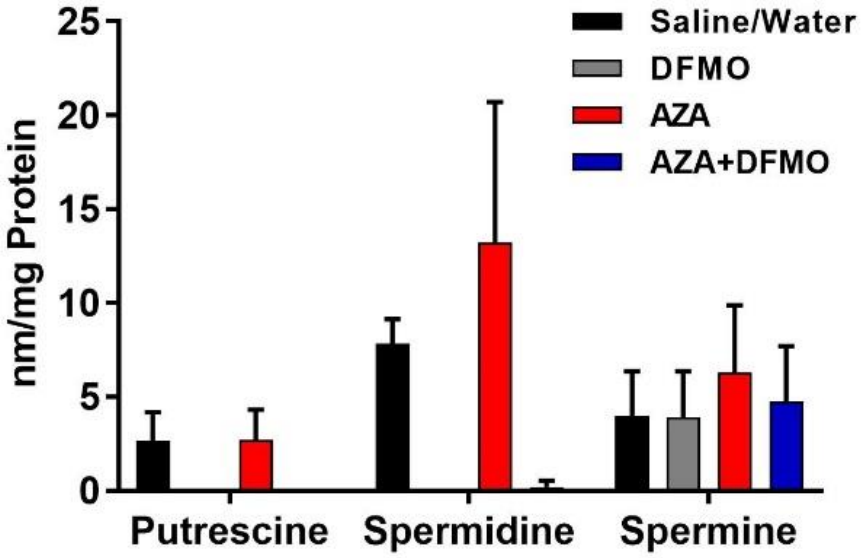

Figure 3.2: VDID8 cells were cultured in 10% FBS RPMI + gentamicin for one week prior to beginning 10 day treatment. Cells were treated with 500nM AZA/saline for 10 days and 5mM DFMO/water for 3 days. AZA+DFMO cells were treated with 500nM AZA for the first 7 days, and 500nM AZA + 5mM DFMO for the final 3 days of treatment. High-performance liquid chromatography (HPLC) analysis of polyamine levels in cultured, treated VDID8 cells are shown. n = 3.

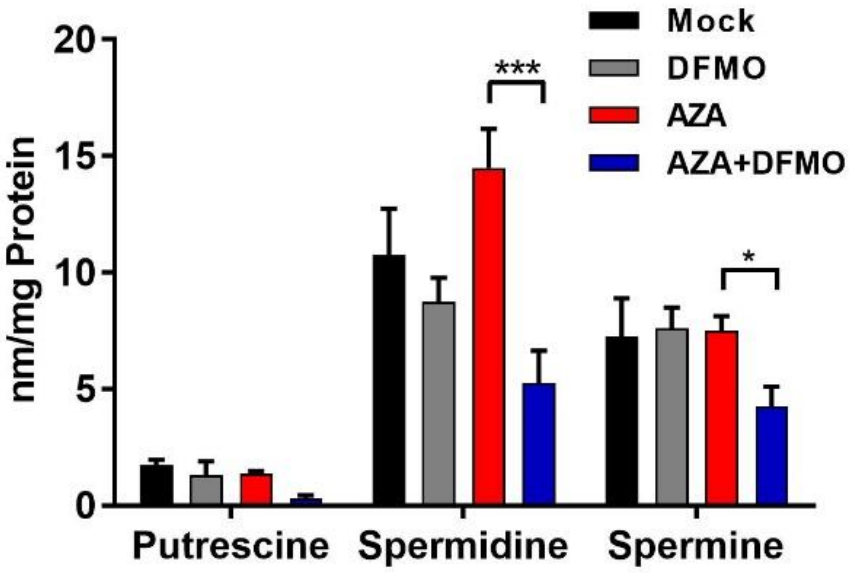

Figure 3.3: Bulk ascites fluid was collected from individual mice treated with DFMO, AZA, or AZA+DFMO. Bulk ascites cells were lysed and washed and remaining cells were prepped for HPLC analysis of polyamine levels. n = 4-10. All data were tested for a Gaussian distribution and found to be normal using Shapiro-Wilk test. Significance was determined using a one way ANOVA.

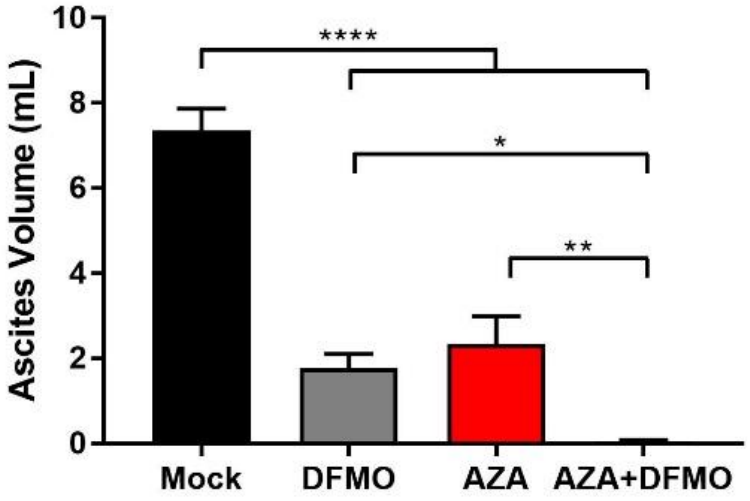

Figure 3.4: Tumor burden, represented by ascites volume, 4 weeks post tumor injection. Representative data (mean +/- SEM shown). n = 10; four biological replicates. Data found to be normal via Shapiro-Wilk test. Significance determined using one-way ANOVA; statistical outliers removed using Peirce's criterion.

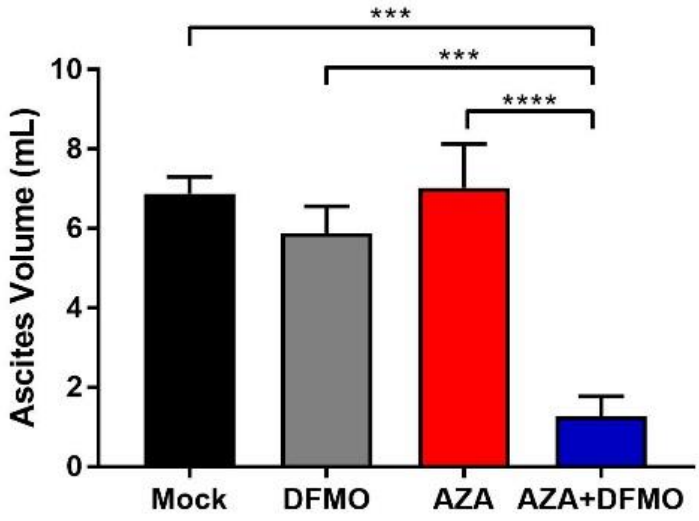

Figure 3.5: Tumor burden, represented by ascites volume, 5 weeks post tumor injection. Representative data (mean +/- SEM shown). n = 10; four biological replicates. Data found to be normal via Shapiro-Wilk test. Significance determined using one-way ANOVA; statistical outliers removed using Peirce's criterion.

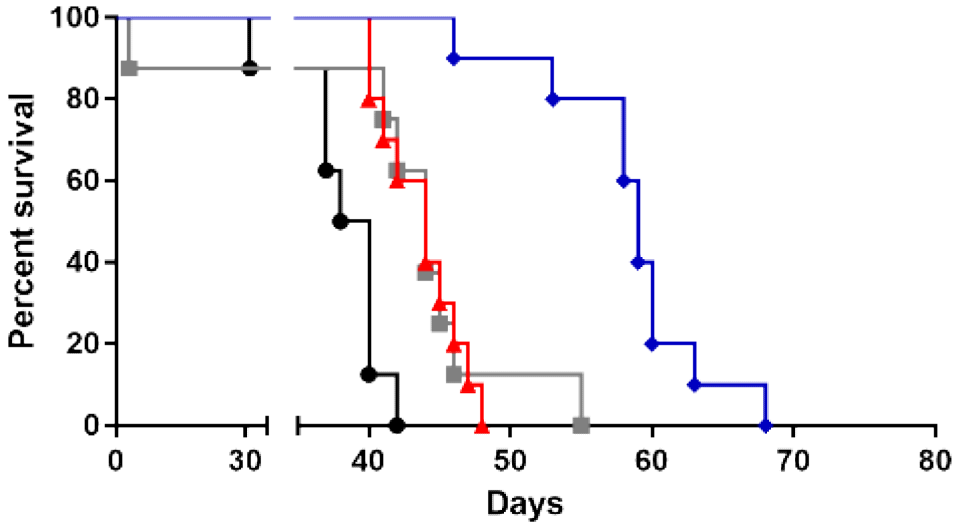

Figure 3.6: Representative survival curve (median survival in days); n = 10; four biological replicates. Significance determined using log-rank Mantel-Cox test.

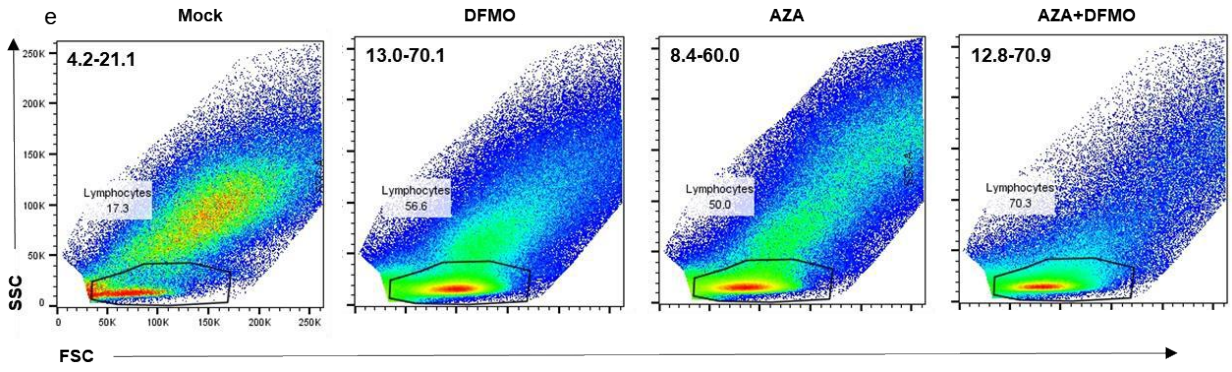

Figure 3.7: Flow cytometry plots of SSC vs. FSC demonstrating an increase in lymphocyte populations in ascites fluid at week 5 post tumor injection with AZA, DFMO, and AZA+DFMO treatment. Range of total lymphocyte population percentages are included in the upper left hand corner for each plot.

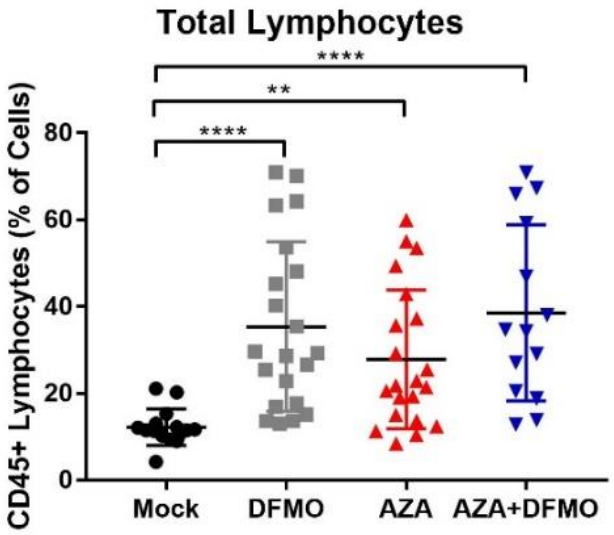

Figure 3.8: Total lymphocyte populations in week 5 bulk ascites fluid of mice; n = 14-21. Data were tested for a Gaussian distribution using Shapiro-Wilk test and found to be normal after log transformation. Significance was determined using one way ANOVA.

3.3.2 AZA+DFMO has few impacts on cell cycle

Because DFMO is FDA approved as an anti-proliferative agent for conditions such as facial hirsutism, we needed to investigate whether the efficacy of combination therapy could be due simply to anti-proliferative effects or perhaps increased cell death or apoptosis (22). We conducted *in vivo* and *in vitro* cell-cycle analyses, determined by BrdU incorporation and 7-AAD staining of DNA content. *In vivo* and *in vitro* data showed that the majority of tumor cells are in the G0-G1 phase (Fig. 3.9 and 3.10). In both sets of data, it appears that AZA+DFMO treatment leads to a G2-M block (Fig. 3.9 and 3.10). While *in vitro* data shows a significant reduction in S phase cells with treatment, *in vivo* conditions, which are influenced by many more variables, differ (Fig. 3.9 and 3.10). This could be due to the greater reduction of polyamines seen *in vitro* versus *in vivo* (Fig. 3.2 and 3.3).

These tumor cell data cannot wholly account for the anti-tumorigenic effect of combination AZA+DFMO in our model. The changes in apoptosis at the low doses of AZA and DFMO used in our study are small as we have previously reported and proliferation *in vivo* is not decreased (17,19). The data do suggest that the combination of AZA and DFMO may lead to an increase of cells in G2-M and this could play a role in the anti-tumorigenic effect observed by combination treatment.

Additionally, microRNA gene expression data was obtained for tumor cells after both *in vitro* culture with DFMO, AZA, and AZA+DFMO, and from GFP+ sorted cells from mice treated *in vivo* (Fig. 3.11 and 3.12). Using an apoptosis gene set enrichment analysis, there were no significant increases in expression of apoptotic

related genes after treatment with AZA, DFMO, or combination AZA+DFMO. Gene enrichment maps provided below for both *in vitro* and *in vivo* results.

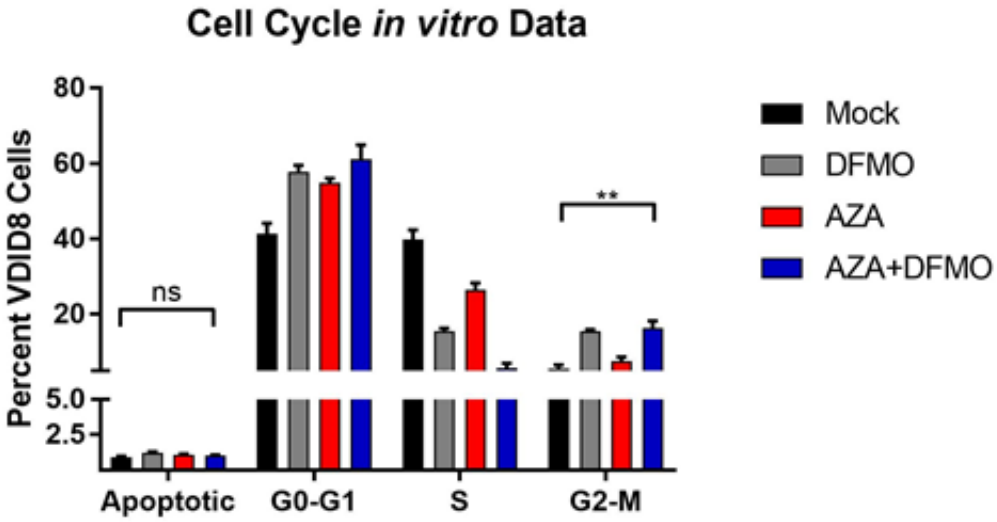

Figure 3.9: Cell cycle analysis of *in vitro* AZA+DFMO treatment of VDID8 cells. There are no statistically significant differences among apoptotic cells. AZA+DFMO *in vitro* leads to a significant increase in G2-M phase cells.

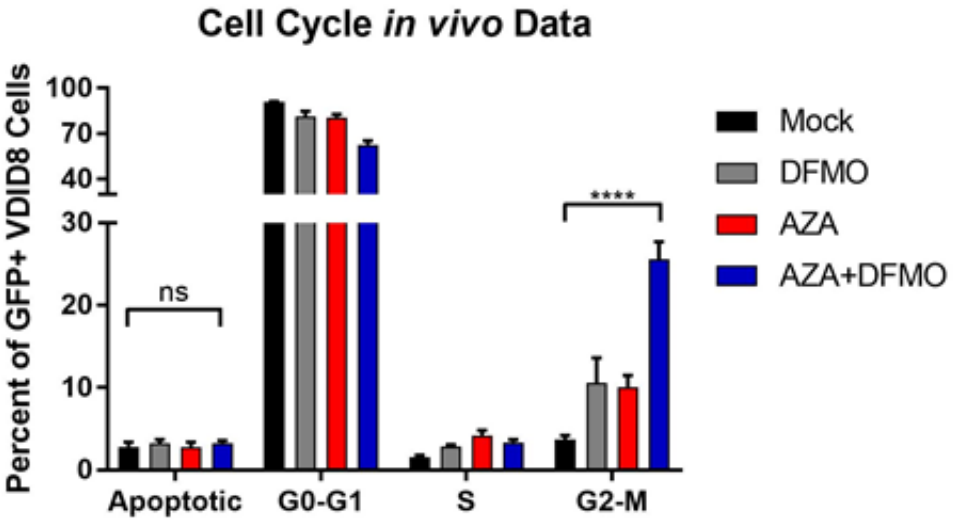

Figure 3.10: Cell cycle analysis of *in vivo* AZA+DFMO treatment of mice previously injected IP with VDID8 cells. There are no statistically significant differences among apoptotic cells. AZA+DFMO *in vivo* leads to a significant increase in G2-M phase cells.

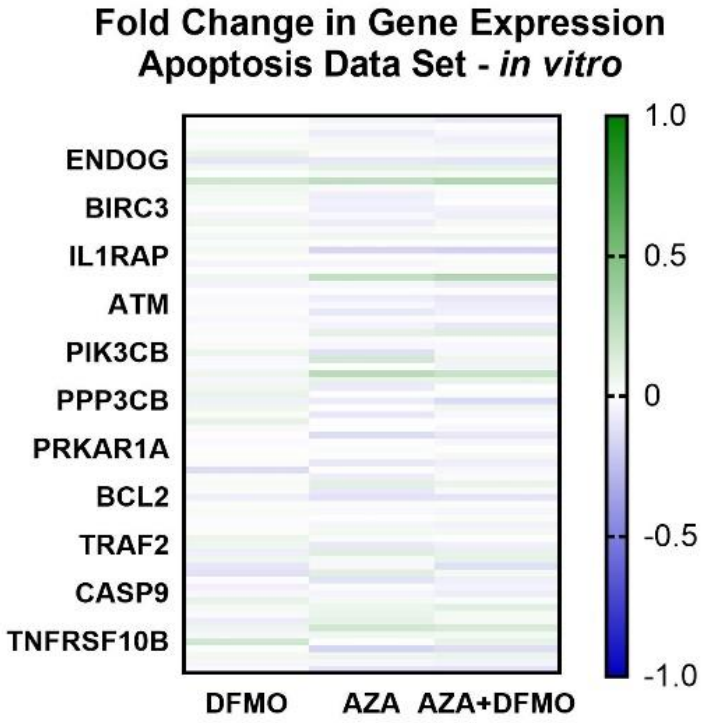

Figure 3.11: Gene set enrichment analysis for DFMO, AZA, and AZA+DFMO treated VDID8 cells. No major fold changes in gene expression were observed with treatment compared to mock cells.

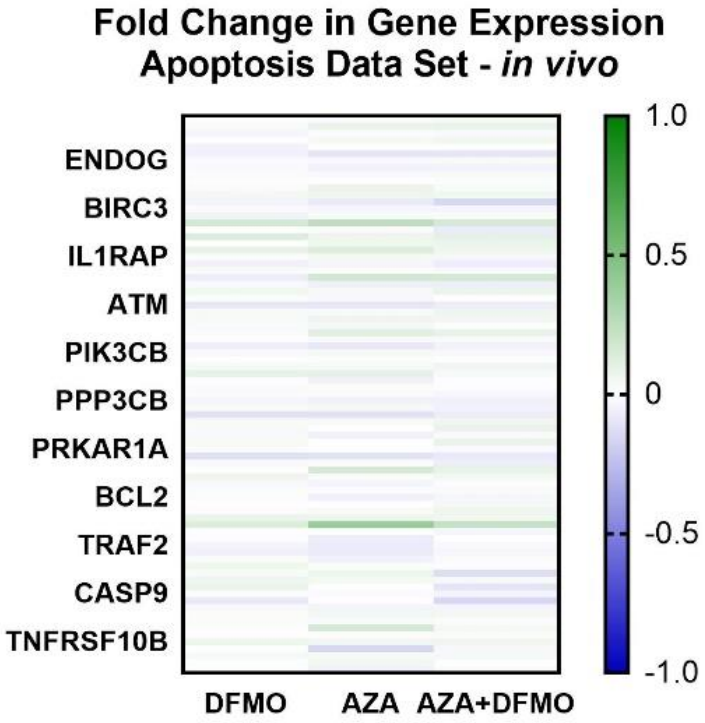

Figure 3.12: Gene set enrichment analysis for GFP+ isolated tumor cells from mice treated with DFMO, AZA, and AZA+DFMO. No major fold changes in gene expression were observed with treatment compared to mock mice.

3.3.3 Combination treatment leads to increased lymphocyte populations

To pursue further whether changes in lymphocyte populations might account for the dramatic increase in survival observed with AZA+DFMO combination therapy, the numbers and activity of specific lymphocyte subpopulations in hemorrhagic ascites fluid at week 5 post tumor injection were analyzed. Single agent AZA or DFMO led to significant increases in T cell, NK cell, and IFNγ+ lymphocyte populations examined in the tumor microenvironment (Fig 3.13 – 3.19). In most cases, combination therapy did not alter immune populations over what was observed with single agents (Fig 3.13 – 3.18). The exception however, was a significant increase in IFNγ+ NK cells observed in combination treated mice versus AZA or DFMO alone (Fig 3.19).

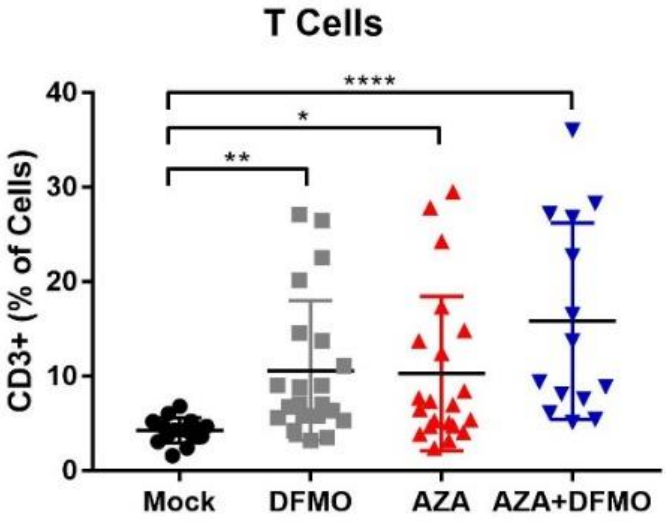

Figure 3.13: Number of total T cells shown as a percent of total cells, isolated from ascites fluid of mice at week 5 post tumor injection.

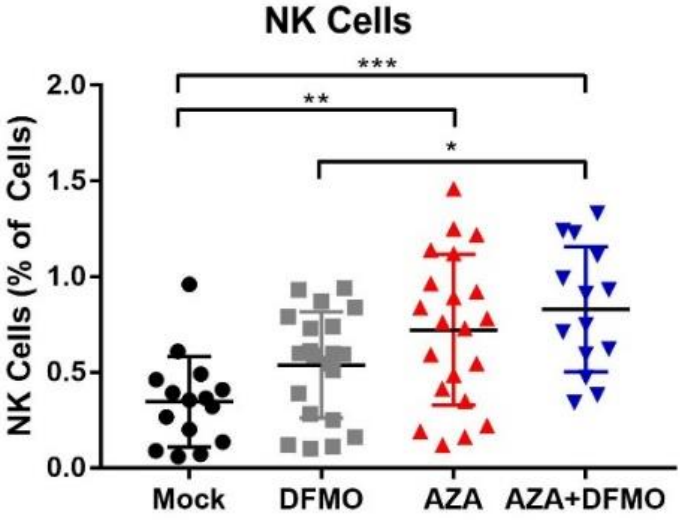

Figure 3.14: Number of total NK cells shown as a percent of total cells, isolated from ascites fluid of mice at week 5 post tumor injection.

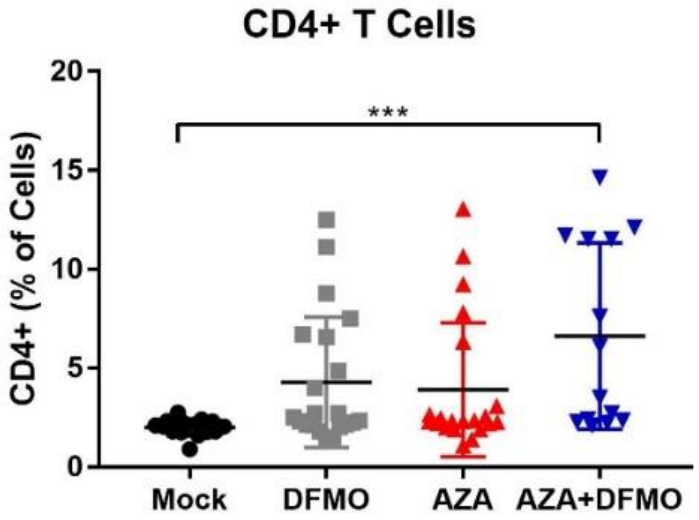

Figure 3.15: Number of total CD4+ “Helper” T cells shown as a percent of total cells, isolated from ascites fluid of mice at week 5 post tumor injection.

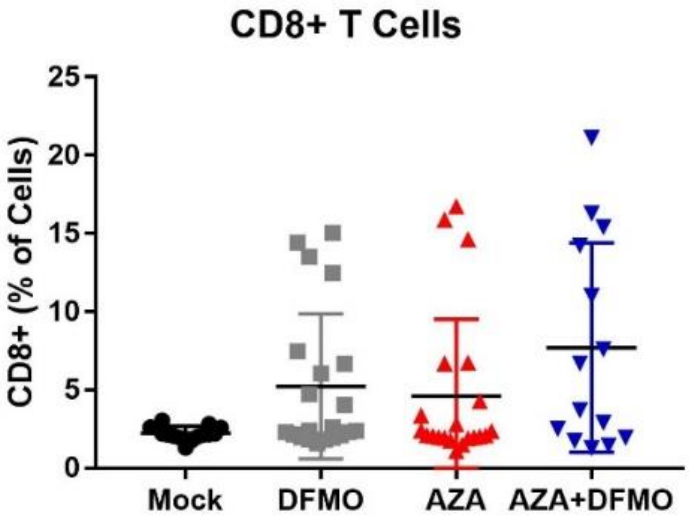

Figure 3.16: Number of total CD8+ cytotoxic T cells shown as a percent of total cells, isolated from ascites fluid of mice at week 5 post tumor injection.

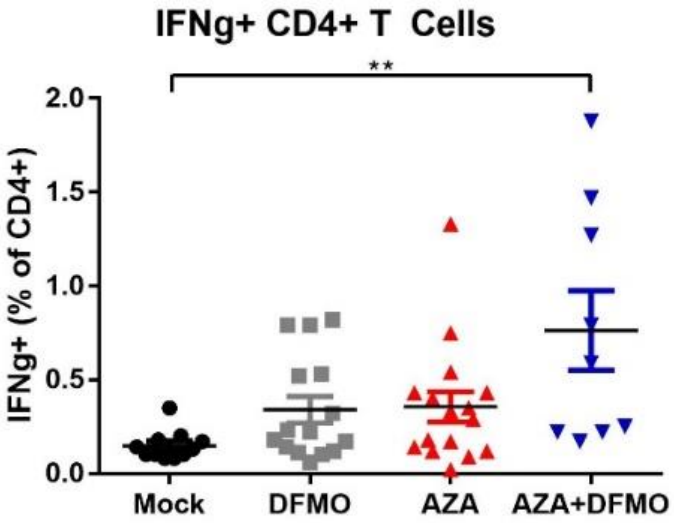

Figure 3.17: Number of IFNγ+ CD4+ T cells, shown as a percentage of CD4+ T cells. IFNγ can be considered a marker of T cell activation, and combination AZA+DFMO leads to increased activated CD4+ T cells.

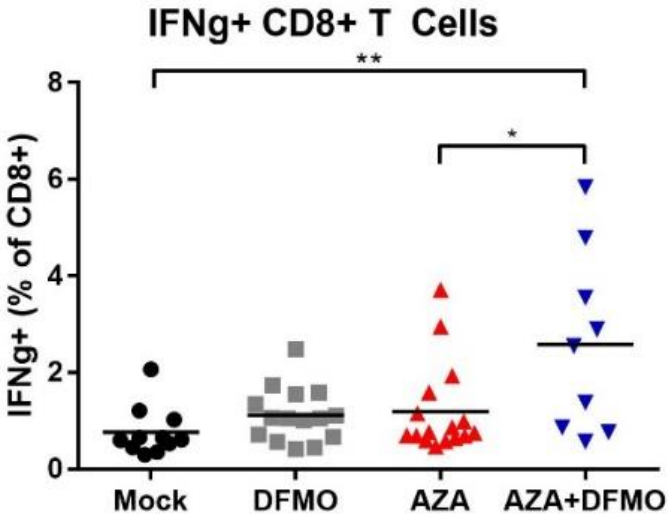

Figure 3.18: Number of IFNγ+ CD8+ T cells, shown as a percentage of CD8+ T cells. AZA+DFMO combination treatment trends toward an increase in activated CD8+ T cells, but is not significant.

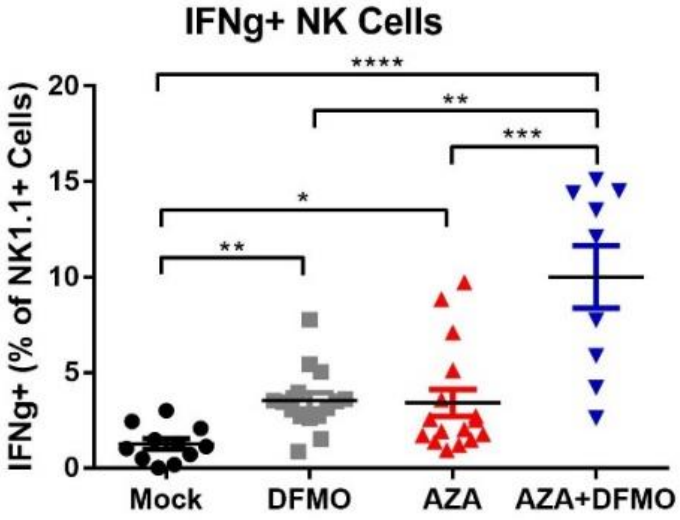

Figure 3.19: Number of IFNγ+ NK cells, shown as a percent of NK cells. Combination treatment leads to significant increases in these IFNγ+ cells compared to both single treatment DFMO or AZA.

3.3.4 Addition of α-PD-1 does not provide added benefit

It was hypothesized that the observed increase in IFNγ+ cells in the model could lead to an increase in PD-L1 expression on the surface of tumor cells, possibly sensitizing the tumor to α-PD-1 therapy. Surface PD-1 expression on T cells is a signature of immune tolerance, and when engaged with its ligand PD-L1 on tumor cells, can limit the T cell's ability to proliferate and perform its effector functions (48,49). We found that GFP+ tumor cells collected from ascites fluid were positive for PD-L1, suggesting that interfering with the PD-1/PD-L1 axis may improve treatment outcome in these mice (Fig 3.20 and 3.21). No changes were observed in the number of PD-1 expressing T cells however, with single agent or combination treatment (Fig 3.20 and 3.21). Nevertheless, there is a population of PD-1+ T cells thus antibody treatment may be beneficial.

Mice were treated with four, 200ug doses of α-PD-1 at days 17, 20, 24, and 27 post tumor injection, as shown in Fig 3.24. This α-PD-1 regimen was found to successfully improve survival in a combination AZA+HDACi treatment regimen, and was therefore tested in this model (17). Addition of α-PD-1 to the combination of DFMO and AZA treatment did not further decrease tumor burden in the mice, nor did it increase survival (Fig 3.25-3.28). The lack of response to α-PD-1 therapy suggests that a T cell response may not be the primary mechanism of action in this combination drug therapy.

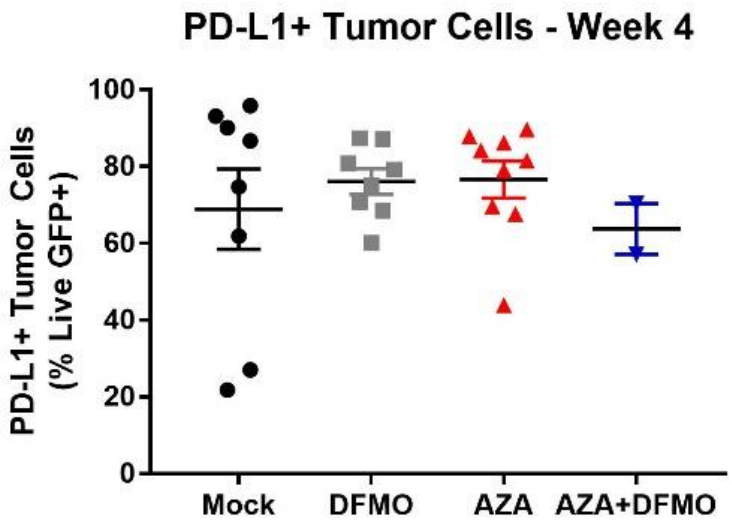

Figure 3.20: Number of PD-L1+ tumor cells, collected from ascites fluid of mice at 4 weeks post tumor cell injection, shown as a percentage of tumor cells.

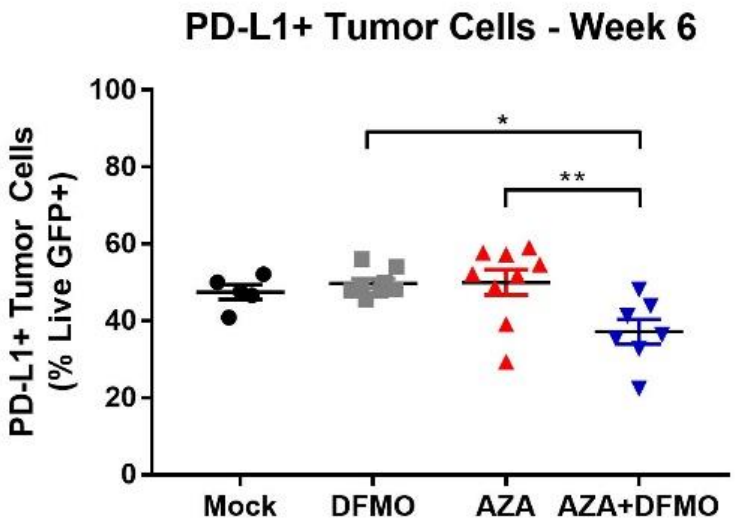

Figure 3.21: Number of PD-L1+ tumor cells, collected from ascites fluid of mice at 6 weeks post tumor cell injection, shown as a percentage of tumor cells.

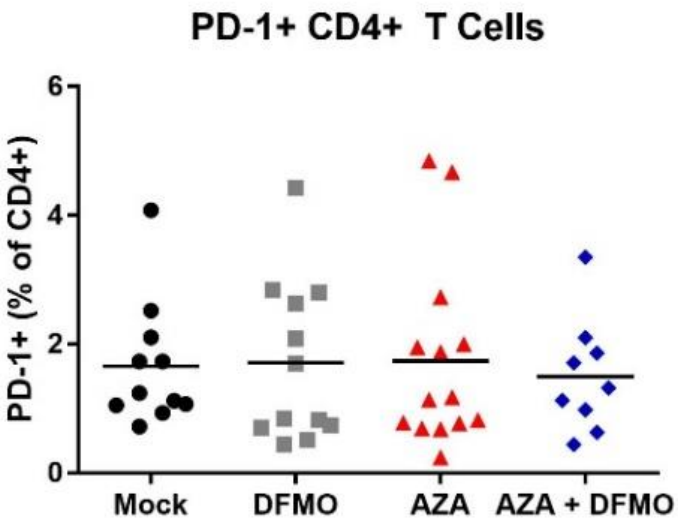

Figure 3.22: Number of PD-1+ CD4+ T cells, shown as a percentage of CD4+ T cells. No changes with treatment were observed, and total PD-1 expressing cell numbers were low.

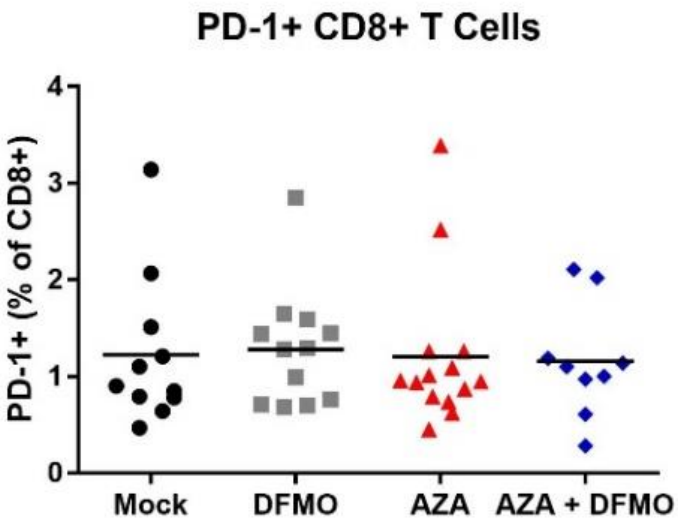

Figure 3.23: Number of PD-1+ CD8+ T cells, shown as a percentage of CD8+ T cells. No changes with treatment were observed, and total PD-1 expressing cell numbers were low.

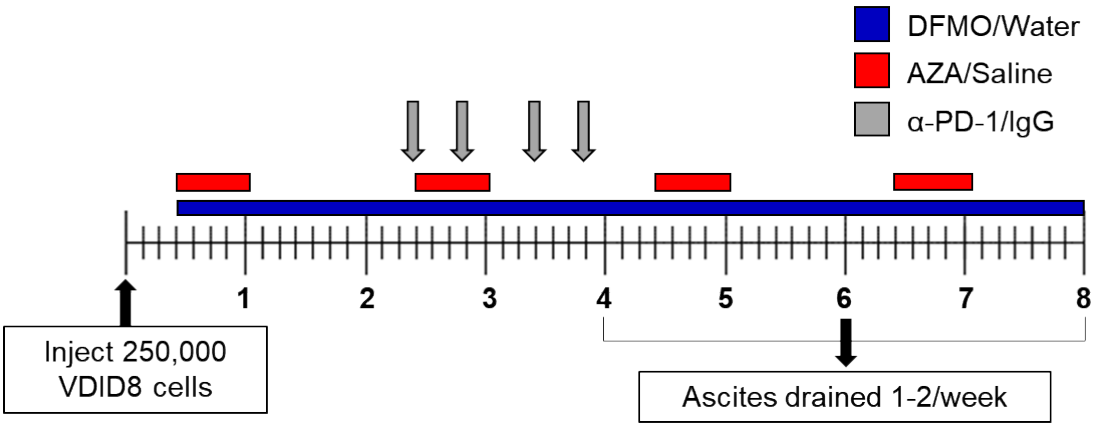

Figure 3.24: Treatment regimen for α-PD-1 therapy. Four, 200ug doses of antibody or IgG control were administered IP to mice at days 17, 20, 24, and 27 post tumor cell injection.

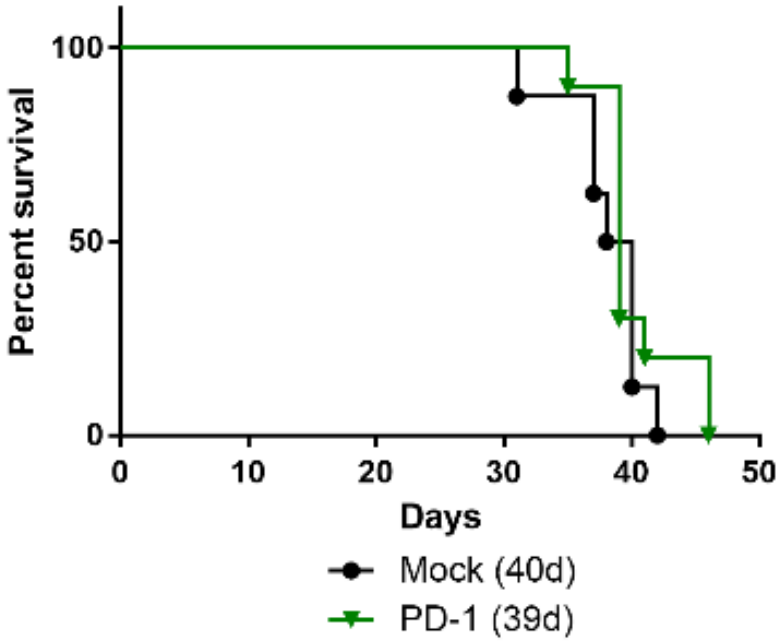

Figure 3.25: Treatment with α-PD-1 therapy alone provided no survival benefit to mice.

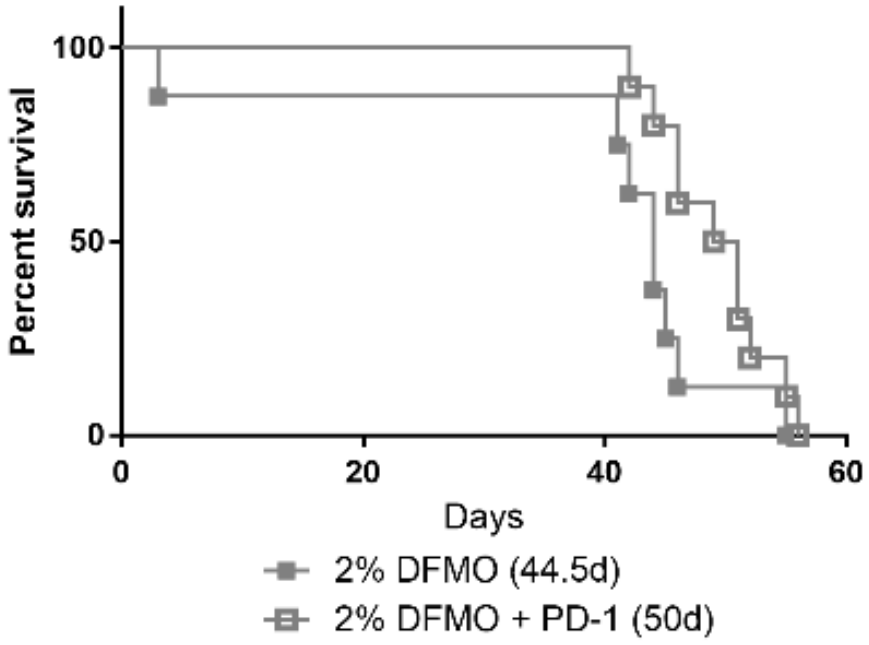

Figure 3.26: Addition of α-PD-1 to DFMO provided a slight benefit in survival to mice, but was not significant (p=0.07).

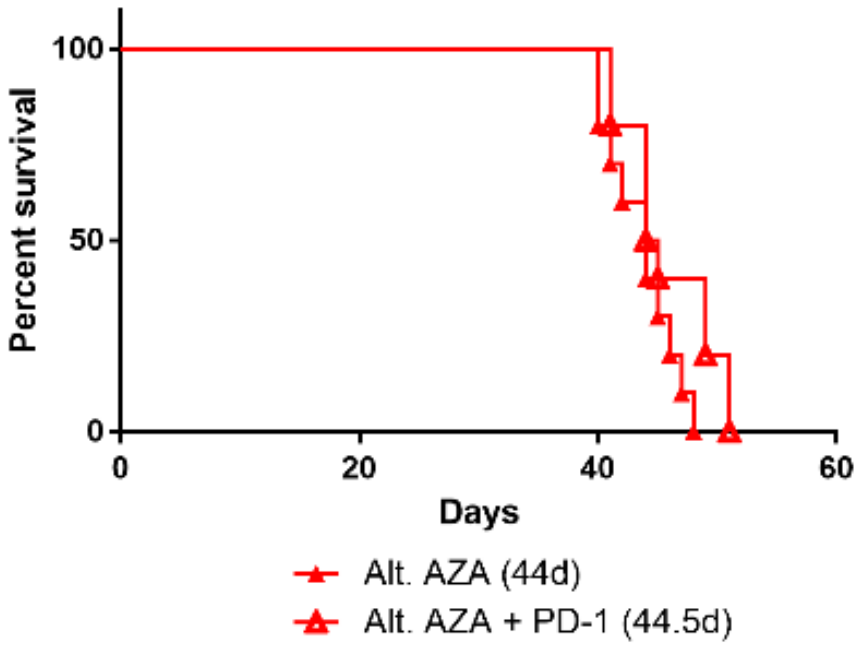

Figure 3.27: Addition of α-PD-1 to AZA provided no survival benefit to mice.

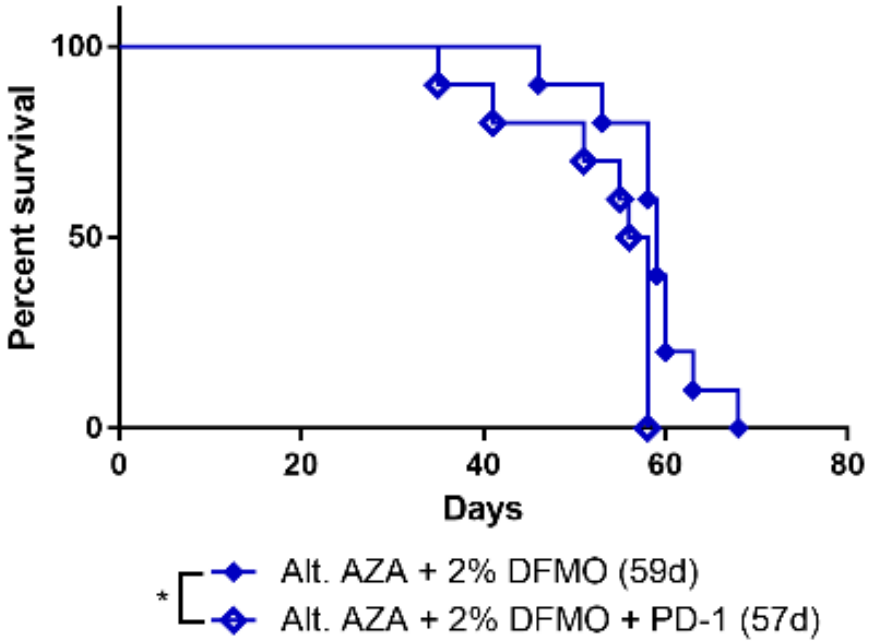

Figure 3.28: Addition of α-PD-1 to combination AZA+DFMO provided no survival benefit to mice, and in fact slightly decreased survival of these mice.

3.4 Discussion

Combination epigenetic and polyamine reducing therapy is an effective treatment strategy for slowing the progression of ovarian cancer in immunocompetent mice, and significantly prolonging survival. This treatment regimen represents the first combination of these two drug therapies in mice, and the first use of DFMO in an immunocompetent mouse model for ovarian cancer (46). While slight impacts to the cell cycle were observed in the form of a G2-M block with AZA+DFMO treatment, more dramatic changes were seen in the overall tumor microenvironment, which comprises the bulk of ascites cells. Treatment with AZA alone led to increased lymphocytes and an increase in IFNγ+ NK cells, CD4+ T cells, and CD8+ T cells, as has been demonstrated before (14,18,19). Signaling of IFNγ via its receptor IFNGR1 on tumor cells can lead to increased expression of PD-L1 on tumor cells, thereby making this increase in IFNγ an attractive candidate for α-PD-1 therapy. However, α-PD-1 therapy had no significant impact on survival in this model when added to the combination AZA and DFMO. These results are in contrast to previous studies using AZA and HDACi where the addition of α-PD-1 produced a significant therapeutic response (18). Histone acetylation is essential for transcription of IFNγ, therefore the use of an HDACi may explain the sensitization to α-PD-1 therapy previously seen, as increasing histone acetylation even further increased IFNγ levels in lymphocytes (47). These data suggest that there may be additional benefit of adding an HDACi to the AZA + DFMO

combination if α-PD-1 is to be used, if such a combination could be used with acceptable levels of toxicity.

While the addition of α-PD-1 modestly decreased survival in Fig 3.28, it is our belief that a difference in median survival of 2 days could likely represent a subtle benefit or could be explained by experimental variability. Other potential explanations for the difference in survival could be engagement of the antibody on PD-1 positive cells, causing inhibitory signaling downstream rendering the cells less effective. Action of this antibody is beneficial to block interactions with PD-L1 positive tumor cells; but perhaps when antibody is given in the AZA+DFMO treated mice, there is not a high enough tumor burden for action of the antibody to be effective, and instead it engages with PD-1 positive T cells only, inhibiting their activity. Furthermore, combination treated AZA+DFMO mice have the lowest number of PD-L1 positive tumor cells in the tumor microenvironment (Fig 3.23), which may explain why addition of α-PD-1 was not beneficial.

Although these increased IFNγ+ pools of lymphocytes did not sensitize the tumor to α-PD-1 therapy, this important cytokine acts not only on tumor cells themselves, but also on surrounding myeloid populations (36). Downstream signaling of IFNγ promotes a myeloid cell to differentiate into an M1 polarized cell, capable of activating T cells via its upregulation of MHC II surface molecules and able to kill tumor cells via nitric oxide dependent mechanisms (36). Investigation of the myeloid and macrophage populations in the tumor microenvironment is thus the next step in determining how the combination AZA+DFMO results in such a significant survival benefit (Fig 3.6) in this ovarian cancer mouse model.

Chapter 2: AZA+DFMO alter TAMs and promote M1 polarization

4.1 Introduction

The DNMTi AZA has been shown to decrease macrophages in the VDID8 model (17,18); however, this work did not distinguish the macrophage phenotype any further. The oncogene MYC is overexpressed in TAMs and its transcriptional targets promote polarization of the pro-tumorigenic M2 macrophage (36). AZA has been shown to decrease expression of MYC in a non-small cell lung cancer model, thus treatment with AZA may reduce M2 polarization (18). Furthermore, DFMO treatment decreases enzyme activity of the essential M2 enzyme arginase, further inhibiting development of this phenotype (26,30). Taken together, combination AZA+DFMO has the potential to not only decrease TAMs in the tumor microenvironment, but perhaps inhibit their polarization toward an M2 macrophage. The observed increases in IFNγ+ lymphocytes may additionally promote M1 polarization. We therefore investigated macrophage populations in the tumor microenvironment of our AZA+DFMO treated mice.

4.2 Methods

Immunocompetent C57BL/6 mice were injected IP with 250,000 VDID8 syngeneic MOSE cells. Mice were treated IP with AZA (0.5 mg/kg) or saline vehicle, DFMO (2% in water), or combination AZA and DFMO beginning three days post tumor injection (Fig 3.1). Hemorrhagic ascites fluid consistently develops

at approximately 4-5 weeks post VDID8 injection and is an accurate measurement of tumor burden in mice, allowing observation of tumor growth in real time (42,43).

When ascites fluid is collected from the mice, the cells obtained represent the tumor microenvironment and can be further analyzed to help illustrate the mixed population of cells surrounding the tumor. Ascites was collected, filtered, incubated in ACK buffer (Quality Biological) to lyse red blood cells, and washed. Cells were blocked with FcR Blocking Reagent (Miltenyi Biotec 130-092-575) and stained for cell-surface markers including Live/Dead (eBioscience 65-0865-14), CD45 (BD Biosciences 563891), F4/80 (BioLegend 123113), CD11b (BioLegend 101222), MHC II (isotype control 400627; BioLegend 107619), CD206 (BioLegend 141708), CD11c (BD Biosciences 564079), and GrB (BioLegend 108407). Flow cytometry acquisition was performed on an LSR II cytometer (BD Biosciences), and data were analyzed using FlowJo software version 10.2.

To assess gene expression of macrophages in the tumor microenvironment, processed ascites cells were suspended in PBS and sorted immediately on a BSL-2 FACSAria II. M1 macrophages were sorted on a gate as follows: CD45+ L/D- F4\80+ CD11b+ MHC II+ CD206- CD11c-. M2 macrophages were sorted on a gate as follows: CD45+ L/D- F4\80+ CD11b+ MHC II- CD206+ CD11c-. Total RNA was isolated from sorted macrophages using TRIzol reagent according to the manufacturer's protocol (Invitrogen, Carlsbad, CA). 200 ng of RNA was used for cDNA synthesis using qScript cDNA SuperMix (Quanta Biosciences, Gaithersburg, MD), followed by SYBR green-mediated real-time PCR (Universal SYBR Green Supermix, BioRad, Hercules, CA) using custom primers specific for

Arg1, Fizz1, and iNOS2. In each experiment, samples were performed in duplicate, normalized to β-actin as an internal control, and fold change in expression relative to M1 or M2 macrophage was determined using the 2-ΔΔCt algorithm. Thermocycling was performed on a Bio-Rad iQ2 real-time PCR detection system and data collected using the iQ5 optical system software.

ELISA assays were performed on serum collected from bulk ascites fluid of individually treated mice via centrifugation at low speed (1000rpm) for 15 minutes. Supernatant was collected and stored at -80C. Circulating CSF-1 levels in mice treated with IgG vs. CSF1R was detected using an ELISA kit (R&D Systems Kit #MMC00) according to instructions.

4.3 Results

4.3.1 AZA+DFMO reduce population of macrophages

Myeloid immune cell populations were next examined to determine whether a decrease in immunosuppression may account for the striking differences in survival. Myeloid derived suppressive cells *(*MDSCs) are suppressive immune cells sometimes present in the tumor microenvironment, high levels of which are associated with a poor prognosis in ovarian cancer (10). No significant decrease in non-lymphocyte or MDSC populations were observed after treatment with AZA and DFMO (Fig 4.1 and 4.2). Instead, total macrophage populations in the tumor microenvironment were consistently decreased with AZA treatment, and decreased even further with the addition of DFMO (Fig 4.3).

Macrophages are professional antigen presenting cells capable of activating T cells. Surface expression of MHC II is essential for interaction with T cells, and the number of MHC II positive cells was increased with AZA, DFMO, and AZA+DFMO treatment compared to vehicle (Fig 4.4 and 4.5). Importantly, MHC II expressing cells were increased significantly with combination treatment compared to single agent AZA, suggesting a possible explanation for the dramatic increase in survival (Fig 4.4). In contrast, untreated mice had high populations of macrophages negative for the MHC II surface protein (Fig 4.5). These data suggest that macrophages may play an important role in tumor response to the combination drug therapy.

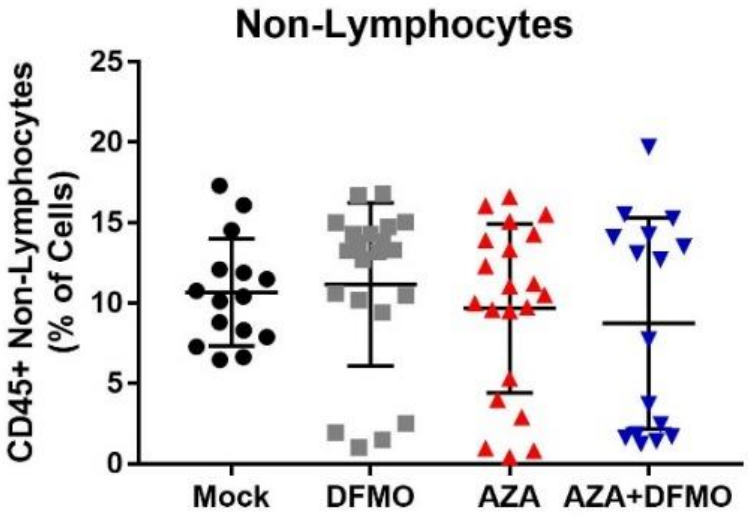

Figure 4.1: Total non-lymphocyte cells in the tumor microenvironment, as a percentage of total cells collected from ascites fluid. No changes with treatment were observed. n = 14-21.

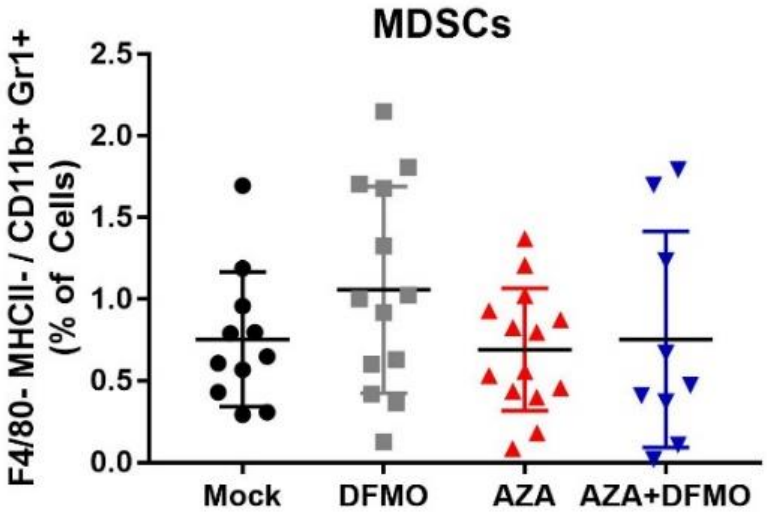

Figure 4.2: Total MDSCs in the tumor microenvironment, as a percentage of total cells. No changes with treatment were observed, and overall populations of MDSCs were low. n = 14-21.

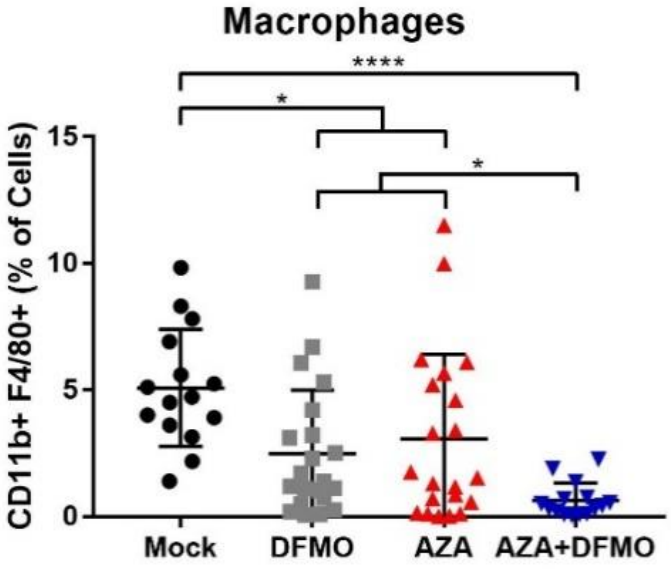

Figure 4.3: Total macrophages in the tumor microenvironment as a percentage of total cells. collected from ascites fluid. Single agent DFMO and single agent AZA both significantly reduce macrophage populations; however combined AZA+DFMO even further decreases macrophages, significantly compared to single agent therapies. n = 14-21.

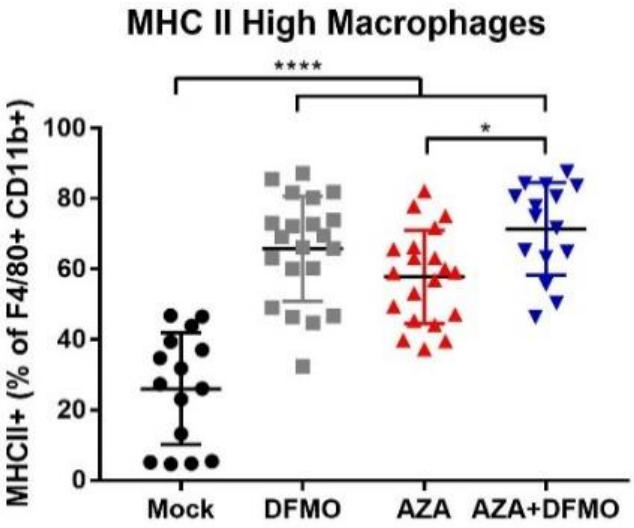

Figure 4.4: Macrophages positive for the surface marker MHC II, and therefore capable of presenting antigen to CD4+ T cells. Data presented as a percentage of F4\80+ CD11b+ macrophages. n = 14-21.

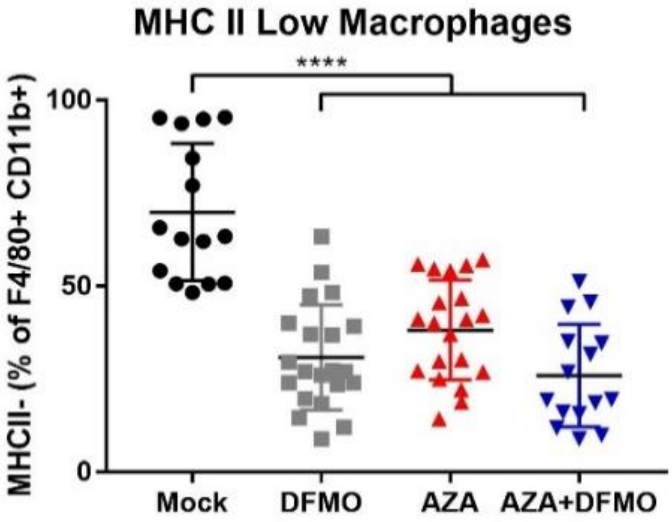

Figure 4.5: Macrophages negative for the surface marker MHC II, and therefore unable to present antigen to CD4+ T cells. Data presented as a percentage of F4\80+ CD11b+ macrophages.

4.3.2 Treatment promotes M1 over M2 polarization

Next, surface markers were examined to distinguish between classical (M1) and alternative (M2) polarized macrophages. High populations of M2 macrophages are associated with a poor prognosis due to their ability to promote tumor growth (9,11,33). Because the surface marker CD206 is upregulated on M2 macrophages, flow cytometry was used to analyze macrophages high for CD206 and low for MHC II—a surface marker for M1 macrophages. Although total macrophages were decreased by the treatments, an increase in M1 macrophages were observed in the remaining macrophage population for all treatment groups (Fig 4.6), as well as a decrease in M2 macrophages (Fig 4.7). MHC II- CD206+ and MHC II+ CD206- macrophages were then sorted via flow cytometry, and RNA was isolated to perform RT-PCR on M1- and M2-specific genes (30,50-52). As expected, CD206+ macrophages demonstrated increased expression of Arg1 and Fizz1 compared to CD206- macrophages (Fig 4.8 and 4.9), and MHC II+ macrophages had increased expression of iNOS2 compared to MHC II- macrophages (Fig 4.10). These data confirm that macrophages expressing high levels of CD206 in our model also retain gene expression patterns that are characteristic of alternatively polarized M2 macrophages.

Interestingly, the decrease in M2 macrophages observed in AZA+DFMO treated mice was not a durable response, and as tumor burden increased in these mice, the relative proportion of M2 macrophages increased as well (Fig 4.11). Macrophages in vehicle treated mice were therefore assessed at three different

time points to determine whether M2 macrophages increase as the disease progresses. Indeed, relative levels of M2 macrophages increased as tumor burden increased in these mice, suggesting the importance of macrophages in disease progression of this ovarian cancer model (Fig. 4.12).

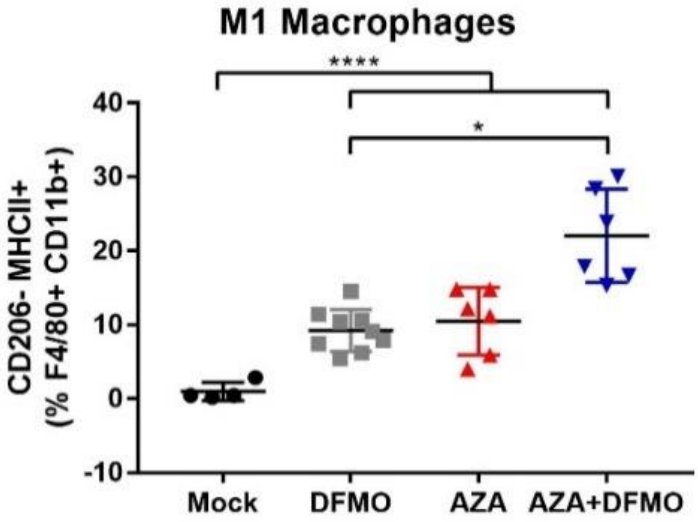

Figure 4.6: M1 macrophages (CD206- MHC II+) in the tumor microenvironment, as a percentage of F4\80+ CD11b+ macrophages. AZA+DFMO treated mice demonstrate significantly increased populations of M1 macrophages, compared to mock and DFMO alone treated mice. n=10.

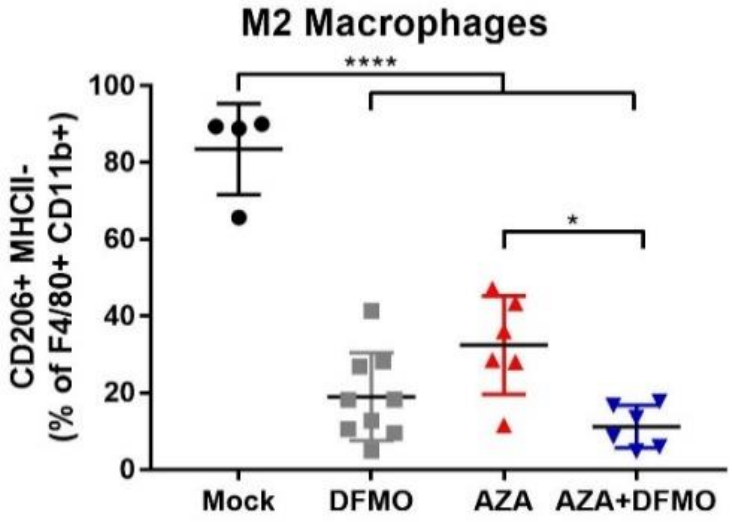

Figure 4.7: M2 macrophages (CD206+ MHC II-) in the tumor microenvironment, as a percentage of F4\80+ CD11b+ macrophages. AZA+DFMO treated mice demonstrate significantly decreased populations of M2 macrophages, compared to mock and AZA alone treated mice. n=10.

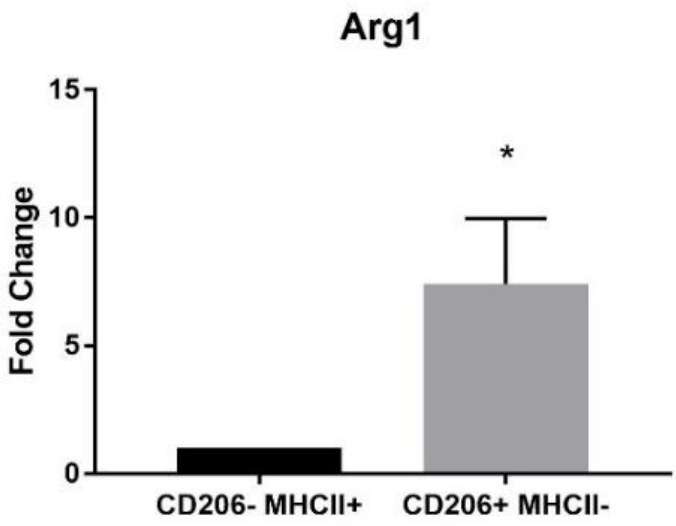

Figure 4.8: qRT-PCR for Arg1 on sorted macrophages. Data confirms that CD206+ MHC II- macrophages exhibited gene expression signatures typical of M2 polarization. n=3.

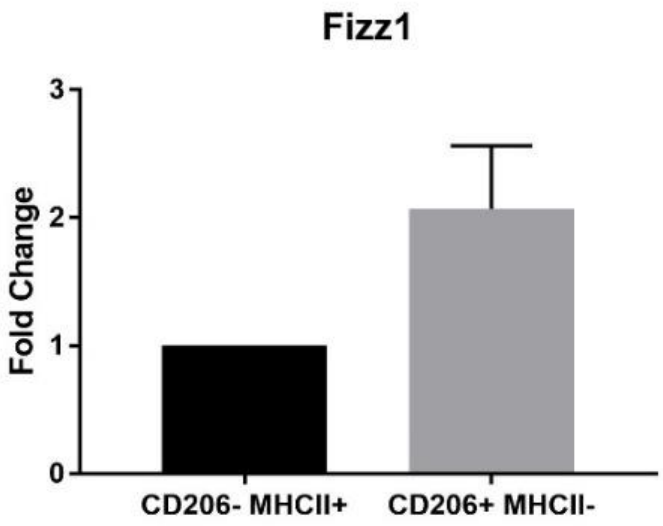

Figure 4.9: qRT-PCR for Fizz1 on sorted macrophages Data confirms that CD206+ MHC II- macrophages exhibited gene expression signatures typical of M2 polarization. n=3.

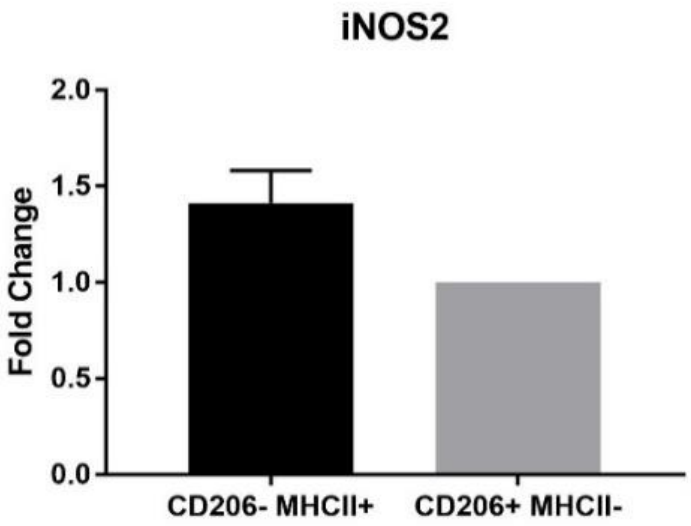

Figure 4.10: qRT-PCR for iNOS2 on sorted macrophages. Data confirms that CD206- MHC II+ macrophages exhibited gene expression signatures typical of M1 polarization. n=3.

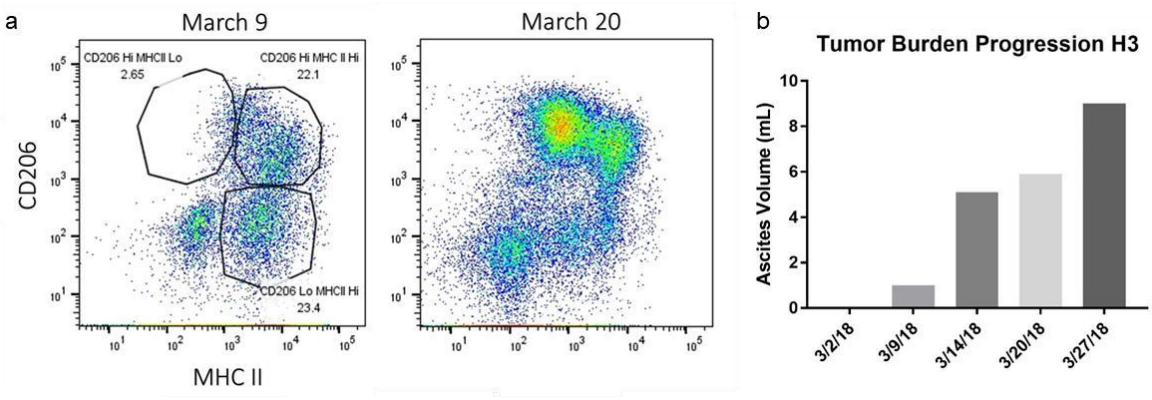

Figure 4.11: a) Representative flow cytometry data shown for one mouse treated with combination AZA+DFMO *in vivo.* At a later time point, there are significantly increased proportions of M2 macrophages high in CD206 and low in MHC II surface expression. b) Paired tumor burden, represented by ascites volume for the same mouse whose cells are shown in 4.11a. The mice's tumor burden is increased at the later time point, coinciding with an increase in M2 macrophages. Please note that this data is shown for only one mouse; thus no statistical analyses were performed.

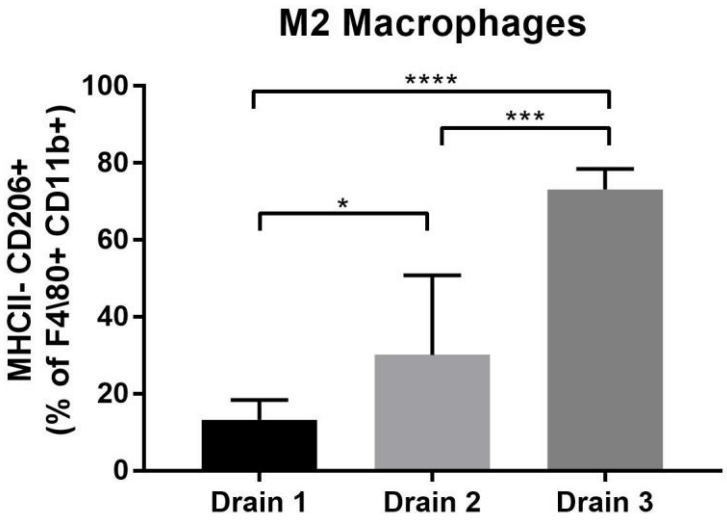

Figure 4.12: Percentage of M2 macrophages (MHCII- CD206+) increase with tumor burden in vehicle treated mice. Drain 1 was performed at week 4 post tumor cell injection; drain 2 at week 5 and drain 3 at week 6.

4.3.3 Macrophage depletion diminishes AZA+DFMO efficacy

To test whether the increase in M1 macrophages was important in the response to AZA and DFMO treatment, macrophages were blocked in the ovarian cancer mouse model using an antibody to CSF1R, an essential growth receptor for macrophages (53) (Fig 4.13). Treatment with α-CSF1R resulted in decreased macrophages in the tumor microenvironment (Fig 4.14) and a consequential increase in M-CSF levels in ascites fluid as measured by ELISA (Fig 4.15). Increased M-CSF indicates that the α-CSF1 receptor block antibody is functional, as more ligand (M-CSF) is free, and less ligand is engaged with its receptor (53).

Initially, the AZA+DFMO combination treatment still resulted in decreased tumor burden in mice, even with the observed decrease in macrophages; however, over time, tumor burden increased more rapidly in AZA+DFMO mice receiving α-CSF1R (Fig 4.16 and 4.17). This depletion in macrophages also led to a decrease in overall survival, compared with AZA+DFMO mice that received IgG control (Fig 4.18).

Analysis via flow cytometry of M1 and M2 surface markers showed that with IgG control, AZA+DFMO mice had increased M1 macrophages and decreased M2 macrophages compared to vehicle, as was previously seen (Fig 4.19 and 4.20; Fig 4.6 and 4.7). Interestingly, while AZA+DFMO mice maintained low M2 macrophages in the presence of α-CSF1R (consistent with the action of α-CSF1R, Fig 4.14), M1 macrophages were significantly decreased compared to AZA+DFMO mice receiving IgG control (Fig 4.19 and 4.20). These results indicate

that the presence of M1 macrophages is important for the mechanism of action of this combination drug therapy, as AZA+DFMO treated mice receiving α-CSF1R had decreased survival and increased tumor burden compared to IgG control.

Also important to note from this data is the fact that simply decreasing macrophages in this model had no benefit to survival (Fig. 4.18), even though M2 macrophages were decreased as a result of α-CSF1R (Fig. 4.21). It appears that the re-programming and re-directing of macrophages to the M1 polarization phenotype is important, not necessarily decreasing M2 macrophages. Lastly, mice treated with AZA+DFMO in the presence of CSF1R showed the previously observed increase in activated, IFNγ+ CD4 T cells, CD8 T cells, and NK cells during both the second and third drain (Fig. 4.22 – 4.27); thus, depletion of macrophages did not impact the lymphocyte response. This data may suggest that the M1 macrophages are not only activating T cells as part of an adaptive response, but may be playing an innate tumoricidal role directly toward the tumor cells.

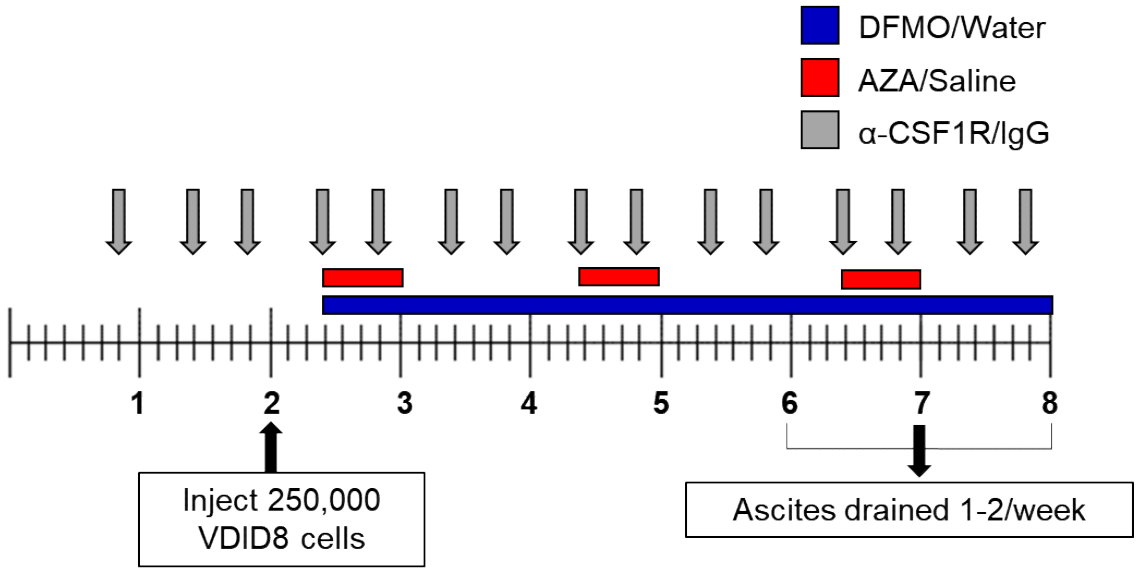

Figure 4.13: Treatment regimen for α-CSF1R block antibody or IgG control antibody. Three, 200ug doses of antibody were administered IP to mice prior to injection of VDID8 tumor cells to deplete macrophages for the duration of tumor development. Twice weekly 200ug doses of antibody were also administered IP for the duration of the experiment to keep macrophage levels low. n=10.

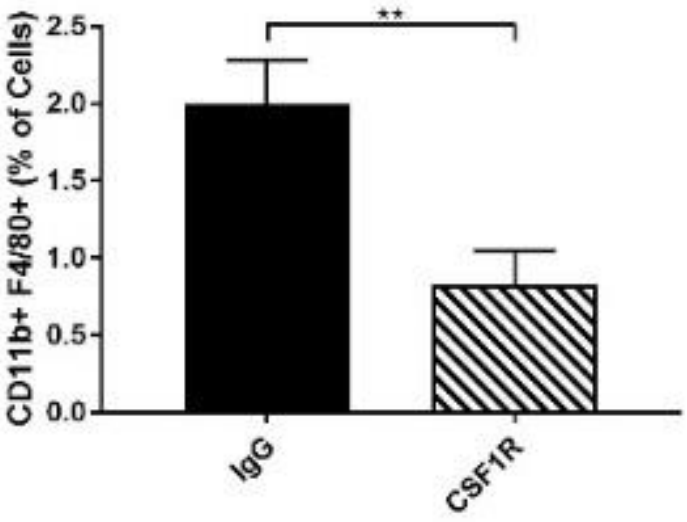

Figure 4.14: Significantly reduced macrophage population, as a percentage of total cells, with α-CSF1R treatment. Decrease observed at week 7 on schematic in Fig 4.11, otherwise known as the first ascites drain.

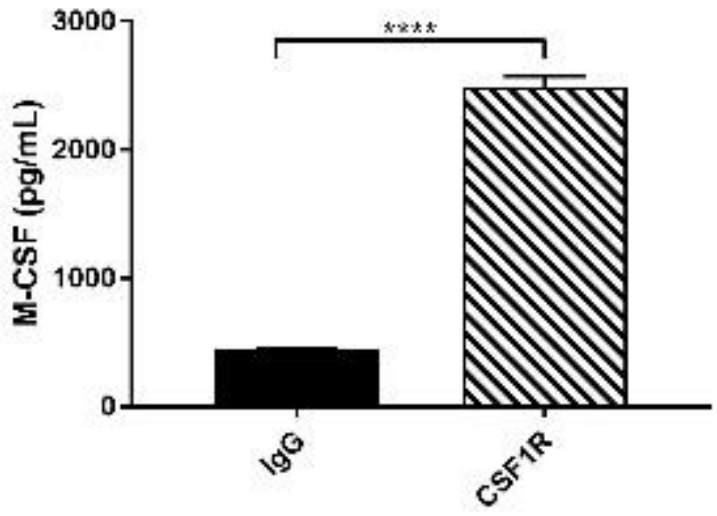

Figure 4.15: Significantly increased circulating M-CSF cytokine levels in bulk ascites fluid as measured via ELISA. n=10.

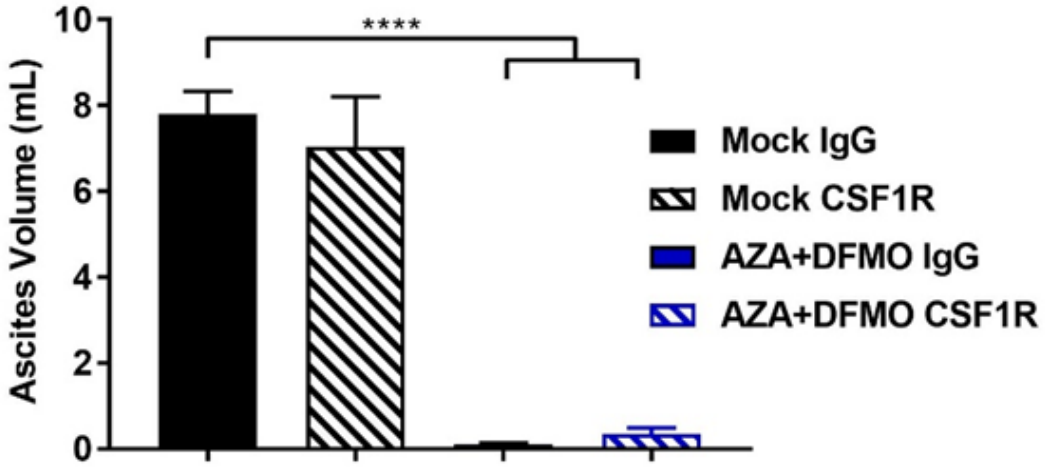

Figure 4.16: Tumor burden represented by ascites volume in mice treated with AZA+DFMO in presence of CSF1R antibody or IgG control during the second drain (week 8 on schematic in Fig 4.11).

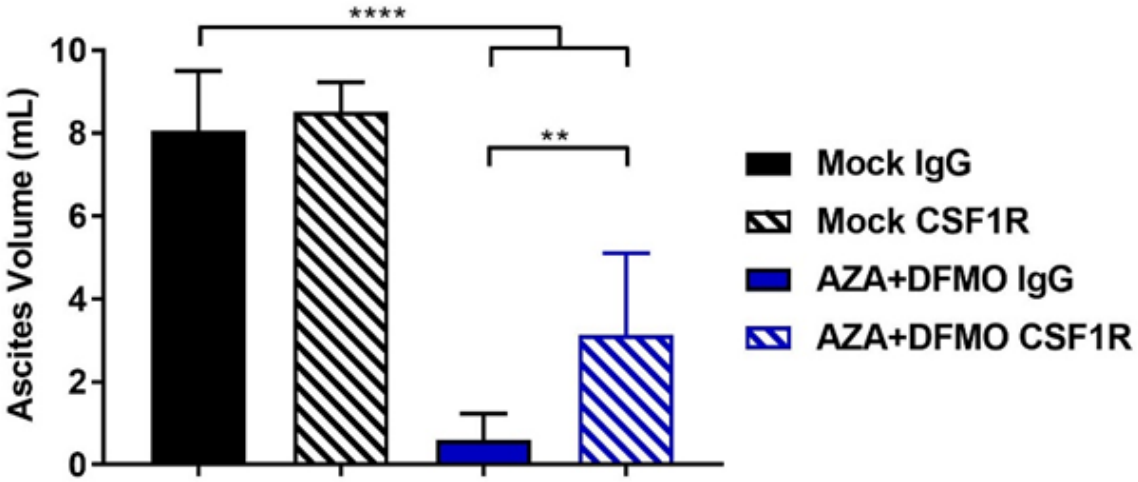

Figure 4.17: Tumor burden during the third drain (week 9 on schematic in Fig 4.11) demonstrating an increase in tumor burden in AZA+DFMO mice receiving CSF1R.

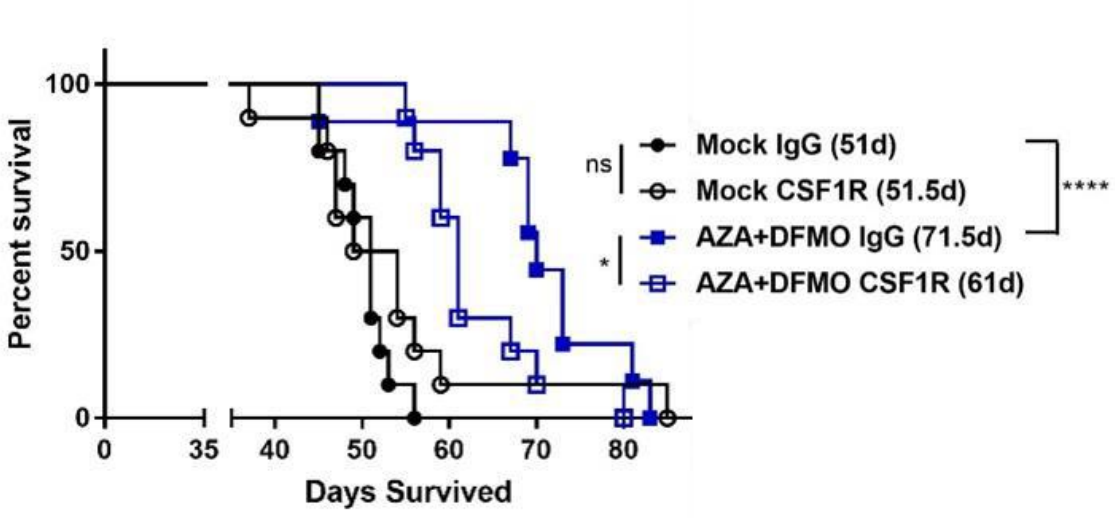

Figure 4.18: Survival curve of AZA + DFMO treated mice receiving CSF1R antibody. Mice with decreased macrophages due to the antibody demonstrated a decrease in survival compared to AZA+DFMO mice receiving IgG.

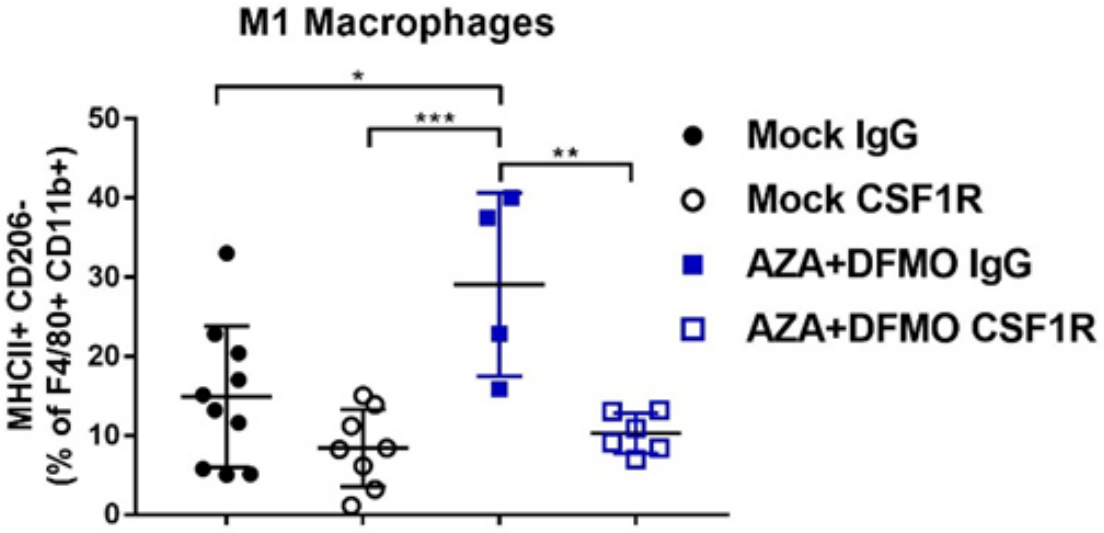

Figure 4.19: M1 macrophages (CD206- MHC II+) analyzed via flow cytometry at the second drain. AZA+DFMO treated mice receiving CSF1R show no increase in M1 macrophages.

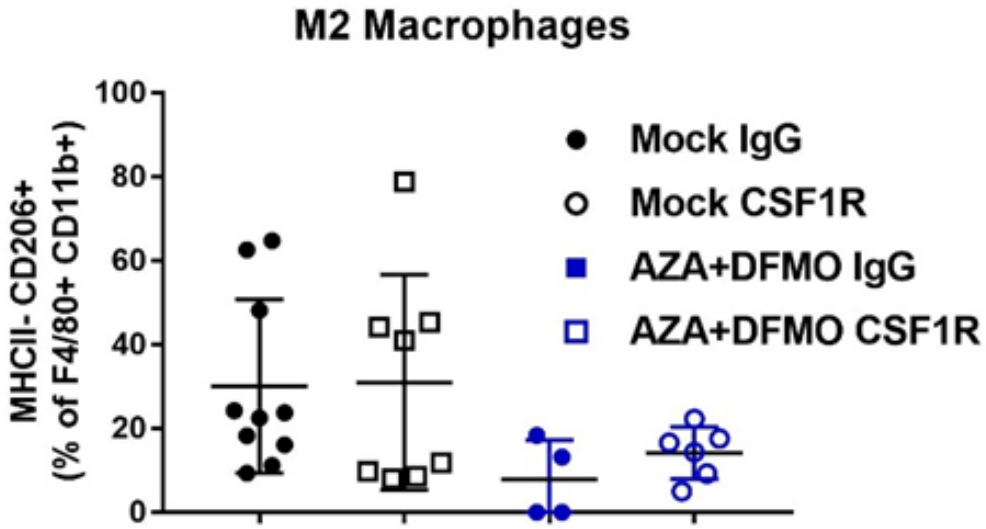

Figure 4.20: M2 macrophages (CD206+ MHC II-) analyzed via flow cytometry at the second drain. M2 macrophages were reduced in both AZA+DFMO treatment arms, compared to mock treated mice.

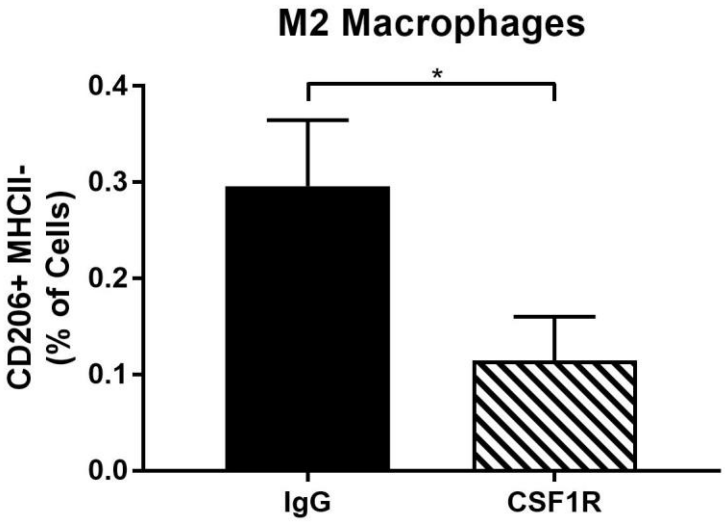

Figure 4.21: M2 macrophages (CD206+ MHC II-) analyzed via flow cytometry at the first drain in mock mice receiving either α-CSF1R or IgG control. M2 macrophages were reduced in mice receiving α-CSF1R, compared to IgG control.

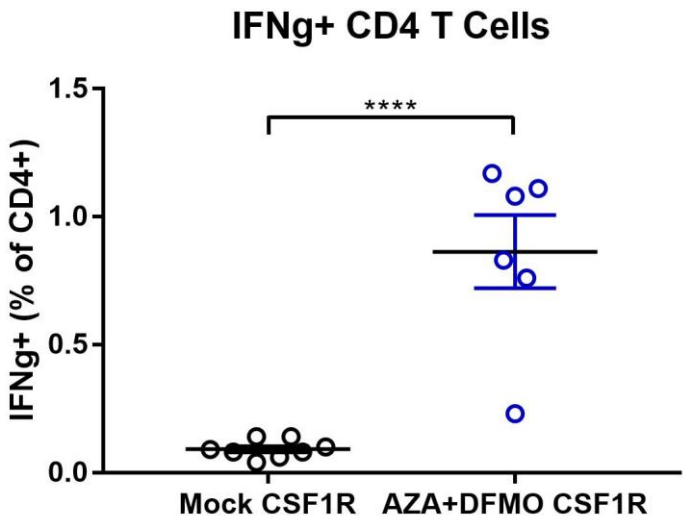

Figure 4.22: Number of IFNγ+ CD4+ T cells, shown as a percentage of CD4+ T cells during the second drain. IFNγ can be considered a marker of T cell activation, and combination AZA+DFMO leads to increased activated CD4+ T cells even in the presence of α-CSF1R block.

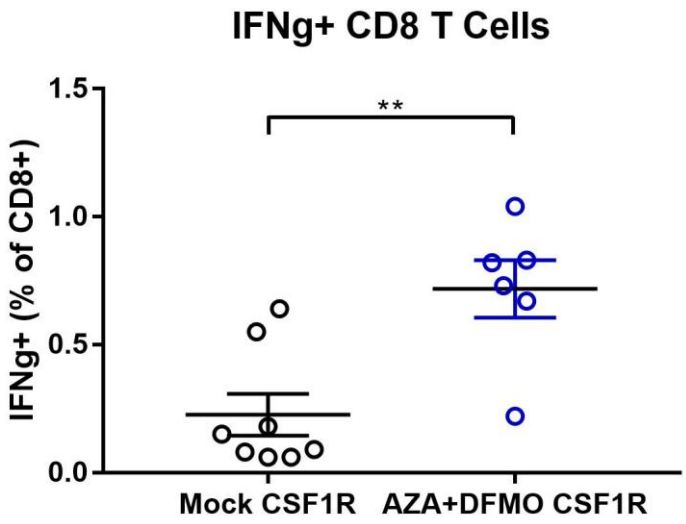

Figure 4.23: Number of IFNγ+ CD8+ T cells, shown as a percentage of CD8+ T cells during the second drain. IFNγ can be considered a marker of T cell activation, and combination AZA+DFMO leads to increased activated CD8+ T cells even in the presence of α-CSF1R block.

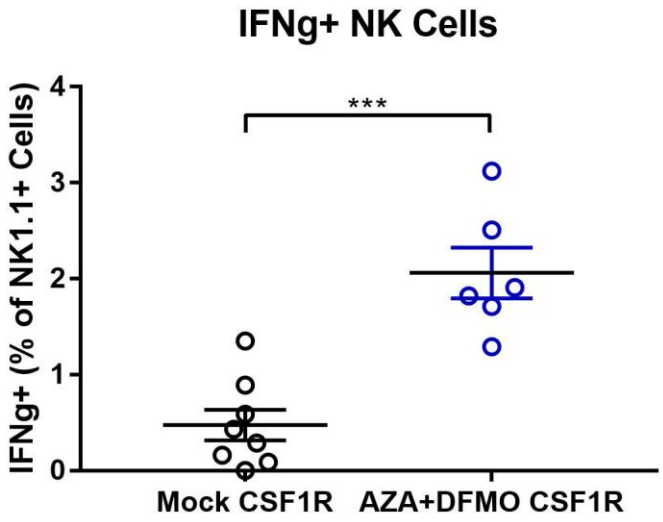

Figure 4.24: Number of IFNγ+ NK cells, shown as a percentage of NK cells during the second drain. IFNγ can be considered a marker of NK cell activation, and combination AZA+DFMO leads to increased activated NK cells even in the presence of α-CSF1R block.

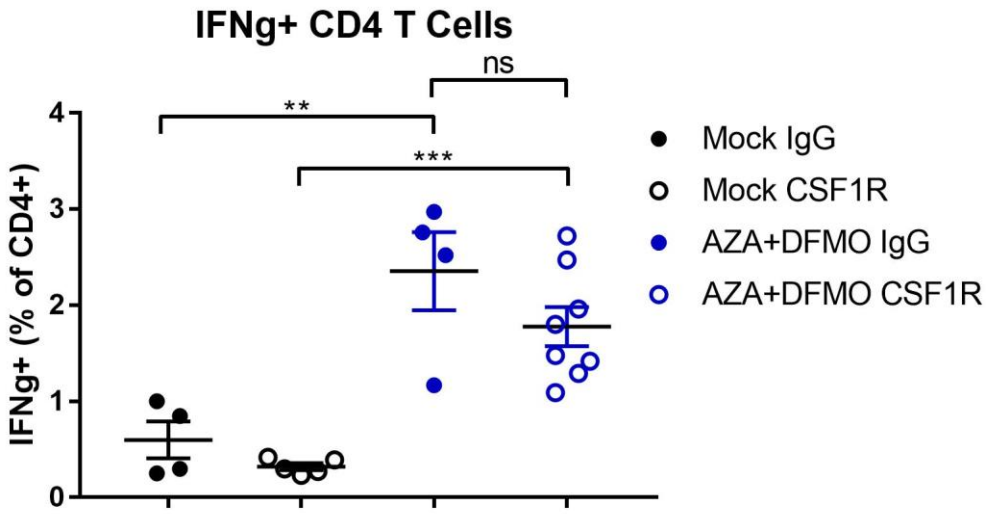

Figure 4.25: Number of IFNγ+ CD4+ T cells, shown as a percentage of CD4+ T cells during the third drain. IFNγ can be considered a marker of T cell activation, and combination AZA+DFMO leads to increased activated CD4+ T cells even in the presence of α-CSF1R block.

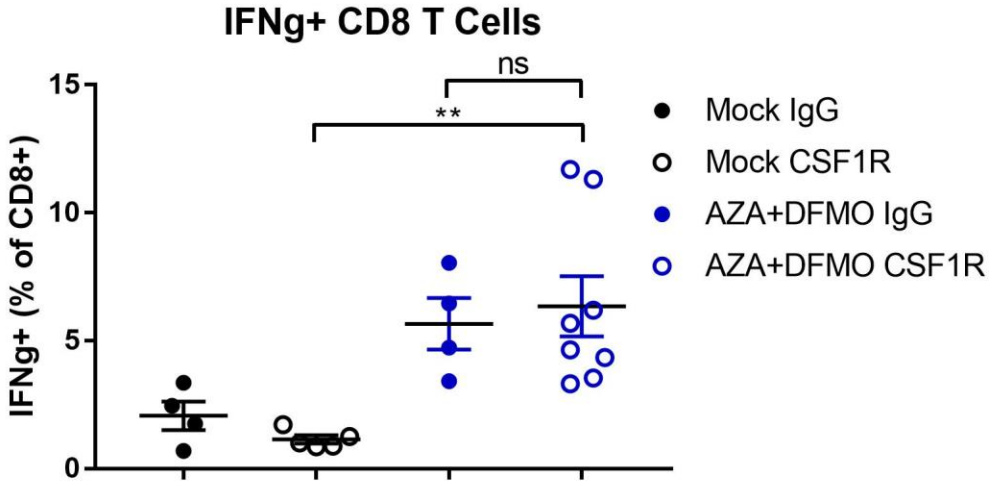

Figure 4.26: Number of IFNγ+ CD8+ T cells, shown as a percentage of CD8+ T cells during the second drain. IFNγ can be considered a marker of T cell activation, and combination AZA+DFMO leads to increased activated CD8+ T cells even in the presence of α-CSF1R block.

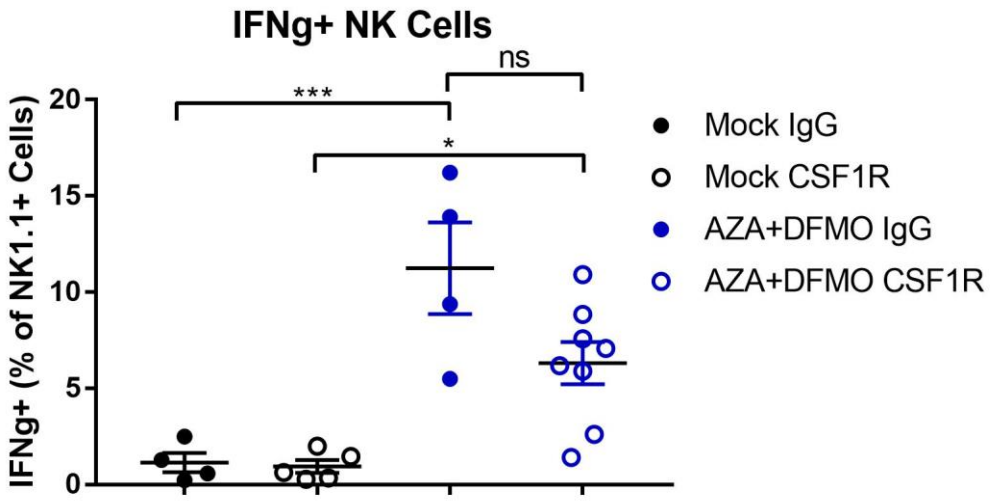

Figure 4.27: Number of IFNγ+ NK cells, shown as a percentage of NK cells during the second drain. IFNγ can be considered a marker of T cell activation, and combination AZA+DFMO leads to increased activated NK cells even in the presence of α-CSF1R block.

4.4 Discussion

Analysis of the tumor microenvironment after the combination treatment with AZA and DFMO indicates that changes to macrophage polarization are critically important in this model. AZA treatment has been shown to decrease macrophages in the tumor microenvironment, though no distinction was made in these studies as to the polarization status of these macrophages (17,18). As the understanding of macrophages deepens, research has discovered that these cells once thought of as permanent, differentiated cells, are in fact quite plastic and able to respond to multiple signals including cytokines and chemokines that direct their behavior and alter their phenotype. Classically polarized M1 macrophages, induced by cytokines such as IFNγ and IL-12, upregulate expression of MHC II and can have tumoricidal functions. M1 macrophages metabolize arginine via iNOS to nitric oxide (NO), creating an oxidizing environment that is damaging to surrounding cells. DFMO treatment has been found to potentiate NO production in LPS-stimulated macrophages *in vitro* (40). Additionally, DFMO, via product inhibition through the increase in ODC substrate, ornithine, inhibits the enzyme arginase I, which is essential for function of alternatively polarized M2 macrophages. Inhibition of arginase I could lead to increased amounts of its substrate arginine, potentially providing more of the metabolite for use by M1 macrophages and iNOS. We hypothesize that treatment with DFMO may therefore increase M1 macrophages by making more of its essential metabolite arginine available, while AZA may help

increase M1 macrophages via its interferon response and production of IFNγ, a cytokine which drives M1 polarization.

Depletion of macrophages in the tumor microenvironment using a CSF1R antibody significantly diminished the efficacy of combination AZA and DFMO, and decreased the levels of M1 macrophages while maintaining levels of IFNγ+ lymphocytes. Tumor burden recurred more rapidly and survival was diminished in mice with fewer macrophages, suggesting that these M1 macrophages could have a tumoricidal role in ovarian tumors. This work represents the first combination of these two distinct treatment strategies in any cancer. The impact of AZA and DFMO on macrophages in the tumor microenvironment may not be specific to ovarian cancer, and could therefore possibly translate to other macrophage-rich tumors such as breast and pancreatic cancers. Furthermore, the use of two well-tolerated and clinically approved drugs offers potential to test a third drug in combination to further prolong survival. Exploration of additional drugs that potentiate M1 macrophages is important, as these tumoricidal cells have potential to decrease tumor burden and help activate the immune system against cancer.

Chapter 3: AZA+DFMO in solid tumor models

5.1 Introduction

While the results seen in the VEGF-β-Defensin ID8 model for high grade serous ovarian cancer are encouraging, it is important to determine whether this drug combination could be applicable in other forms of solid tumor, and perhaps other tumors rich in macrophages. The p53-/- ID8 ovarian tumor cell line developed by the McNeish lab forms both hemorrhagic ascites and small solid tumors along the ovaries and bladder (44). Importantly, the hemorrhagic ascites that develops in this model is not correlated with survival; thus, as the model currently exists, ultrasound is the only imaging technique available to monitor tumor burden in these mice (44). Another limitation of the VDID8 model is that it doesn't accurately model the most common mutations seen in high grade serous ovarian cancer (HGSOC), including but not limited to Trp53, Brca1, Brca2, Nf1, and Rb1 (44). In fact, the McNeish lab found that the parental ID8 cell line developed by Dr. Roby in 2000 was wildtype for all of these common HGSOC mutations (44). Therefore studying the combination AZA+DFMO in a model with mutations common to HGSOC is essential in determining how the drugs may work in patients.

In addition to testing AZA+DFMO in a p53-/- HGSOC mouse model, we decided to test the drug combination in a breast cancer model that is also p53 null. The 2208L model developed by the Medina and Rosen labs at Baylor college of Medicine is as mentioned above, also a p53-/- tumor model (45). The 2208L is an aggressive, infiltrating ductal carcinoma-like mouse tumor that is rich in MDSCs. .

Also unique to this model is that the breast cancer cells have not been cultured on plastic and have only been passaged in mice, making them a better, less altered, model for *in vivo* tumor conditions (45).

5.2 Methods

Immunocompetent C57BL/6 mice were injected IP with 5,000,000 p53-/- ID8 syngeneic MOSE cells. Mice were treated IP with AZA (0.5 mg/kg) or saline vehicle, DFMO (2% in water), or combination AZA and DFMO beginning three days post tumor injection (Fig 5.1). Hemorrhagic ascites fluid consistently develops at approximately 7-8 weeks post p53-/- ID8 injection (44).

Cellular ascites collected from these mice, was further analyzed to characterize the mixed population of cells surrounding the disseminated tumor cells. Solid tumors were not harvested or analyzed. Ascites was collected, filtered, incubated in ACK buffer (Quality Biological) to lyse red blood cells, and washed. Cells were blocked with FcR Blocking Reagent (Miltenyi Biotec 130-092-575) and stained for cell-surface markers including Live/Dead (eBioscience 65-0865-14), CD45 (BD Biosciences 563891), F4/80 (BioLegend 123113), CD11b (BioLegend 101222), MHC II (isotype control 400627; BioLegend 107619), CD206 (BioLegend 141708), CD11c (BD Biosciences 564079), Ly6C (BD Biosciences 562728), and Ly6G (BD Biosciences 563005). Flow cytometry acquisition was performed on an LSR II cytometer (BD Biosciences), and data were analyzed using FlowJo software version 10.2.

For the 2208L breast cancer model, tumor tissue (2mm) is inserted into the mammary fat pad of 6-8 week old immunocompetent BALB/c wildtype mice. Breast tumor measurements are obtained once weekly and tumors were harvested at pre-determined time points. Mice were treated IP with AZA (0.5 mg/kg) or saline vehicle, DFMO (2% in water), or combination AZA and DFMO beginning three days post tumor implant.

5.3 Results

5.3.1 AZA+DFMO in p53-/- ovarian cancer model

Mice treated with single agent AZA have a slight benefit in survival (median survival 67.5 days) compared to untreated mice who have a median survival of 60 days in this p53-/- ID8 model (Fig. 5.2). Interestingly, there is a significant difference between treatment with single agent DFMO in this model versus single agent AZA, as DFMO alone dramatically increases survival in these mice to a median of 85.5 days. It remains true however that mice treated with combination therapy exhibit the largest increase in overall survival with a median survival of 91 days (Fig. 5.2).

Myeloid immune cell populations were next examined to determine whether combination AZA+DFMO had similar actions on immunosuppressive cells in this p53-/- HGSOC model. MDSCs are suppressive immune cells often present in the tumor microenvironment, high levels of which are associated with a poor prognosis in ovarian cancer, other solid tumors and metastatic disease (10). No significant decrease in non-lymphocyte or MDSC populations (both monocyte derived and

granulocyte derived) was observed after treatment with AZA and DFMO (Fig 5.3 – 5.5). Interestingly, total macrophage populations were also not affected by treatment and it appears that single agent AZA treatment may trend toward increased macrophages at this time point in the hemorrhagic ascites fluid (Fig 5.6). It is possible that the immune cell populations in the hemorrhagic ascites fluid may not mimic the tumor microenvironment of the solid tumor in this model. Future experiments should include immunohistochemistry of the solid tumors isolated from mice to determine what immune cells are physically infiltrating the tumor.

Assessment of only total macrophage populations in the tumor microenvironment is not sufficient to gain an accurate view of the distribution and behavior of macrophage in and around solid tumors. Although AZA treatment appears to increase total macrophages in the hemorrhagic ascites fluid, perhaps this is due to recruitment of M1 anti-tumorigenic macrophages, rather than an increase in M2 immunosuppressive macrophages (36). Therefore we next examined within these total macrophage populations, whether they were more representative of an M1 macrophage (CD206- MHC II+) or an M2 macrophage (CD206+ MHC II-). Mice treated with single agent DFMO demonstrated an increase in the population of M1 macrophages in the hemorrhagic ascites, paired with a dramatic decrease in M2 macrophages (Fig 5.7, 5.8). Treatment with single agent AZA and combination AZA+DFMO however, led to no significant changes in either M1 or M2 macrophages (Fig 5.7, 5.8).

Another important myeloid cell capable of activating T cells and increasing an immune response are dendritic cells, which we also looked at in the tumor

microenvironment of these p53-/- mice. No significant changes were observed in dendritic cell populations, although single agent AZA did trend toward an increase (Fig 5.9). These data are intriguing because in regards to survival, the AZA+DFMO treated mice did have the longest overall median survival, yet they do not appear to have the changes in macrophage polarization observed in the VDID8 model (Chapter 2). Again, immune cells surrounding and infiltrating the solid tumors in this p53-/- ID8 model may be more important, and should be investigated in future experiments.

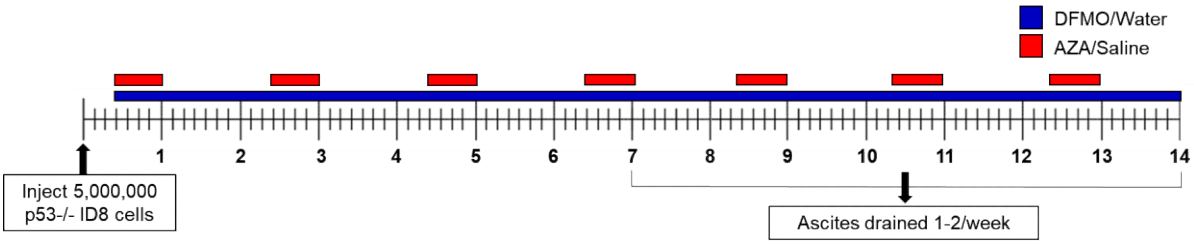

Figure 5.1: Tumor cell injection and treatment schematic. Mice were injected IP with 5,000,000 p53-/- ID8 cells and treated with 0.5 mg/kg of AZA/saline IP 5 days a week, every other week. 2% DFMO was provided in water bottles. Mice were treated throughout the duration of the experiment. Upon 25-30% weight gain, ascites fluid was drained from mice and processed for analysis of the tumor microenvironment. n=10.

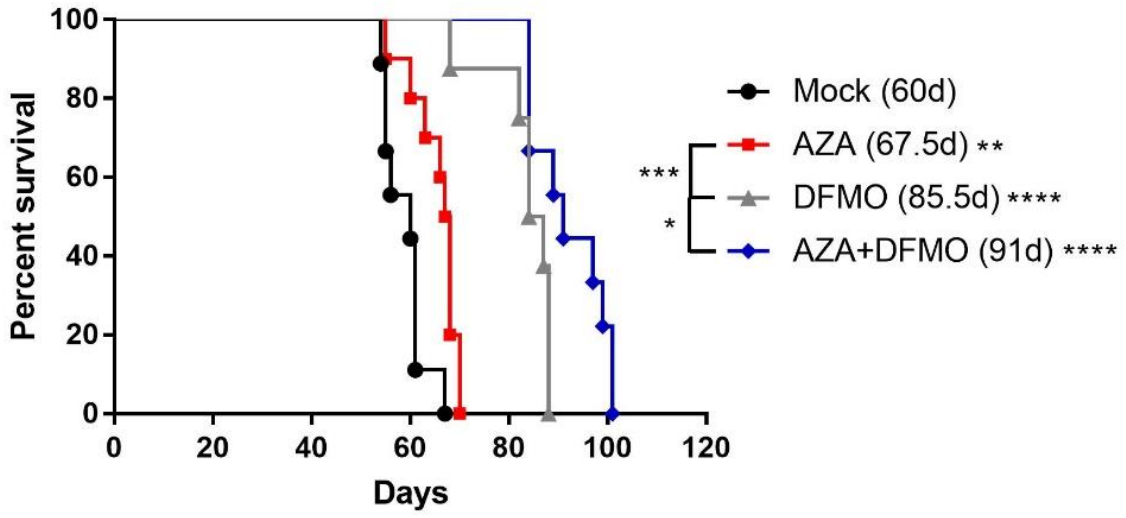

Figure 5.2: Survival curve (median survival in days); n = 10 mice per group. Significance determined using log-rank Mantel-Cox test.

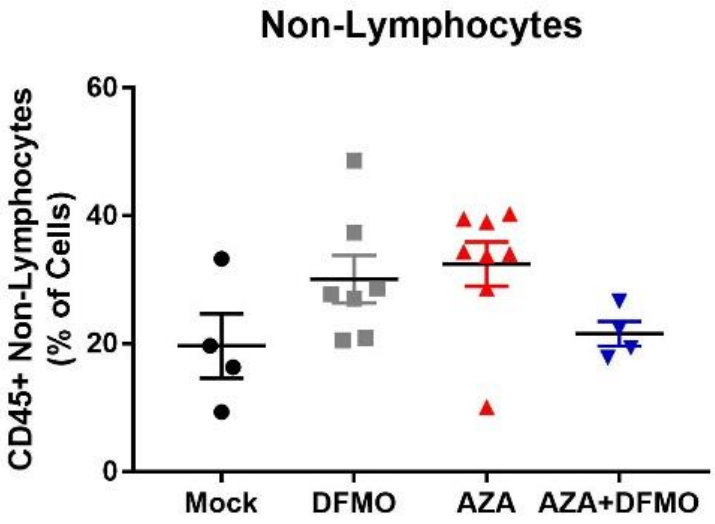

Figure 5.3: Total non-lymphocyte cells in the tumor microenvironment, as a percentage of total cells collected from ascites fluid. No changes with treatment were observed. n =10.

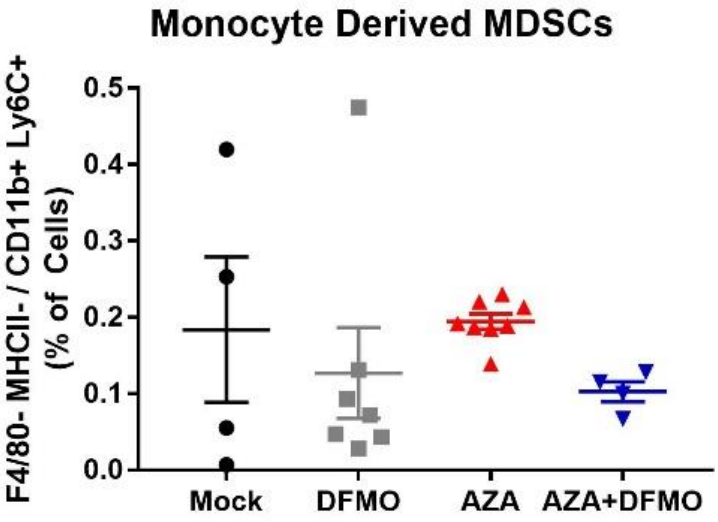

Figure 5.4: Total monocyte derived MDSCs in the tumor microenvironment, as a percentage of total cells. No changes with treatment were observed, and overall populations of MDSCs were low. n=10.

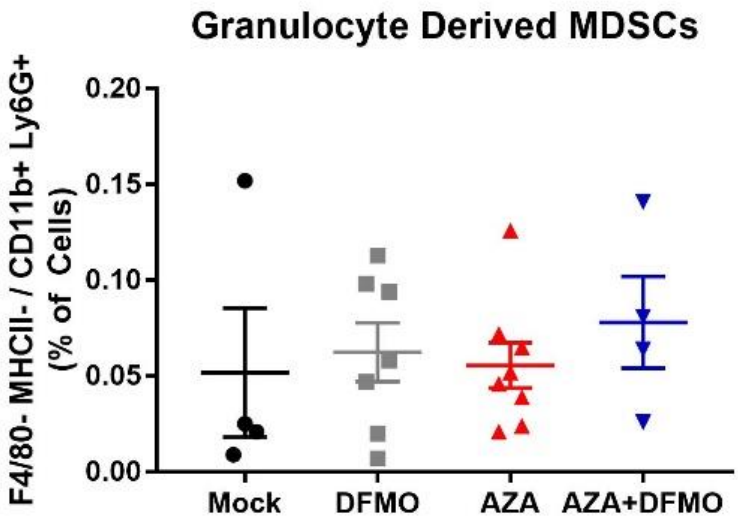

Figure 5.5: Total granulocyte derived MDSCs in the tumor microenvironment, as a percentage of total cells. No changes with treatment were observed, and overall populations of MDSCs were low. n=10.

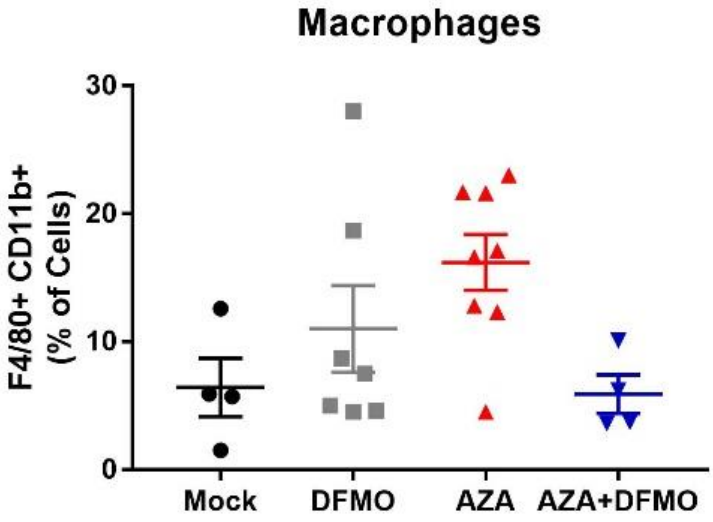

Figure 5.6: Total macrophages in the tumor microenvironment, as a percentage of total cells. No significant changes were observed with treatment, although it appears that single agent AZA treatment trends toward increased macrophages in the hemorrhagic ascites fluid. n=10.

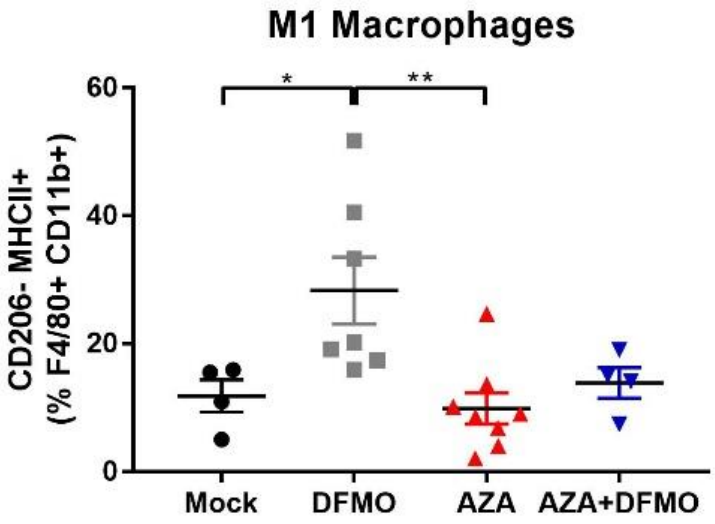

Figure 5.7: M1 macrophages (CD206- MHC II+) in the tumor microenvironment, as a percentage of F4\80+ CD11b+ macrophages. n=10.

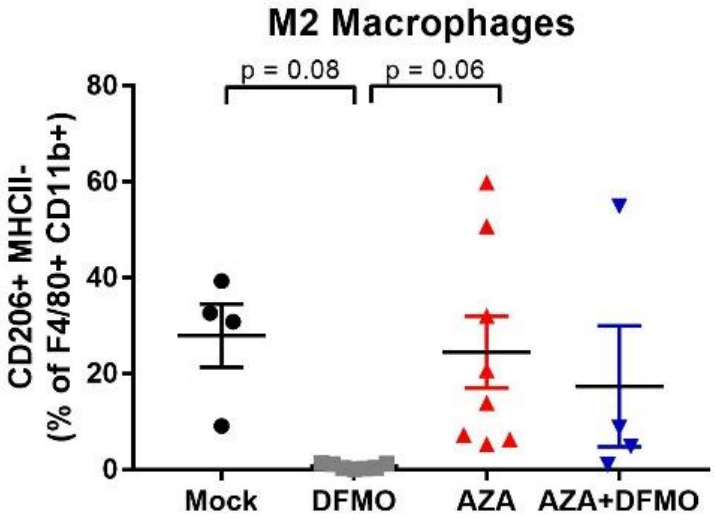

Figure 5.8: M2 macrophages (CD206+ MHC II-) in the tumor microenvironment, as a percentage of F4\80+ CD11b+ macrophages. n=10.

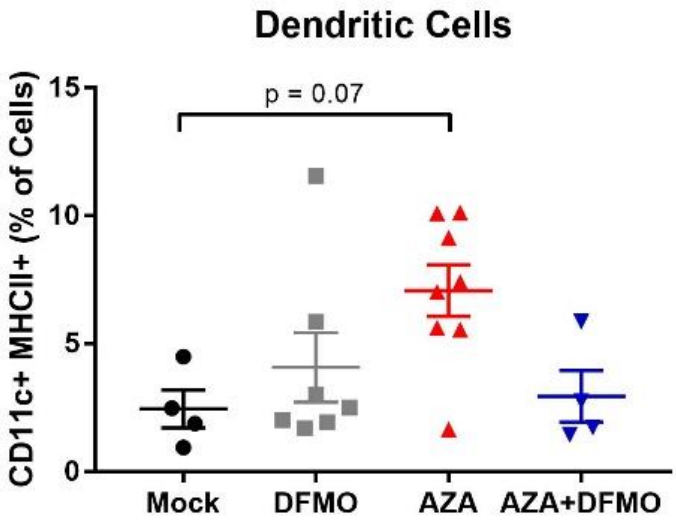

Figure 5.9: Total dendritic cells in the tumor microenvironment, shown as a percentage of total cells. Single agent AZA treatment trends toward an increase in this cell population which is indicative of an anti-viral interferon response (14,17,18). n=10.

5.3.2 DFMO alone reduces tumor burden in 2208L breast model

Combination AZA+DFMO treated mice in the 2208L breast tumor model had increased survival and decreased tumor burden as measured in weeks 3 through 6 post tumor implant surgery (Fig 5.10 – 5.14). Interestingly, this benefit in survival and tumor burden appears to again be driven by DFMO. Single agent AZA treatment had no impact on tumor size in these mice, and no benefit in survival (Fig 5.10 – 5.14).

Myeloid immune cell populations were next examined to determine whether combination AZA+DFMO had similar actions on immunosuppressive cells in this 2208L breast cancer model. No significant changes to total MDSC or macrophage populations were observed with treatment (n=3 mice per group), except perhaps a trend toward an increase in total macrophages with DFMO treatment (Fig 5.15 and 5.16).

It is essential to investigate macrophage populations further because depending on the suite of genes expressed, a macrophage in the tumor microenvironment could be either pro- or anti-tumorigenic. In this experiment, we were unable to consider the surface protein CD206 which is upregulated on M2 polarization macrophages, and instead examined M1 surface markers including MHC II and CD86. The surface molecule CD86 is upregulated on activated macrophages and dendritic cells, and is known as a co-stimulatory molecule that interacts with CD28 on T cells, aiding in their activation and proliferation (36). Therefore macrophages positive for both MHC II and CD86 would be considered M1 macrophages, capable of T cell activation (36). Combination AZA+DFMO

resulted in a trending increase in M1 macrophages, however changes were not significant possibly due to low sample number (Fig 5.17).

Another myeloid derived cell capable of T cell activation, and in fact the most adept cell type at T cell activation, is the dendritic cell (54). Dendritic cells are phagocytic cells that regularly uptake exogenous antigen from their surrounding environment and in the presence of an infection, will help tailor the immune response by secreting certain cytokines (54). They will additionally upregulate surface expression of MHC II and the co-stimulatory molecules CD80 and CD86 to enable them to present antigen to nearby T cells, thereby activating them (54). The established anti-viral, interferon response induced by AZA treatment should in fact increase activation of dendritic cells, therefore exploring their role in the tumor microenvironment could be important (14,17,18). Firstly, we assessed dendritic cell populations overall in these breast tumors, both as a percentage of CD45+ immune cells and as a percentage of total cells and found that combination AZA+DFMO may increase dendritic cell populations overall in the tumor microenvironment (Fig 5.18 and 5.19). Low sample numbers did not provide enough power for statistical significance; however the data overall are intriguing.

Although AZA did not impact total dendritic cell numbers, it may potentially impact the activation of dendritic cells, which can be assessed through surface expression of the co-stimulatory signaling proteins CD80 and CD86 (54). In fact, even with low sample numbers, we were able to demonstrate a significant increase in activated and mature dendritic cells with AZA treatment, which is in line with the interferon response launched by this drug treatment (Fig 5.20) (14,17,18).

Importantly however, AZA treatment did not prove beneficial to these mice in terms of tumor size or burden, or overall survival (Fig 5.10 – 5.14). It would appear that activating an immune response against this tumor via AZA treatment does not have a sufficient anti-tumorigenic impact, perhaps due to the high populations of myeloid derived suppressor cells and other immunosuppressive cells in the tumor microenvironment. DFMO treatment, which is known to impact these cell populations, has a greater impact on survival and tumor burden in these mice (24,26).

In order for activated dendritic cells to activate T cell populations, they require a favorable microenvironment without high populations of immunosuppressive cells; however even in the combination AZA+DFMO, the addition of AZA did not provide further benefit. There could be other mechanisms at play preventing dendritic cells from activating T cells, or preventing T cells from infiltrating the tumor site. Immunohistochemistry experiments in the future could provide more insights into what cell populations are able to infiltrate the tumor site.

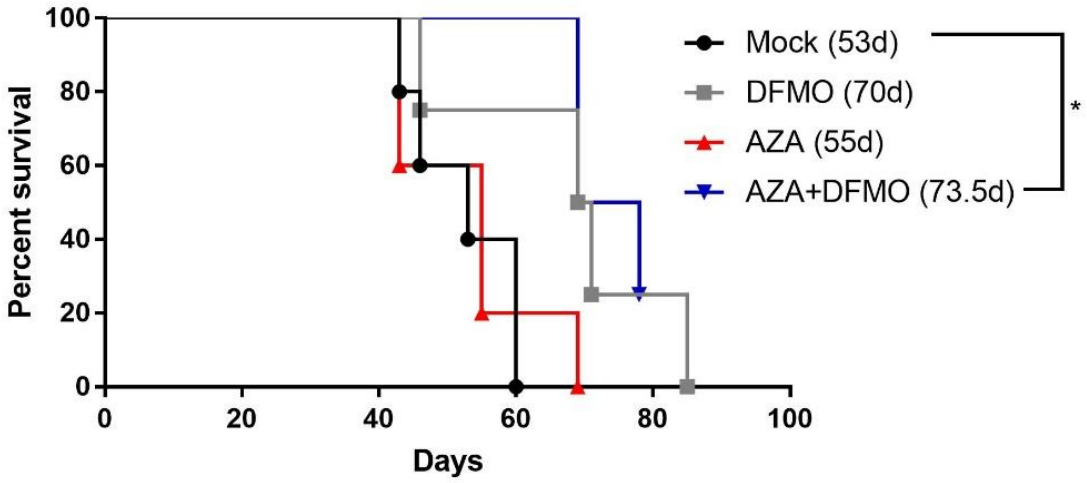

Figure 5.10: Survival curve (median survival in days); n = 4. Significance determined using log-rank Mantel-Cox test.

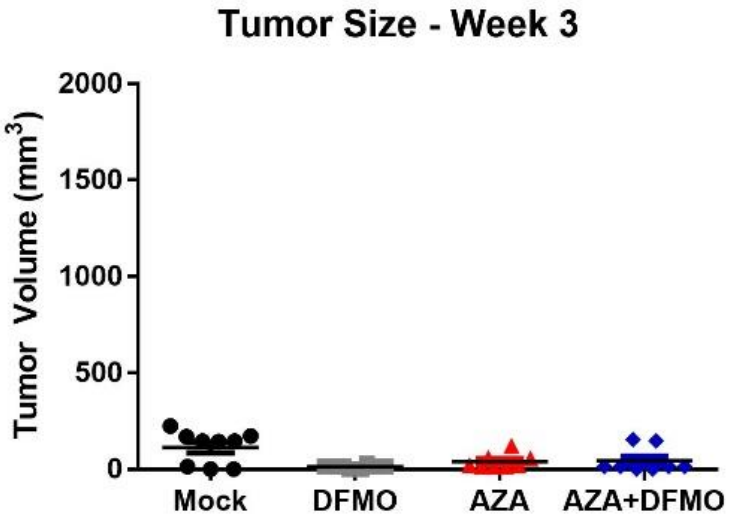

Figure 5.11: Tumor size as measured once weekly in 2208L mice (week 3 post tumor implant). Very little tumor growth is observed at this time point. n=10.

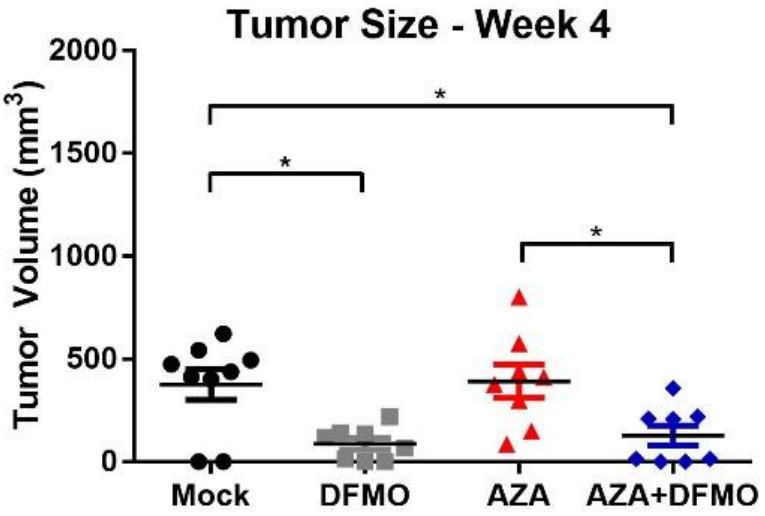

Figure 5.12: Tumor size as measured once weekly in 2208L mice (week 4 post tumor implant). Both untreated and AZA treated mice begin to have increased tumor volume. n=10.

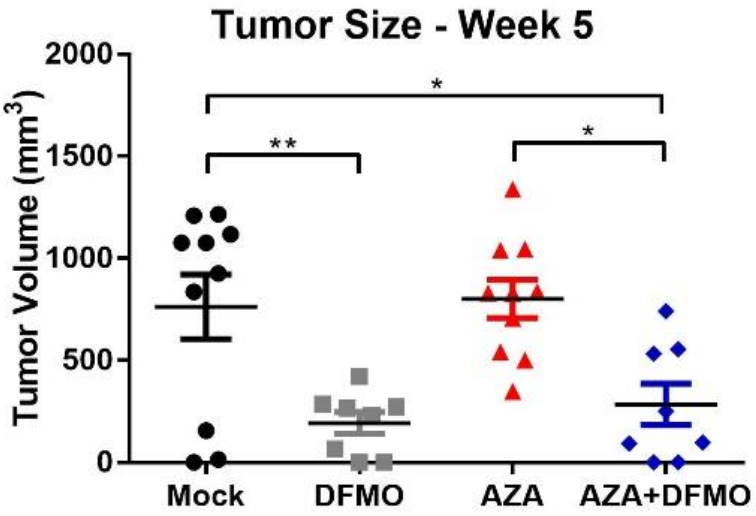

Figure 5.13: Tumor size as measured once weekly in 2208L mice (week 5 post tumor implant). Treatment with DFMO as both a single agent and in combination with AZA maintains low tumor volumes. n=10.

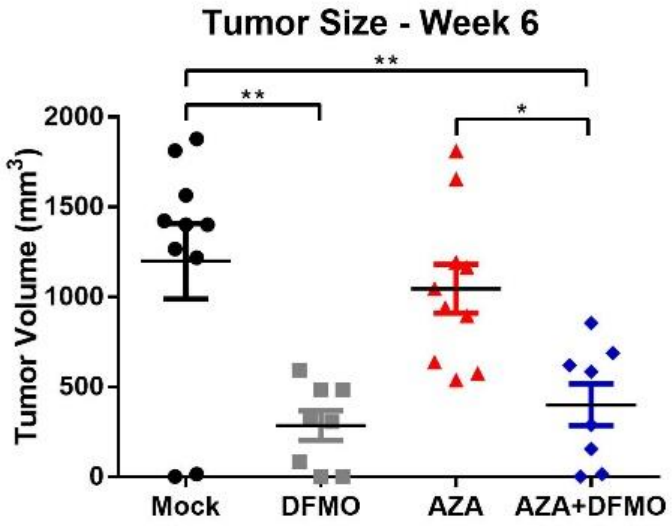

Figure 5.14: Tumor size as measured once weekly in 2208L mice (week 6 post tumor implant). Treatment with DFMO as both a single agent and in combination with AZA maintains low tumor volumes. n=10.

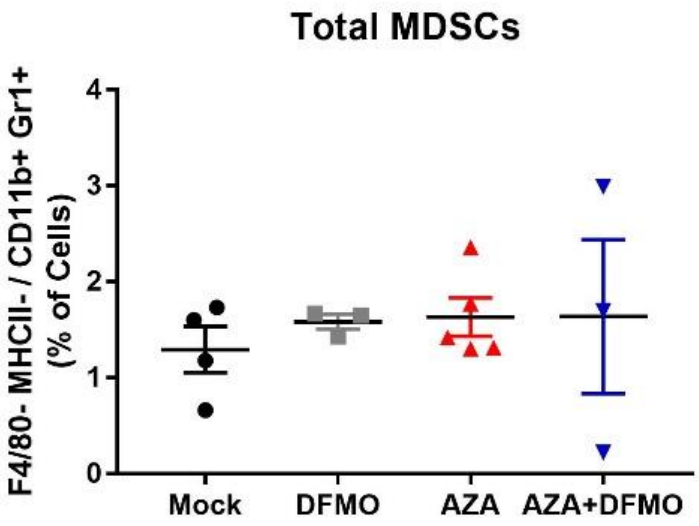

Figure 5.15: Total MDSCs in the tumor microenvironment, as a percentage of total cells. No significant changes were observed with treatment. n=10.

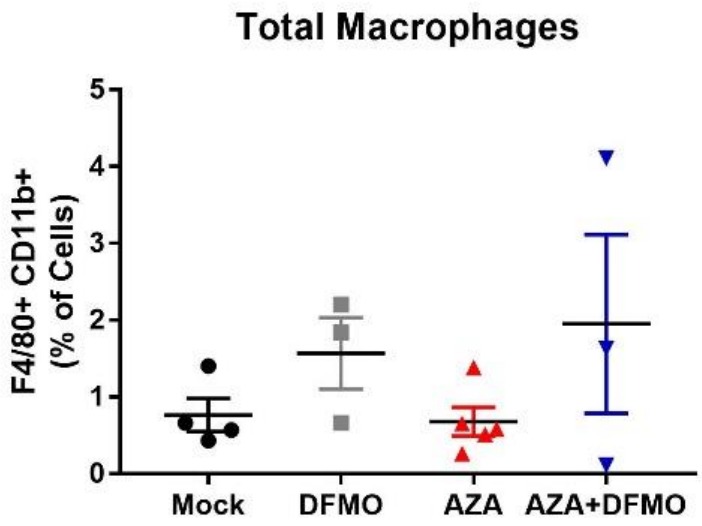

Figure 5.16: Total macrophages in the tumor microenvironment, as a percentage of total cells. No significant changes were observed with treatment, although single agent DFMO is trending toward an *increase* in macrophages, the opposite of what is seen in the VDID8 model. n=3.

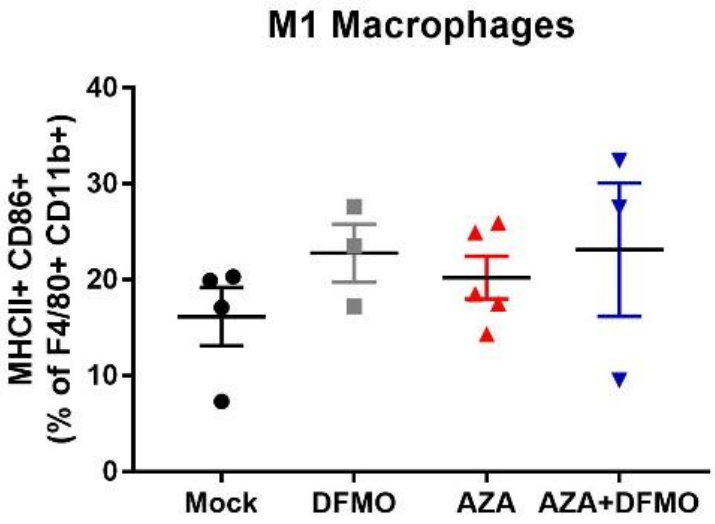

Figure 5.17: M1 macrophages in the tumor microenvironment of the breast 2208L model, shown as a percentage of macrophages. DFMO treatment trends toward an increase in M1 macrophages. n=3.

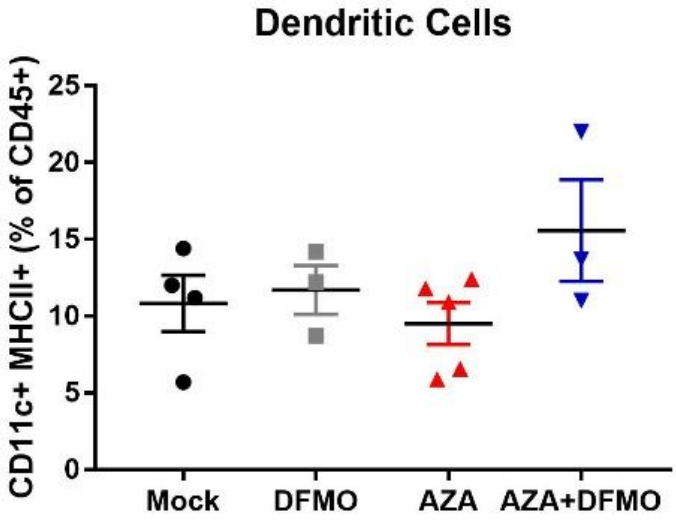

Figure 5.18: Dendritic cells in the tumor microenvironment of the 2208L breast cancer model, shown as a percentage of CD45+ immune cells. No significant changes were observed with treatment. n=3.

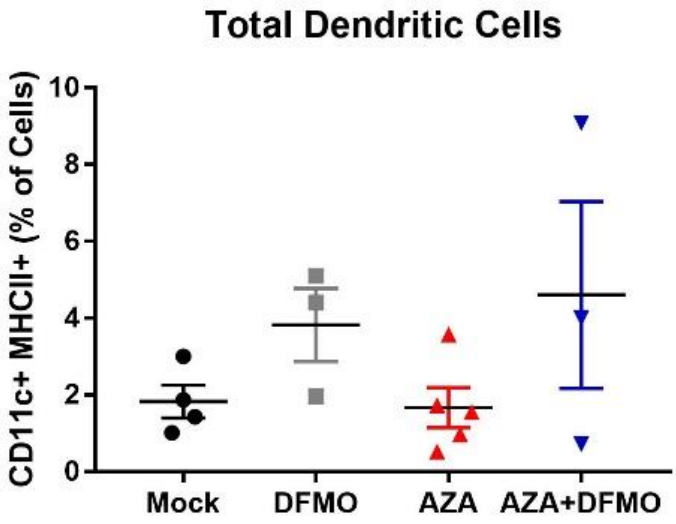

Figure 5.19: Dendritic cells in the tumor microenvironment of the 2208L breast cancer model, shown as a percentage of total cells. No significant changes were observed with treatment. n=3.

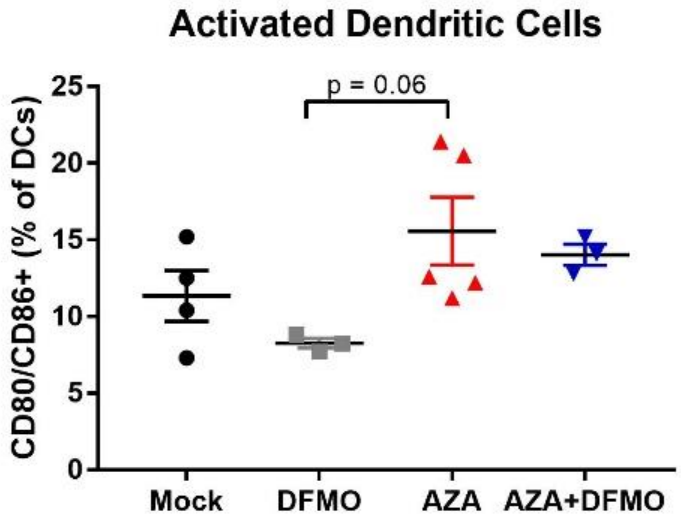

Figure 5.20: Mature or activated dendritic cells in the tumor microenvironment of the 2208L breast cancer model, shown as a percentage of dendritic cells. AZA treatment increases activation of these cells. n=3.

5.3.3 DFMO activates GATA6+ peritoneal macrophages in ovarian tumors

An additional factor to consider when analyzing macrophage populations in the tumor microenvironment is whether these macrophages are tissue resident cells or recruited cells from secondary lymphoid tissue. It is now well understood that certain macrophage populations are seeded out into respective tissue sites during embryogenesis (55). These macrophage subsets include Kupffer cells, Langerhans cells, and alveolar macrophages in liver, skin, and lung tissue respectively (55). In the peritoneum where the tumor microenvironment exists for our VDID8 ovarian cancer mouse model, the tissue resident macrophage population are peritoneal macrophages (53,55). These peritoneal macrophages are known to depend on the transcription factor GATA6 for their differentiation and survival (56,57). Nuclear flow cytometry staining for transcription factors is the most common way to identify T regulatory cells, via expression of the transcription factor Foxp3; therefore identifying macrophages positive for the factor GATA6 will define whether a macrophage is a tissue resident cell or a recruited cell from secondary lymphoid tissue (58,59).

Total macrophages were found to be decreased with DFMO alone and AZA+DFMO during this third ascites drain (Fig 5.21). For logistical reasons, the third drain of ascites fluid at week 6 was analyzed during this experiment. Of these total macrophages, on average roughly 50 percent of the cells were positive for GATA6 and are considered to be peritoneal macrophages, although the data does have wide variation (Fig 5.22). Some mice have a very high percentage of

peritoneal macrophages and others have a lower percentage, which is the case for every treatment arm (Fig 5.22).

Next, the sub-classification of macrophage was examined to see whether peritoneal macrophages had a classically polarized M1 macrophage phenotype or an alternative polarization of M2. As has been observed several times in prior experiments, treatment with DFMO, AZA, and especially AZA+DFMO caused an increase in M1 macrophages in the tumor microenvironment, and a decrease in M2 macrophages (Fig 5.23, 5.24). Again, this data is during the third draining of ascites fluid and therefore the increase in M1 macrophages is not quite as high as that seen in the second drain in Figure 4.6, likely due to the increase in tumor burden at this time (Fig 5.23). Alternatively polarized M2 macrophages remain very low in mice treated with DFMO, but have begun to slightly rise in AZA treated mice (Fig 5.24).

To answer the question of whether peritoneal macrophages were regulated by treatment, cells positive for all three factors (F4\80, CD11b, and GATA6) were further analyzed for markers related to M1 and M2 macrophages (MHC II and CD206). M1-like peritoneal macrophages increased with DFMO treatment, whether it was DFMO alone or in combination with AZA (Fig 5.25), and M2-like peritoneal macrophages decreased with DFMO treatment (Fig 5.26). Interestingly, it does not appear that AZA has a significant impact on this cell population, as M1-like peritoneal macrophages do not increase with AZA treatment compared to mock treated mice, and M2-like peritoneal macrophages only slightly decrease (Fig 5.25, 5.26)

These data are intriguing because AZA treatment does increase M1 macrophages in this VDID8 model, as seen in Figure 4.6 and again in Figure 5.23, similar to the increase seen in DFMO alone; however, AZA treatment does not increase the tissue resident macrophages that are positive for M1-like features (Fig 5.25). These data therefore suggest that AZA treatment is increasing M1 macrophages through another mechanism—namely through recruitment of macrophages from secondary lymphoid tissue. DFMO in contrast, is able to impact macrophages directly at the tissue site (Fig 5.25, 5.26). The differing impacts these drugs have on tissue resident versus recruited macrophages could help to explain the mechanism for why this drug combination works synergistically compared to the single agents. DFMO is able to drive tissue resident macrophages toward a classic polarization that is anti-tumorigenic, while AZA activates an interferon response which includes recruitment of M1 macrophages to the tumor site.

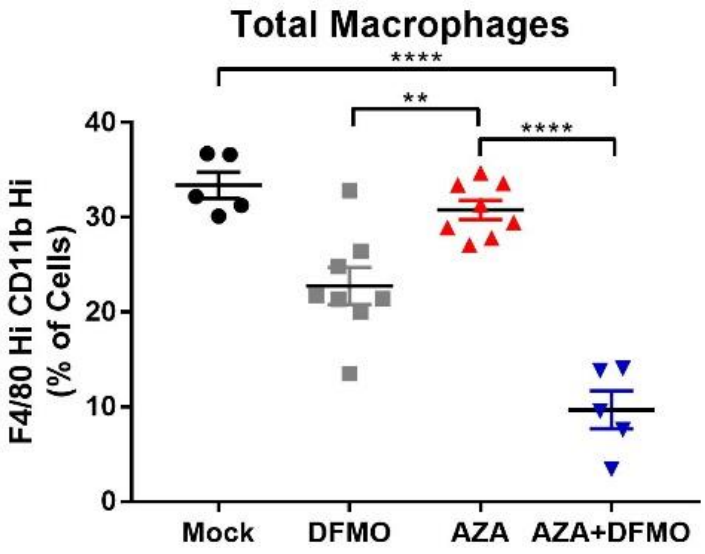

Figure 5.21: Total macrophages in the tumor microenvironment of the VDID8 ovarian cancer mouse model during week 6 post tumor cell injection (drain 3).

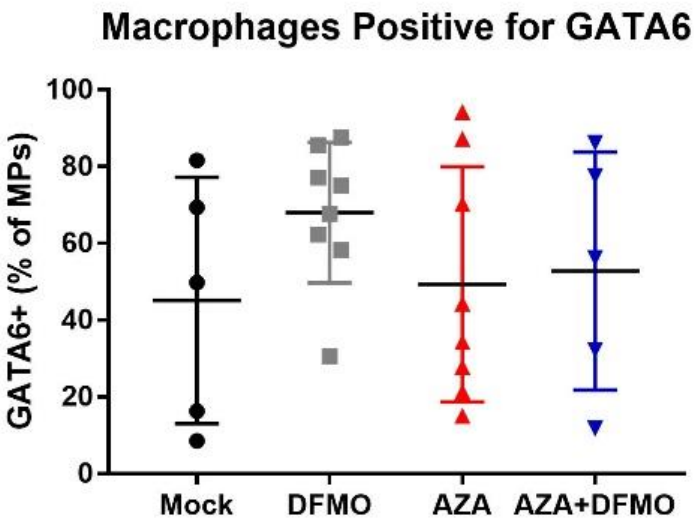

Figure 5.22: Peritoneal macrophages in the tumor microenvironment of the VDID8 model shown as a percentage of macrophages. On average, roughly 50 percent of the macrophages are tissue resident peritoneal macrophages.

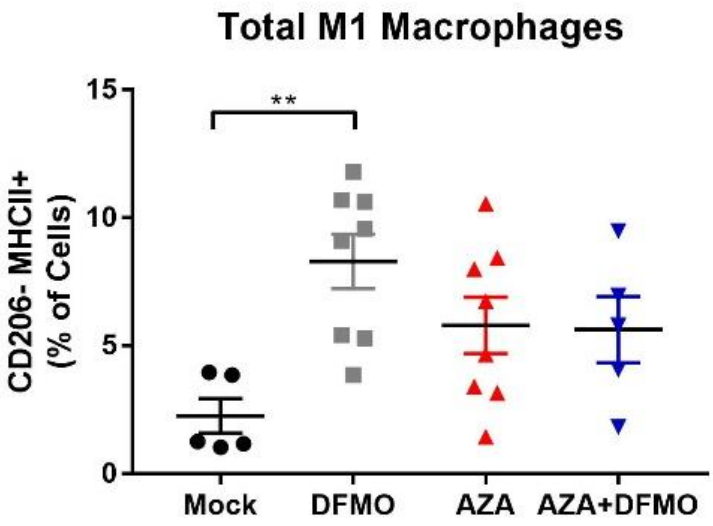

Figure 5.23: Total M1 macrophages as a percentage of cells in DFMO, AZA, and AZA+DFMO treated mice compared to mock mice. All treatment arms show an increase in M1 macrophages, though DFMO alone shows the highest increase during this third drain.

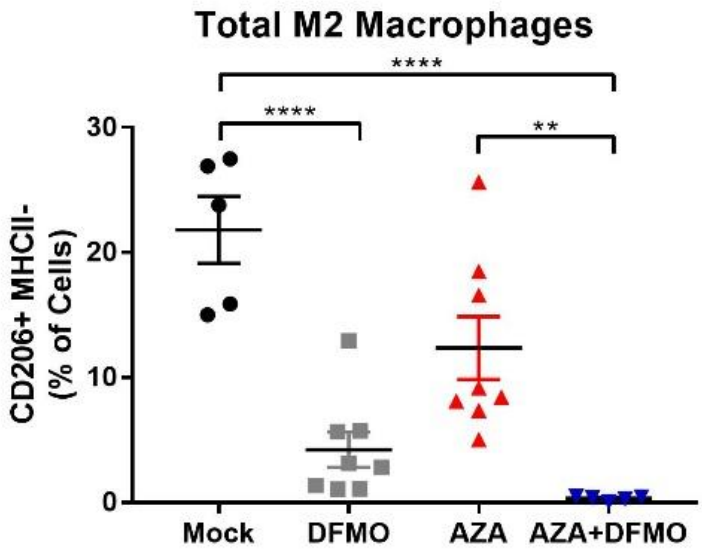

Figure 5.24: Total M2 macrophages as a percentage of cells in DFMO, AZA, and AZA+DFMO treated mice compared to mock mice. Combination treated mice have the lowest population of M2 macrophages during the third ascites drain.

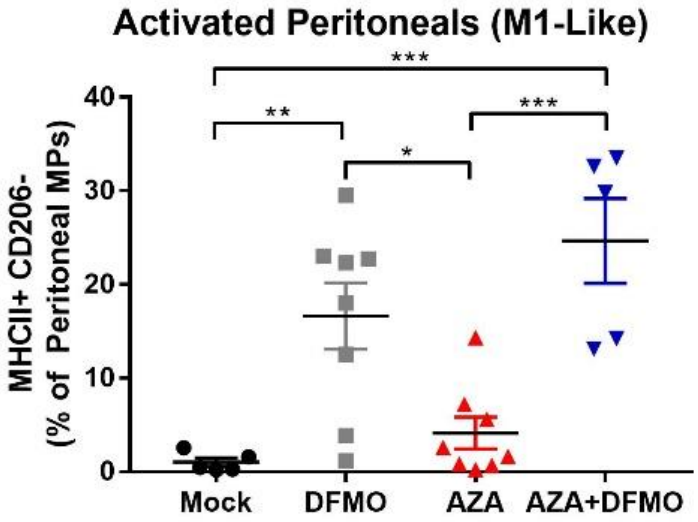

Figure 5.25: Peritoneal macrophages exhibiting an M1-like phenotype positive for MHC II and negative for CD206, shown as a percentage of peritoneal macrophages. Mice treated with DFMO demonstrate an increase in this population.

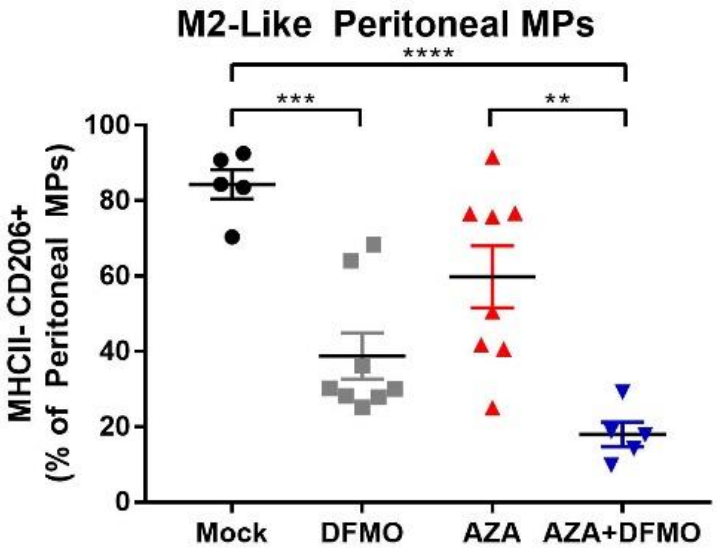

Figure 5.26: Peritoneal macrophages exhibiting an M2-like phenotype negative for MHC II and positive for CD206, shown as a percentage of peritoneal macrophages. Mice treated with DFMO demonstrate a decrease in this population.

5.4 Discussion

The testing of our novel drug combination of AZA and DFMO in two additional solid tumor models has shown that combination AZA+DFMO provides the greatest survival benefit in both the p53-/- solid tumor ID8 ovarian model and the 2208L breast cancer model (Fig 5.2, 5.10). Interestingly however, both of these solid tumor models exhibited significant benefits in terms of survival and tumor burden with DFMO alone over single agent AZA (Fig 5.2, 5.10-5.14). Furthermore, when tissue resident macrophage populations were analyzed in respect to this drug combination in the VDID8 model, it was discovered that DFMO alone had a significant impact on the tissue resident macrophage populations (Fig 5.25, 5.26). It could therefore be possible that DFMO has a greater benefit in solid tumor models due to its ability to act directly at the tumor site on tissue resident macrophages. With AZA's proposed mechanism of action through a system wide interferon/anti-viral response, perhaps the time required to launch this response works against AZA in the solid tumor model. Importantly, the VDID8 ovarian cancer model is an overexpression model of VEGF which produces high volumes of hemorrhagic ascites and increased vasculature. In this model, AZA alone provides a survival benefit very similar to single agent DFMO, perhaps because the increased vasculature allows rapid recruitment of immune cells from the secondary lymphoid tissues.

M1 macrophages were generally increased with treatment in these solid tumors (Fig 5.17, 5.7), though not as dramatically as was seen in the VDID8 model. In the

case of the p53-/- model, the macrophages analyzed are those isolated from hemorrhagic ascites fluid, and therefore may contain a significant population of peritoneal macrophages. It therefore is logical that DFMO treatment is able to impact these macrophages (Fig 5.7, 5.8) while AZA treatment appears to have less of an impact. Data from the breast model does represent immune cells in the physical solid tumor, and there appears to be a modest increase in M1 macrophages with all treatment arms (Fig 5.17). AZA treatment was also found to increase activation and maturation of dendritic cells in both solid tumor models (Fig 5.9, 5.20). These data are also in line with AZA's interferon response, however again, it appears that this increase in activated dendritic cells was not sufficient to elicit a major benefit to survival or tumor burden (Fig 5.2, 5.10-5.14). Overall, combination AZA+DFMO had a significant benefit to survival in both the p53-/- ovarian ID8 model and 2208L breast model, but the impacts on immune cell populations and their contribution to this survival benefit are less clear.

Conclusions and Future Directions

6.1 Summary

Combination epigenetic and polyamine reducing therapy is an effective treatment strategy for ovarian cancer in immunocompetent mice, prolonging survival and decreasing tumor burden significantly. This treatment regimen represents the first combination of these two drug therapies in mice, and the first use of DFMO in an immunocompetent mouse model for ovarian cancer (60). Treatment with AZA alone led to an increase in IFNγ+ NK cells, CD4+ T cells, and CD8+ T cells, as has been demonstrated before (13,17,18). Signaling of IFNγ via its receptor IFNGR1 on tumor cells can lead to increased expression of PD-L1 on tumor cells, thereby making this increase in IFNγ an attractive candidate for α-PD-1 therapy. However, α-PD-1 therapy had no significant impact on survival in this model when added to the combination AZA and DFMO. These results are in contrast to previous studies using AZA and HDACi where the addition of α-PD-1 produced a significant therapeutic response (17). Histone acetylation is essential for transcription of IFNγ, therefore the use of an HDACi may explain the sensitization to α-PD-1 therapy previously seen, as increasing histone acetylation even further increased IFNγ levels in lymphocytes (61).

Analysis of the tumor microenvironment after the combination treatment with AZA and DFMO indicated that the impacts on macrophage polarization are critically important in this model. AZA treatment has been shown to decrease macrophages in the tumor microenvironment, though previously no distinction was

made as to the polarization status of these macrophages (17,18). As the understanding of macrophages deepens, research has discovered that these cells once thought of as permanent, differentiated cells, are in fact quite plastic and able to respond to multiple signals including cytokines and chemokines that direct their behavior and alter their phenotype. Classically polarized M1 macrophages, induced by cytokines such as IFNγ and IL-12, upregulate expression of MHC II and can have tumoricidal functions. M1 macrophages metabolize arginine via iNOS to nitric oxide (NO), creating an oxidizing environment that is damaging to surrounding cells. DFMO treatment has been found to potentiate NO production in LPS-stimulated macrophages *in vitro* (40). Additionally, DFMO, via product inhibition through the increase in ODC substrate, ornithine, inhibits the enzyme arginase I, which is essential for function of alternatively polarized M2 macrophages (22,30). Inhibition of arginase I could lead to increased amounts of its substrate arginine, potentially providing more of the metabolite for use by M1 macrophages and iNOS (30,36). Treatment with DFMO may therefore increase M1 macrophages by making more of its essential metabolite arginine available, while AZA may help increase M1 macrophages via its interferon response and production of IFNγ, a cytokine which drives M1 polarization (14,17,18,36).

Depletion of macrophages in the tumor microenvironment using a CSF1R antibody significantly diminished the efficacy of combination AZA and DFMO, and decreased the levels of M1 macrophages. Tumor burden recurred more rapidly and survival was diminished in mice with fewer macrophages, suggesting that these M1 macrophages could have a tumoricidal role in ovarian tumors.

Importantly, the CSF1R antibody depletes peritoneal macrophages, and has not been shown to reduce recruited macrophages from secondary lymphoid tissue (53). Experiments assessing GATA6 positive macrophages in the VDID8 ovarian model showed that DFMO alone had a significant impact on the tissue resident macrophage populations (Fig 5.24, 5.25). It could therefore be possible that depleting the peritoneal macrophages with the CSF1R antibody prevented DFMO's action on the tissue resident macrophages, resulting in fewer M1 macrophages in the tumor microenvironment (Fig 4.17). AZA treatment in this CSF1R antibody block experiment could still have been able to activate an interferon response and recruit M1 macrophages from the periphery, but perhaps this effect was not enough. In fact, the survival curve for mice receiving CSF1R antibody in combination with AZA+DFMO looks similar to that of a mouse receiving single agent AZA (Fig 4.16, 3.4). These data are in line with DFMO's proposed action on tissue resident macrophages—by depleting these macrophages, DFMO is less able to alter macrophage polarization, and there is a resultant decreased survival.

6.2 Future Directions

This work represents the first combination of these two distinct treatment strategies of epigenetic therapy and polyamine reducing therapy in any cancer. The impact of AZA and DFMO on macrophages in the tumor microenvironment may not be specific to ovarian cancer, and could therefore possibly translate to other macrophage-rich tumors. Furthermore, the use of two well-tolerated and

clinically approved drugs offers potential to test a third drug in combination to further prolong survival. Examples of additional drug combinations could include polyamine transport inhibitors, additional epigenetic therapies such as HDACis, or possibly therapeutic antibodies that deplete M2 macrophages such as α-IL-10R. Exploration of additional drugs that potentiate M1 macrophages is important, as these tumoricidal cells have potential to decrease tumor burden and help activate the immune system against cancer.

In addition to exploring the potential for additional drugs in this combination AZA+DFMO treatment regimen, the role of NK cells in the treatment response could also be further investigated. Combination AZA and DFMO led to a pronounced increase in NK cells positive for IFNγ, significantly more than that of either single agent alone (Fig 3.17). One possibility is that these high levels of IFNγ are precisely what helps to promote the polarization of M1 macrophages, as this cytokine is known to stimulate M1 polarization (36). The potential that these NK cells are playing an additional anti-tumorcidal role however cannot be ruled out. Depletion experiments against NK cells could provide some insight into this question.

Another unanswered question that could potentially be investigated would be the precise role of M1 macrophages against the tumor. These macrophages could be directly tumoricidal via nitric oxide pathways, or they could be activating T cells and in fact it is the CD8+ T cells and NK cells that are primarily responsible for cytotoxicity. Furthermore, how exactly the tumor cell is impacted by these drugs is still an unanswered question—is the immune system actively killing tumor cells or

is it halted growth? Cell cycle experiments suggest that apoptosis is not a primary mechanism, nor is halted growth, so perhaps immunological forms of cell death are at play including necroptosis (programmed necrosis), pyroptosis (inflammatory cell death), or simple necrosis (sudden cell death due to injury). The mechanism of tumor cell death is an interesting question that could still be explored in this model.

Lastly, experiments exploring the role of tissue resident versus recruited macrophages by looking at levels of the transcription factor GATA6 suggested an important role for DFMO on peritoneal macrophages (Fig. 6.1). Additionally, the CSF1R depletion experiment which depletes tissue resident peritoneal macrophages but not necessarily recruited macrophages from the bone marrow suggested that the combined impact (DFMO on tissue resident, and AZA on recruited macrophages) is a major factor to the efficacy of this combination therapy. To truly discover the impact of recruited macrophages, the same AZA+DFMO experiment could be repeated in a mouse knockout model for CCR2, the essential chemokine receptor that recruits macrophages from the bone marrow and secondary lymphoid tissue (62). If single agent DFMO performs similarly in this CCR2 knockout, one could make the reasonable conclusion that its impacts are primarily on tissue resident macrophages. It would also be anticipated that single agent AZA could have less of an impact if the recruited M1 macrophages are essential to its mechanism. Alternatively, AZA may still have a benefit if the primary role of these macrophages is to activate T cells in the secondary lymphoid tissues.

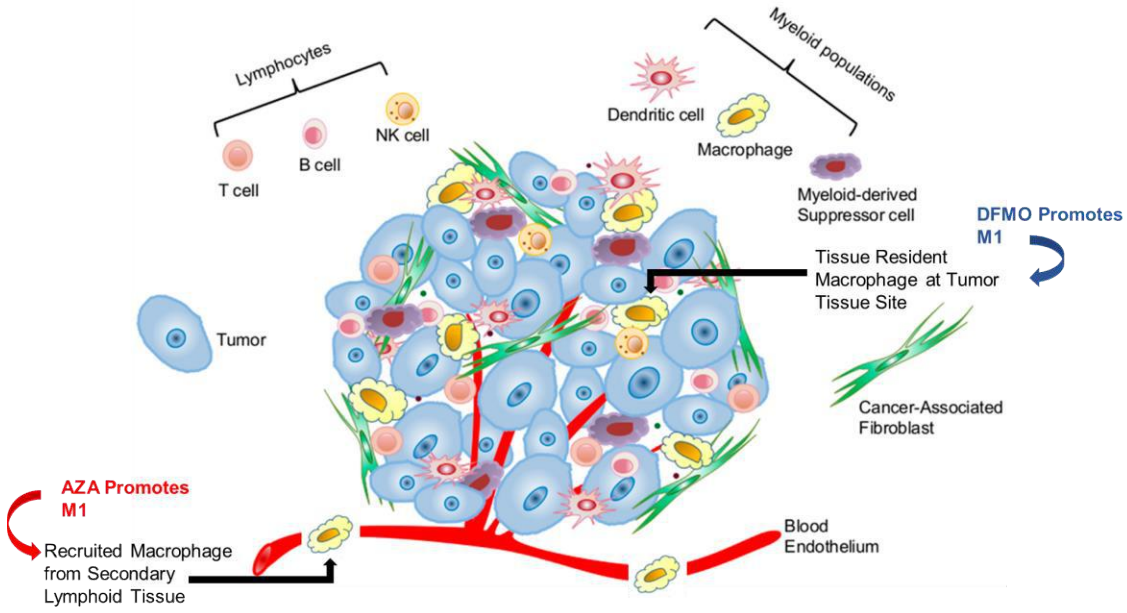

Figure 6.1: Schematic demonstrating hypothesis that DFMO treatment works at the tumor tissue site, and is able to promote tissue resident macrophages toward M1 polarization. In contrast AZA treatment, which elicits a type I interferon response, leads to recruitment of M1 macrophages from secondary lymphoid tissue. The two drugs combined thus lead to the largest increase in M1 macrophages in the tumor microenvironment, and the strongest benefit in survival. Schematic adapted from published figure: Cui and Guo, *Int. J. Mol. Sci.* (63).

REFERENCES

1. Torre LA, Trabert B, DeSantis CE, Miller KD, Samimi G, Runowicz CD*, et al.* Ovarian cancer statistics, 2018. CA Cancer J Clin **2018**;68:284-96
2. Siegel RL, Miller KD, Jemal A. Cancer statistics, 2018. CA Cancer J Clin **2018**;68:7-30
3. Hwang TJ, Franklin JM, Chen CT, Lauffenburger JC, Gyawali B, Kesselheim AS*, et al.* Efficacy, Safety, and Regulatory Approval of Food and Drug Administration-Designated Breakthrough and Nonbreakthrough Cancer Medicines. J Clin Oncol **2018**;36:1805-12
4. Preston CC, Goode EL, Hartmann LC, Kalli KR, Knutson KL. Immunity and immune suppression in human ovarian cancer. Immunotherapy **2011**;3:539-56
5. Brahmer JR, Tykodi SS, Chow LQ, Hwu WJ, Topalian SL, Hwu P*, et al.* Safety and activity of anti-PD-L1 antibody in patients with advanced cancer. N Engl J Med **2012**;366:2455-65
6. Chester C, Dorigo O, Berek JS, Kohrt H. Immunotherapeutic approaches to ovarian cancer treatment. J Immunother Cancer **2015**;3:7
7. Alipour S, Zoghi S, Khalili N, Hirbod-Mobarakeh A, Emens LA, Rezaei N. Specific immunotherapy in ovarian cancer: a systematic review. Immunotherapy **2016**;8:1193-204
8. Leffers N, Gooden MJ, de Jong RA, Hoogeboom BN, ten Hoor KA, Hollema H*, et al.* Prognostic significance of tumor-infiltrating T-lymphocytes in primary and metastatic lesions of advanced stage ovarian cancer. Cancer Immunol Immunother **2009**;58:449-59
9. Zhang M, He Y, Sun X, Li Q, Wang W, Zhao A*, et al.* A high M1/M2 ratio of tumor-associated macrophages is associated with extended survival in ovarian cancer patients. J Ovarian Res **2014**;7:19
10. Wu L, Deng Z, Peng Y, Han L, Liu J, Wang L*, et al.* Ascites-derived IL-6 and IL-10 synergistically expand CD14(+)HLA-DR(-/low) myeloid-derived suppressor cells in ovarian cancer patients. Oncotarget **2017**;8:76843-56
11. Yuan X, Zhang J, Li D, Mao Y, Mo F, Du W*, et al.* Prognostic significance of tumor-associated macrophages in ovarian cancer: A meta-analysis. Gynecol Oncol **2017**;147:181-7

12. Wrangle J, Wang W, Koch A, Easwaran H, Mohammad HP, Vendetti F*, et al.* Alterations of immune response of Non-Small Cell Lung Cancer with Azacytidine. Oncotarget **2013**;4:2067-79

13. Li H, Chiappinelli KB, Guzzetta AA, Easwaran H, Yen RW, Vatapalli R*, et al.* Immune regulation by low doses of the DNA methyltransferase inhibitor 5-azacitidine in common human epithelial cancers. Oncotarget **2014**;5:587-98

14. Chiappinelli KB, Strissel PL, Desrichard A, Li H, Henke C, Akman B*, et al.* Inhibiting DNA Methylation Causes an Interferon Response in Cancer via dsRNA Including Endogenous Retroviruses. Cell **2015**;162:974-86

15. Roulois D, Loo Yau H, Singhania R, Wang Y, Danesh A, Shen SY*, et al.* DNA-Demethylating Agents Target Colorectal Cancer Cells by Inducing Viral Mimicry by Endogenous Transcripts. Cell **2015**;162:961-73

16. Wang L, Amoozgar Z, Huang J, Saleh MH, Xing D, Orsulic S*, et al.* Decitabine Enhances Lymphocyte Migration and Function and Synergizes with CTLA-4 Blockade in a Murine Ovarian Cancer Model. Cancer Immunol Res **2015**;3:1030-41

17. Stone ML, Chiappinelli KB, Li H, Murphy LM, Travers ME, Topper MJ*, et al.* Epigenetic therapy activates type I interferon signaling in murine ovarian cancer to reduce immunosuppression and tumor burden. Proc Natl Acad Sci U S A **2017**;114:E10981-E90

18. Topper MJ, Vaz M, Chiappinelli KB, DeStefano Shields CE, Niknafs N, Yen RC*, et al.* Epigenetic Therapy Ties MYC Depletion to Reversing Immune Evasion and Treating Lung Cancer. Cell **2017**;171:1284-300 e21

19. Tsai HC, Li H, Van Neste L, Cai Y, Robert C, Rassool FV*, et al.* Transient low doses of DNA-demethylating agents exert durable antitumor effects on hematological and epithelial tumor cells. Cancer Cell **2012**;21:430-46

20. Juergens RA, Wrangle J, Vendetti FP, Murphy SC, Zhao M, Coleman B*, et al.* Combination epigenetic therapy has efficacy in patients with refractory advanced non-small cell lung cancer. Cancer Discov **2011**;1:598-607

21. Selvakumaran M, Liebermann D, Hoffman B. The proto-oncogene c-myc blocks myeloid differentiation independently of its target gene ornithine decarboxylase. Blood **1996**;88:1248-55

22. Casero RA, Jr., Murray Stewart T, Pegg AE. Polyamine metabolism and cancer: treatments, challenges and opportunities. Nat Rev Cancer **2018**

23. Choi YH, Park HY. Anti-inflammatory effects of spermidine in lipopolysaccharide-stimulated BV2 microglial cells. J Biomed Sci **2012**;19:31

24. Hayes CS, Shicora AC, Keough MP, Snook AE, Burns MR, Gilmour SK. Polyamine-blocking therapy reverses immunosuppression in the tumor microenvironment. Cancer Immunol Res **2014**;2:274-85

25. Chamaillard L, Catros-Quemener V, Delcros JG, Bansard JY, Havouis R, Desury D*, et al.* Polyamine deprivation prevents the development of tumour-induced immune suppression. Br J Cancer **1997**;76:365-70

26. Ye C, Geng Z, Dominguez D, Chen S, Fan J, Qin L*, et al.* Targeting Ornithine Decarboxylase by alpha-Difluoromethylornithine Inhibits Tumor Growth by Impairing Myeloid-Derived Suppressor Cells. J Immunol **2016**;196:915-23

27. Ai L, Mu S, Wang Y, Wang H, Cai L, Li W*, et al.* Prognostic role of myeloid-derived suppressor cells in cancers: a systematic review and meta-analysis. BMC Cancer **2018**;18:1220

28. Rollins-Smith LA, Ruzzini AC, Fites JS, Reinert LK, Hall EM, Joosse BA*, et al.* Metabolites involved in immune evasion by Batrachochytrium dendrobatidis include the polyamine spermidine. Infect Immun **2019**

29. Chaturvedi R, Asim M, Hoge S, Lewis ND, Singh K, Barry DP*, et al.* Polyamines Impair Immunity to Helicobacter pylori by Inhibiting L-Arginine Uptake Required for Nitric Oxide Production. Gastroenterology **2010**;139:1686-98, 98 e1-6

30. Bronte V, Zanovello P. Regulation of immune responses by L-arginine metabolism. Nat Rev Immunol **2005**;5:641-54

31. Bussiere FI, Chaturvedi R, Cheng Y, Gobert AP, Asim M, Blumberg DR*, et al.* Spermine causes loss of innate immune response to Helicobacter pylori by inhibition of inducible nitric-oxide synthase translation. J Biol Chem **2005**;280:2409-12

32. Hardbower DM, Asim M, Luis PB, Singh K, Barry DP, Yang C*, et al.* Ornithine decarboxylase regulates M1 macrophage activation and mucosal inflammation via histone modifications. Proc Natl Acad Sci U S A **2017**;114:E751-E60

33. Galli SJ, Borregaard N, Wynn TA. Phenotypic and functional plasticity of cells of innate immunity: macrophages, mast cells and neutrophils. Nat Immunol **2011**;12:1035-44

34. Bingle L, Brown NJ, Lewis CE. The role of tumour-associated macrophages in tumour progression: implications for new anticancer therapies. J Pathol **2002**;196:254-65

35. Tamura R, Tanaka T, Yamamoto Y, Akasaki Y, Sasaki H. Dual role of macrophage in tumor immunity. Immunotherapy **2018**;10:899-909

36. Mantovani A, Marchesi F, Malesci A, Laghi L, Allavena P. Tumour-associated macrophages as treatment targets in oncology. Nat Rev Clin Oncol **2017**;14:399-416

37. Partecke LI, Gunther C, Hagemann S, Jacobi C, Merkel M, Sendler M*, et al.* Induction of M2-macrophages by tumour cells and tumour growth promotion by M2-macrophages: a quid pro quo in pancreatic cancer. Pancreatology **2013**;13:508-16

38. Klug F, Prakash H, Huber PE, Seibel T, Bender N, Halama N*, et al.* Low-dose irradiation programs macrophage differentiation to an iNOS(+)/M1 phenotype that orchestrates effective T cell immunotherapy. Cancer Cell **2013**;24:589-602

39. Zhang M, Caragine T, Wang H, Cohen PS, Botchkina G, Soda K*, et al.* Spermine inhibits proinflammatory cytokine synthesis in human mononuclear cells: a counterregulatory mechanism that restrains the immune response. J Exp Med **1997**;185:1759-68

40. Baydoun AR, Morgan DM. Inhibition of ornithine decarboxylase potentiates nitric oxide production in LPS-activated J774 cells. Br J Pharmacol **1998**;125:1511-6

41. Roby KF, Taylor CC, Sweetwood JP, Cheng Y, Pace JL, Tawfik O*, et al.* Development of a syngeneic mouse model for events related to ovarian cancer. Carcinogenesis **2000**;21:585-91

42. Conejo-Garcia JR, Benencia F, Courreges MC, Kang E, Mohamed-Hadley A, Buckanovich RJ*, et al.* Tumor-infiltrating dendritic cell precursors recruited by a beta-defensin contribute to vasculogenesis under the influence of Vegf-A. Nat Med **2004**;10:950-8

43. Zhang L, Yang N, Garcia JR, Mohamed A, Benencia F, Rubin SC*, et al.* Generation of a syngeneic mouse model to study the effects of vascular endothelial growth factor in ovarian carcinoma. Am J Pathol **2002**;161:2295-309

44. Walton J, Blagih J, Ennis D, Leung E, Dowson S, Farquharson M*, et al.* CRISPR/Cas9-Mediated Trp53 and Brca2 Knockout to Generate Improved Murine Models of Ovarian High-Grade Serous Carcinoma. Cancer Res **2016**;76:6118-29

45. Pfefferle AD, Agrawal YN, Koboldt DC, Kanchi KL, Herschkowitz JI, Mardis ER*, et al.* Genomic profiling of murine mammary tumors identifies potential personalized drug targets for p53-deficient mammary cancers. Dis Model Mech **2016**;9:749-57

46. Peirce CS. The numerical measure of the success of predictions. Science **1884**;4:453-4

47. Kabra PM, Lee HK, Lubich WP, Marton LJ. Solid-phase extraction and determination of dansyl derivatives of unconjugated and acetylated polyamines by reversed-phase liquid chromatography: improved separation systems for polyamines in cerebrospinal fluid, urine and tissue. J Chromatogr **1986**;380:19-32

48. Wherry EJ, Kurachi M. Molecular and cellular insights into T cell exhaustion. Nat Rev Immunol **2015**;15:486-99

49. Zehn D, Wherry EJ. Immune Memory and Exhaustion: Clinically Relevant Lessons from the LCMV Model. Adv Exp Med Biol **2015**;850:137-52

50. Lawrence T, Natoli G. Transcriptional regulation of macrophage polarization: enabling diversity with identity. Nat Rev Immunol **2011**;11:750-61

51. Sica A, Mantovani A. Macrophage plasticity and polarization: in vivo veritas. J Clin Invest **2012**;122:787-95

52. Martinez FO, Gordon S. The M1 and M2 paradigm of macrophage activation: time for reassessment. F1000Prime Rep **2014**;6:13

53. MacDonald KP, Palmer JS, Cronau S, Seppanen E, Olver S, Raffelt NC*, et al.* An antibody against the colony-stimulating factor 1 receptor depletes the resident subset of monocytes and tissue- and tumor-associated macrophages but does not inhibit inflammation. Blood **2010**;116:3955-63

54. Roche PA, Furuta K. The ins and outs of MHC class II-mediated antigen processing and presentation. Nat Rev Immunol **2015**;15:203-16

55. Mass E, Ballesteros I, Farlik M, Halbritter F, Gunther P, Crozet L*, et al.* Specification of tissue-resident macrophages during organogenesis. Science **2016**;353

56. Gautier EL, Shay T, Miller J, Greter M, Jakubzick C, Ivanov S*, et al.* Gene-expression profiles and transcriptional regulatory pathways that underlie the identity and diversity of mouse tissue macrophages. Nat Immunol **2012**;13:1118-28

57. Gautier EL, Ivanov S, Williams JW, Huang SC, Marcelin G, Fairfax K*, et al.* Gata6 regulates aspartoacylase expression in resident peritoneal macrophages and controls their survival. J Exp Med **2014**;211:1525-31

58. Crellin NK, Garcia RV, Levings MK. Flow cytometry-based methods for studying signaling in human CD4+CD25+FOXP3+ T regulatory cells. J Immunol Methods **2007**;324:92-104

59. Hsieh CS, Lee HM, Lio CW. Selection of regulatory T cells in the thymus. Nat Rev Immunol **2012**;12:157-67

60. Manetta A, Satyaswarcoop PG, Podczaski ES, Hamilton T, Ozols RF, Mortel R. Effect of alpha-difluoromethylornithine (DFMO) on the growth of human ovarian carcinoma. Eur J Gynaecol Oncol **1988**;9:222-7

61. Peng M, Yin N, Chhangawala S, Xu K, Leslie CS, Li MO. Aerobic glycolysis promotes T helper 1 cell differentiation through an epigenetic mechanism. Science **2016**;354:481-4

62. Willenborg S, Lucas T, van Loo G, Knipper JA, Krieg T, Haase I*, et al.* CCR2 recruits an inflammatory macrophage subpopulation critical for angiogenesis in tissue repair. Blood **2012**;120:613-25

63. Cui Y, Guo G. Immunomodulatory Function of the Tumor Suppressor p53 in Host Immune Response and the Tumor Microenvironment. Int J Mol Sci **2016**;17

This page is intentionally left blank.

Curriculum Vitae

MEGHAN TRAVERS
1830 Eastern Avenue, Baltimore, MD 21231
(508) 446-2853 · mtravers@jhmi.edu

EDUCATION

Ph.D., Cellular and Molecular Medicine
Johns Hopkins University School of Medicine (SOM), Baltimore, MD, June 2019
Dissertation: DFMO and 5-azacytidine increase M1 macrophages in an ovarian cancer mouse model.
Advisor: Dr. Cynthia Zahnow

Bachelor of Science, Biological Engineering
Cornell University, Ithaca, NY, May 2009

RESEARCH EXPERIENCE

Johns Hopkins University SOM, Cancer Epigenetics
Dr. Cynthia Zahnow *May 2016 - Present*
Doctoral Research

- Studying the use of novel epigenetic drug combination treatment strategies in a murine model for high grade serous ovarian cancer.
- Investigating the recruitment and activation of immune cells in response to treatment with epigenetic therapies, with a particular focus on alterations to macrophages in the tumor microenvironment.

Johns Hopkins University SOM, Retrovirus Lab
Dr. Kenneth Witwer *Sep 2015 – Dec 2015*
Graduate Student Rotation Project

- Investigated the role of exosomes in HIV infection including viral production and infectivity in both T cell and macrophage primary cell cultures.
- Presented data obtained during a three month rotation project at the International Society for Extracellular Vesicles annual conference in Rotterdam, The Netherlands.

Northeastern University, DNA Damage
Dr. Penny Beuning *May 2014 – Dec 2014*
Masters Student Volunteer

- Assisted PhD candidate with research on DNA damage and repair in *E. coli* upon exposure to alkylating agents.

PUBLICATIONS

- **Travers, M.**, Brown, S. et al. (2019). *DFMO and 5-azacytidine increase M1 macrophages in the tumor microenvironment of an ovarian cancer mouse model*. Cancer Research. In press.
- Zhang, H., Pandey, S., **Travers, M.**, et al. (2018). *Targeting CDK9 Reactivates Epigenetically Silenced Genes in Cancer.* Cell. Vol 175 Issue 5.
- Liao, Z., Muth, D., Eitan, E., **Travers, M.**, et al. (2017). *Serum extracellular vesicle depletion processes affect release and infectivity of HIV-1 in culture.* Scientific Reports. 7, Article number: 2558.
- Stone, M., Chiappinelli, K., Li, H., Murphy, LM, **Travers, M.**, et al. (2017). *Epigenetic therapy activates type I interferon signaling in murine ovarian cancer to reduce immunosuppression and tumor burden.* Proceedings of the National Academy of Sciences. Vol 114 No 51.

ABSTRACTS AND PRESENTATIONS

- **Travers, M.**, Brown, S. et al. (2019, June). *DFMO and 5-azacytidine promote TAMs toward an M1 polarization in the tumor microenvironment of an ovarian cancer mouse model*. Invited speaker to the Gordon Research Seminar on Polyamines, Waterville Valley, NH.
- **Travers, M.**, Brown, S. et al. (2019, April). *DFMO and 5-azacytidine increase M1 macrophages in the tumor microenvironment of an ovarian cancer mouse model*. Poster presentation at the annual American Association for Cancer Research meeting, Atlanta, GA.
- **Travers, M.**, Brown, S. et al. (2018, June). *DFMO and 5-azacytidine increase M1 macrophages in the tumor microenvironment of an ovarian cancer mouse model*. Poster presentation at the annual Sidney Kimmel Comprehensive Cancer Center (SKCCC) Fellow Research Day, Baltimore, MD.
    - Awarded Honorable Mention in Translational Research.
- **Travers, M.**, Liao, Z., et al. (2016, May). *Extracellular vesicles in culture medium influence cell survival and response to HIV infection*. Poster presentation at the annual meeting of the International Society for Extracellular Vesicles, Rotterdam, The Netherlands.

TEACHING EXPERIENCE

Johns Hopkins Collaborative Teaching Fellow *Sep 2018 – Dec 2018*

- Instruct undergraduate freshmen in introductory chemistry course alongside the mentorship of Dr. George Greco and Dr. Judy Levine at Goucher College.
- Gained valuable experience leading lecture and laboratory sections for a class of 50 students with variable backgrounds in science.

Johns Hopkins University Teaching Academy *June 2017 – Present*

- Participated in three-day teaching institute workshop focused on teaching as scholarship.
- Learned skills for planning courses, incorporating active learning, ensuring the classroom is inclusive, and evaluating student's learning in a way that is both fair to them and informative to the teacher.

Johns Hopkins University School of Public Health *Sep – Oct 2017*
Teaching Assistant *Sep – Oct 2018*

- Worked alongside Dr. Alan Scott for two terms as the teaching assistant for Principles of Immunology I, a graduate-level course with over 70 enrolled students.
- Led review sessions for midterm and final exams and received a majority "excellent" (82%) rating from student course evaluations.

Johns Hopkins University School of Medicine *Jan 2017 – Nov 2017*
Pollard Scholar

- Taught first-year graduate students material from three courses: Pathways and Regulation, Cellular Structure and Dynamics, and Molecular Biology and Genomics.
- Taught a 1-hour, once-weekly class addressing challenging concepts.

Cornell University, *Teaching Assistant, Biochemistry* *Sep 2008 – Dec 2008*

Cornell University, *Academic Excellence Workshop Facilitator*
Calculus I and Calculus II *Aug 2006 – Dec 2008*

ACADEMIC SERVICE

Student Representative
Cellular and Molecular Medicine Student Senate *June 2018 – June 2019*

PROFESSIONAL AFFILIATIONS

American Association for Cancer Research, Associate Member

HONORS

Honorable Mention in Translational Research

- SKCCC Fellow Research Day, June 2018.

Collaborative Teaching Fellow, Johns Hopkins School of Medicine, August 2018.

ENGINEERING EXPERIENCE

DePuy Synthes, Raynham, MA *Apr 2014 – Aug 2015*
Regulatory Affairs, Spine Medical Devices

- Data management for Unique Device Identification (UDI) spine regulatory database to ensure compliance with new Federal Drug Administration (FDA) regulations.
- Verify initial records and maintain compliance of the regulatory database.

E.A. Engineering, Science, and Technology, Warwick, RI *Aug 2009 – Apr 2014*
Engineer

- Excelled in Data Management role for large-scale air sampling project. Analyzed data trends and conducted review of data anomalies. Compiled all verified data and presented results in an effective and efficient manner.
- Prepared conceptual, preliminary, and final designs for nature-like fishway bypass channels.
- Conducted two major developmental analyses to determine economic viability of multi-dam and power generating facilities for Federal Energy Regulatory Commission.